INVESTIGATION OF DAILY TO SEASONAL VARIATION IN GREENHOUSE GAS EMISSION AND CYCLING IN AGRICULTURAL RIPARIAN ZONE SOILS

A thesis submitted to the Faculty of Graduate and Postdoctoral Affairs
in partial fulfillment of the requirements for the degree of

Master of Science

In

Earth Sciences

Carleton University
Ottawa, Ontario

ABSTRACT:

Agricultural riparian zone microecosystems provide opportunity for mitigation of pollution transport and greenhouse gas emissions. In order to make recommendations to farmers as to best management practices, temporal variations in gas fluxes between the soil and atmosphere must be considered, and the controls on soil-gas behaviour must be better understood. In this study, CO_2, O_2, CH_4, and N_2O subsurface concentrations and surface fluxes were monitored with an average temporal resolution of 4 hours, along with soil temperature, soil moisture content, and barometric pressure from the beginning of May until the end of November 2021 at an active, arborous, agricultural riparian zone in St. Albert, Ontario. The results show varying control of barometric pressure, soil temperature, and moisture content on short-term changes in soil gas concentrations and emissions depending on the overall environmental conditions under which these changes in controlling parameters occur.

ACKNOWLEDGMENTS:

Firstly, thanks are due to my supervisor, Richard Amos, who has led by example in being thorough, methodical, and curious, helping develop my abilities in scientific research. Steadfast, calm, and even-tempered in his encouragement and advice, he has played a large part in the completion of this work and has been an invaluable mentor and role model. Additional sources of scientific inspiration, valuable insight, and support include David Blowes, Oliver Blume, Ian Clark, Emilia Craiovan, Amanda Halstead, Kyle Horner, David Lapen, Carol Ptacek, David Rudolph, Andrew Schietzsch, Mark Sunohara, and Geng Xiaoyuan. In times where social interactions were sparse, the conversations and experiences shared with Andrew Hicks in the lab and in celebration of his completed thesis; with George Bao in the field; and with Colleen Harper virtually, and outside for lunch, carried significant weight.

To my friends and family, thank you. Thank you for understanding my tardiness, my late nights and early mornings working, and my abrupt departures to the field. Thank you for coaxing me from work when I needed it, and for understanding and supporting me when it wasn't possible.

TABLE OF CONTENTS:

LIST OF FIGURES:

LIST OF TABLES:

1 INTRODUCTION

Greenhouse gases (GHG) persist as a global topic of interest, as concentrations of carbon dioxide (CO_2), nitrous oxide (N_2O), and methane (CH_4) in the atmosphere continue to increase and contribute to climate change (Global Monitoring Laboratory, 2022; IPCC, 2013; Gregorich et al. 2005). The ability of soils to behave as a source or sink within their roles in the nitrogen and carbon cycles, along with the growing concern around climate change demands that GHG behaviour within these soils be better understood (Smith et al., 2018; Paustian et al., 2016). Agricultural soils are of particular interest and importance due to their constant manipulation and maintenance along with their geographic prevalence and significant GHG contributions in Canada. Roughly 160 million acres of agricultural land exists in Canada (Statistics Canada, 2022), with its soil contributing 24 Mt CO_2 equivalent of GHGs to the atmosphere (3.3% of the nation's total anthropogenic emissions) in 2019 (ECCC, 2021). Land/soil modification via fertilizer/manure application, tilling, installation of drainage systems, artificial riparian zone creation, dredging, and natural vegetation clearing/brushing introduces many controlled variables to the emission of GHGs in Canadian agricultural riparian zones. The presence of these numerous controlled variables gives these soils the unique ability to be studied over a wide range of conditions in order to better understand GHG behaviour, as well as the potential to be actively managed in order to reduce GHG emissions.

Agricultural beneficial management practices (BMPs) can be implemented to aid in reduction of GHG emissions or water contamination while contributing economic benefit (or lack of economic detriment) to farmers (Sunohara et al., 2016; Crabbé et al., 2012; Pearce & Yates, 2017). Examples of some BMPs include riparian buffer areas, grazing management, manure storage, and limited tillage, etc. (Pearce & Yates, 2017). Controlled tile drainage (CTD) is used to control the water table level in agricultural fields by regulating how much water is drained from the field into the drainage ditches via a network of subsurface tiles, controlled with flashboard risers at the drainage outlets. CTD is able to reduce transport of nutrients by increasing uptake by crops, and increasing crop yield (Gilliam et al., 1979; Evans et al., 1995). However, the elevated water tables brought on by CTD systems contribute to increased surface runoff, as well as promoting anaerobic conditions with high soil moisture content, increasing the potential for greater nitrous oxide and methane emissions compared to uncontrolled tile drainage (UCTD) systems (which are similar systems, but without the ability to control field water saturation or drainage discharge (Evans et al., 1995)) (Blume, O., 2019; Evans et al., 1995).

Riparian zones in an agricultural context are the microecosystems that lie within the interface between land (crop field) and aquatic environment (drainage ditch) (Vidon et al., 2010). The vegetation that exists within these riparian zones can help the area act as a buffer strip, reducing the loss of sediment, soil, and pollutants from the field into the drainage system, while contributing to the sequestration of carbon (Gumiere et al., 2011; Arora et al., 2010; Baskerville et al., 2021). Riparian vegetation can slow surface water flow and settle out sediment while its roots will strengthen the soil and prevent erosion (Nigel et al., 2014). In particular, riparian buffer strips are able to reduce nitrate (NO_3^-) export into the drainage system via dilution,

vegetation uptake, immobilization, and denitrification (Oertel et al., 2016). With the slowing of run off through these riparian zones, pesticide retention has also been found to occur through infiltration, sorption, and sediment deposition (Arora et al., 2010). If these riparian zones are managed correctly, they have also been found to sequester atmospheric carbon dioxide in the growth and burial of biomass (Borin et al., 2010; Baskeville et al., 2021).

With soil moisture content, temperature, physical, and biogeochemical properties being the main controllers of soil gas production, consumption, and transport, the soil conditions in agricultural riparian zones brought on by CTD and riparian vegetation have the potential to significantly influence soil gas behaviour and emissions (Smith et al., 2018; Oertel et al., 2016). The production or consumption of CH_4, CO_2, and N_2O from soil is a result of microbial activity, root respiration, heterotrophic respiration, and chemical decay (Oertel et al., 2016).

1.1 BIOLOGIC PROCESSES

1.1.1 CO_2:

Soil is the source for 60-90% of CO_2 emissions from an ecosystem (Kuzyakov, Y., 2006). CO_2 production in soil is mainly the result of heterotrophic (soil organism) and autotrophic (root) respiration (Oertel et al., 2016; Tan, K. H., 2009; Trumbore, S. E., 1993). Where both of these components of soil respiration share the same general equation (Tan, K. H., 2009; Stumm & Morgan, 2012):

$$C_6H_{12}O_6 + 6O_2 \rightarrow 6CO_2 + 6H_2O \qquad (1)$$

Heterotrophic respiration pertains to microorganisms oxidizing available carbohydrates in the soil (products of decomposition) to acquire the energy necessary for metabolism and growth (Tan, K. H., 2009; Stumm & Morgan, 2012). Root respiration involves the use of photosynthates (product of photosynthesis) for root maintenance and growth (Pregitzer et al., 2007). Dense populations of heterotrophs (microorganisms and mycorrhizae) congregate within the rhizosphere (root zone), as beneficial chemicals/nutrients are secreted by plant roots (Tan, K. H., 2009). This can cause difficulty in distinguishing between autotrophic and heterotrophic respiration in the rhizosphere, leading to the common simplification of considering root respiration to include all respiration processes within the root zone (Hanson, et al., 2000). However, it should be understood that the two respiration processes in the rhizosphere react differently to changing environmental conditions (Hanson, et al., 2000; Kuzyakov, Y., 2006).

1.1.2 CH_4:

Between 70 and 80% of CH_4 in the atmosphere originates from biologic processes, much of which is microbiological activity within the soil (Le Mer & Roger, 2001). Methanogenic and methanotrophic bacteria play a role in the consumption and production of both CH_4 and CO_2 (Le Mer & Roger, 2001). Each of these bacterial populations dominate under different environmental conditions but will often remain present under their specific unfavourable conditions (Le Mer & Roger, 2001). For example, under anaerobic conditions, methanotrophs and methanogens are

present simultaneously, where methanogens dominate, consuming CO_2 to produce CH_4 via methanogenesis (Le Mer & Roger, 2001; Dutaur & Verchot, 2007):

$$4H_2 + CO_2 \rightarrow CH_4 + 2H_2O \quad (2)$$

This reduction of CO_2 is unfavourable if oxygen, nitrate, ferric iron, or manganese(IV) are readily available in its place, as they require less energy to be reduced (Smith et al., 2018). If these conditions were to become aerobic, methanotrophs would begin to thrive, consuming CH_4 (and readily available O_2) and producing CO_2 via methanotrophy (Le Mer & Roger, 2001; Dutaur & Verchot, 2007):

$$CH_4 + 2O_2 \rightarrow CO_2 + 2H_2O \quad (3)$$

1.1.3 N_2O:

Roughly 60% of global N_2O emissions are from soils, with agricultural soils in particular contributing significantly (Butterbach-Bahl et al., 2013). N_2O and N_2 production in soil is mainly controlled by nitrifying and denitrifying bacteria (Le Mer & Roger, 2001; Butterbach-Bahl et al., 2013). Nitrification is the two-step process of converting ammonium (NH_4^+) or ammonia (NH_3) into nitrate (NO_3^-), with an intermediate product of nitrite (NO_2^-), where each step of the reaction requires aerobic conditions (Smith et al., 2018; Butterbach-Bahl et al., 2013):

$$NH_4^+ + \frac{3}{2}O_2 \rightarrow NO_2^- + H_2O + 2H^+ \quad (4)$$

$$NH_3 + O_2 \rightarrow NO_2^- + 3H^+ \quad (5)$$

$$NO_{2^-} + \frac{1}{2}O_2 \rightarrow NO_3^- \quad (6)$$

Denitrification is the stepwise reduction of NO_3^- under anaerobic conditions, potentially producing NO_2^-, NO, N_2O, and N_2 (Smith et al., 2018; Butterbach-Bahl et al., 2013):

$$NO_{3^-} \rightarrow NO_2^- \rightarrow NO \rightarrow N_2O \rightarrow N_2 \quad (7)$$

The amount of NO_2^-, NO, N_2O, or N_2 produced, or the end product of the stepwise reduction is determined by environmental conditions (Smith et al., 2018; Butterbach-Bahl et al., 2013).

The intermediate products formed during these major N_2O controlling microbial processes can be removed from the system via reactions within plant bodies such as assimilatory denitrification (where NO_3^- is transformed into NH_4^+ under anaerobic conditions) or immobilization (uptake of NO_3^- by plants) (Smith et al., 2018).

1.2 SOIL GAS TRANSPORT

Soil gas concentrations at a particular place and time in a soil profile and surface fluxes are the result of the balance between biogeochemical reactions previously described and soil gas transport processes (Molins & Mayer, 2007). Diffusion is considered the major process for gas exchange between the soil and atmosphere, as well for gas transport within the soil (Smith et al., 2018; Kayler et al., 2010; Thorstenson & Pollock, 1989; Molins & Mayer, 2007; Blume, O., 2019). Molecular diffusion is the process by which gases will move from areas of high concentration to areas of low concentration in order to reach a state of maximum entropy (and by which the rate of movement is determined by the magnitude of the concentration gradient) (Appelo & Postma, 2005). With the soil gas reactions described above producing and consuming components of soil gas depending on environmental conditions which vary spatially and temporally, there are constant differences in gas concentrations within the soil profile, causing diffusion to occur.

Advection is another gas transport mechanism to consider (Amos et al., 2005; Molins & Mayer, 2007), where there is transport/movement of the bulk fluid (gas), which all constituents within the gas mass are subject to (Warrick, A. W., 2002). This mass flow can occur within the soil profile, as well as between the soil and the atmosphere and is brought on by pressure gradients, potentially caused by wind action, barometric pressure changes, changes in temperature, water table/soil moisture content variations, and by consumption or production of gases (Molins & Mayer, 2007; Smith et al., 2018). Changes in barometric pressure will cause differences in pressure between soil gas and the atmosphere, influencing transport. An increase in barometric pressure will inhibit upward transport of soil gas and gas effluxes, potentially causing advective transport of atmospheric gas into the soil, whereas low atmospheric pressures will promote advective upward transport of gas and soil gas efflux (all while maintaining the diffusive component of transport driven by concentration gradients throughout any changes in advective transport) (Olenka et al., 2019; Laemmel et al., 2017; Maier et al., 2012).

1.3 RIPARIAN ZONE ENVIRONMENTS

Riparian zones being in proximity to streams (with anthropological controls, in an agricultural context), their soils are subject to unique conditions. For example, high water tables prevail in riparian zones, often giving these areas relatively high soil moisture content (Kachenchart et al., 2012; Gunderson et al., 2010). Riparian zones are also subject to frequent water table fluctuations, potentially creating conditions favourable to the formation of discrete anaerobic and aerobic zones (microsites) within the soil (Kachenchart et al., 2012).

Riparian zone vegetation plays a significant role in influencing the soil moisture content, temperature, and soil organic carbon (SOC) (Baskerville et al., 2021). Where large trees are able to provide shade during agronomic seasons in forested riparian zones, the air and shallow soil temperatures will tend to be lower, and the soil moisture content may be higher by way of less evaporation compared to herbaceous riparian zones or bare fields (Baskerville et al., 2021; Moore et al., 2005; Wynn & Mostaghimi, 2006). Shade provided by forest canopies also tends to buffer diurnal temperature variations (Moore et al., 2005; Wynn & Mostaghimi, 2006), as well as

provide protection from wind, potentially shielding the soil from wind induced mass flux events (Smith et al., 2018). However, during winter months, the loss of the canopy in a deciduous forested riparian zone removes its ability to buffer diurnal temperatures, exposing the soil to a higher number of freeze-thaw events compared to herbaceous riparian zones (Wynn & Mostaghimi, 2006), as well as exposing the soil to wind induced mass flux events (Smith et al., 2018). With a forest canopy, less precipitation may reach the soil, as it is intercepted (Reichstein et al., 2003). The presence of vegetation in general will cause a loss of a certain amount of soil water through the process of transpiration (while different vegetation types will have different transpiration capabilities) (Reichstein et al., 2003). With the thermal and moisture regulation provided by streams, soil closer to the stream (further down the bank slope) has been observed to be subject to fewer freeze-thaw cycles in the winter (Wynn & Mostaghimi, 2006).

As well as the above-ground environmental services provided by riparian zone vegetation, the root systems of different vegetation types can influence soil structure and chemistry (Raich, et al., 2000). Herbaceous vegetation will allocate greater amounts of carbon in the form of photosynthates to the roots compared to arborous vegetation, contributing to a greater diversity of carbon substrates (thus increasing microbiological population and productivity) (Raich, et al., 2000). The deeper root systems of forested riparian zones contributes to increased soil porosity, water retention, and permeability (Cole et al., 2020). This is in part due to the deep root systems of woody vegetation, able to draw moisture from greater depths (and a greater soil volume) compared to herbaceous vegetation which is only able to draw moisture from shallow depths (Wynn & Mostaghimi, 2006). In addition to influencing the microbiological community, plant roots themselves respire, and root respiration rates will vary depending on vegetation type and diurnal/seasonal variations in light, soil temperature, and soil moisture content (Vargas & Allen, 2008).

Vegetation type will influence the soil chemistry, which will in turn influence the soil microbial community by way of nutrient content and carbon availability (Waymouth et al., 2020; Malchair & Carnol, 2009). Carbon (C), nitrogen (N), and phosphorous (P) in the soil are used, immobilized, and released by both the microbial community and the vegetation community (Aponte et al., 2010). Different vegetation communities will be able provide varying amounts of nutrients to the soil by way of litter quality and quantity, as well as root exudates (Aponte et al., 2010). Plant roots will secrete readily available C for microbial respiration, and these exudates will vary between plant species (Malchair & Carnol, 2009). Litter introduction to the soil surface will increase the amount of labile C available, promoting microbiological activity (Maxwell & Coleman, 1995). There are seasonal trends related to the introduction of litter, with surplus in the fall months under deciduous forests (leaf litter). Under certain agricultural riparian zone clearing/brushing techniques, significant amounts of mulch litter is left on the soil surface. In addition to riparian vegetation adding and removing nutrients to and from soil, vegetated riparian zones also have increased capability of attenuating nutrients transported from elsewhere by surface and subsurface waters (Kachenchart et al., 2012). Many of these nutrients will then be taken up by plant and microbiological life (and potentially converted emitted as GHGs, ex. N_2O) (Kachenchart et al., 2012). Due to the often times higher soil moisture content of riparian soils,

there is also greater carbon sequestration and a larger carbon pool in these areas (Gunderson et al., 2010).

Riparian vegetation is a tertiary control on GHG behaviour in soils. Vegetation type and presence influences the soil temperature, moisture content, and physical and chemical parameters. These secondary characteristics then control the biogeochemical reactions producing/consuming GHGs, and the soil gas transport/efflux.

1.4 CONTROLS ON SOIL GAS PRODUCTION, CONSUMPTION, AND TRANSPORT

1.4.1 Moisture Content:

With availability of O_2 in soil being necessary for many of the biogeochemical processes controlling GHG fluxes, soil moisture content plays an important role in controlling gas transport processes and therefore the rate and extent of reactions, as increasing soil moisture content will displace O_2 within soil pore space and inhibit gas diffusion (Oertel et al., 2016). Soil water is also beneficial in acting as a transport medium for reactants necessary to microbiological processes, and in preventing microbe water stress (Schindlbacher et al., 2004). Thus, an optimal moisture content range should exist, where there is sufficient soil water to promote reactant transport and allow for soil aeration and diffusion. Nitrification, methanotrophy, and aerobic soil respiration all require O_2 as a reactant. With increasing soil moisture content over a certain threshold, these processes will be inhibited (Oertel et al., 2016; Serano-Silva et al., 2014; Reichstein et al., 2003). Higher production rates by nitrification have been observed with decreasing soil moisture content, with maximum production at approximately 20% water-filled pore space (WFPS) (Oertel et al., 2016). However, with limited O_2, nitrifying bacteria can use NO_2^- as an electron acceptor, reducing it to NO and N_2O (Smith et al., 2018). Methane oxidation by methanotrophs has been observed to decrease with increasing soil moisture content within the range of 20% water holding capacity (WHC) (Jäckel et al., 2001) and 60% WFPS (Khalil & Baggs, 2005). Below 20% WHC, methanotrophy rates have been observed to decrease, and above 60% WFPS, methanogenesis has been observed to be favoured (Serano-Silva et al., 2014; Jäckel et al., 2001; Khalil & Baggs, 2005). Optimum moisture content for CO_2 emissions/production in general (including soil and root respiration) have been found to range between 20 and 60% WFPS depending on soil and vegetation types, where a cropland will show highest CO_2 emissions at 20% WFPS, a forested site at 40% WFPS, and a wetland at 60% WFPS (Schaufler et al., 2010; Smith et al., 2018).

The role of soil moisture in displacing soil O_2 results in a positive correlation between soil moisture content and soil anaerobic microbiological processes such as methanogenesis and denitrification where NO_3^- and CO_2 have the potential to act as electron acceptors in place of O_2 (Brewer et al., 2018; Smith et al., 2018). N_2O produced by denitrification is more likely to be further reduced to N_2 by denitrifying bacteria if it encounters a saturated, O_2 lacking soil on its emission path (Smith et al., 2018). With unsaturated soil above its place of production, it is less likely to be further reduced, and thus emitted as N_2O. As CO_2 is not as readily available to be reduced compared to NO_3^-, methanogenesis requires longer times under anaerobic conditions to be established (more reduced conditions) (Smith et al., 2018; Oertel et al., 2016).

Methanogenesis has been observed to be 60% more likely at 65% WFPS or higher, reaching maximum rates around 75% WFPS (Brewer et al., 2018). Much like the products of denitrification, the products of methanogenesis can be transported from anaerobic microsites to areas in the soil with greater O_2 content, and can be subject to aerobic processes (where CH_4 produced by methanogenesis can be oxidized to CO_2 via methanotrophy) (Brewer et al., 2018).

1.4.2 Temperature:

Temperature plays an important role in GHG emissions, as it influences the biogeochemical processes producing and consuming GHGs, such as microbial metabolism and plant activity (Schaufler et al., 2010; Oertel et al., 2016). Higher temperatures generally increase microbial metabolism, resulting in higher rates of production from microbially mediated reactions (Smith et al., 2018; Oertel et al., 2016). The relationship between the biologic process rate and the temperature is often described using Q_{10}, quantifying the rate of increase in a biological process for a 10^{o}C change in temperature (Fang et al., 2006). Soil respiration rates will generally increase exponentially with increasing temperatures between 10 and 30°C, where observed Q_{10} values have been around 2.4, as long as water content and soil physical parameters are not limiting (Oertel et al., 2016; Shabaga et al., 2015). Root and heterotrophic portions of soil respiration will react differently to changes in temperature, where root respiration has been observed to be more sensitive (Shabaga et al., 2015; Boone et al., 1998). Rhizosphere respiration in a mixed temperate forest has been observed with a Q_{10} of 4.6, heterotrophic respiration in the same system with a Q_{10} of 2.5, and bulk soil respiration with a Q_{10} of 3.5 (Boone et al., 1998). Heterotrophic respiration slows as temperatures cool below freezing with the absence of free water, but has still been observed at temperatures as low as -7°C (Oertel et al., 2016; Panikov et al., 2006). Temperature is also an important control on methane oxidation, where the reaction rate increases with temperature with observed Q_{10} values of near 1.4 (Smith et al., 2018; Schaufler et al., 2010; Whalen & Reeburgh, 1996). Increasing temperature will also prompt CO_2 to degas from soil water (Lloyd & Taylor, 1994).

With higher soil respiration and methanotrophy rates associated with increased soil temperature, depletion/consumption of O_2 can be accelerated and force the onset of methanogenesis and denitrification (Oertel et al., 2016). Denitrification rates increase with increasing temperature with Q_{10} values having been observed to range between 1.7 and 9.3 within various soils, with a Q_{10} of around 8 when soil moisture and N availability are non-constraining (Abdallah et al., 2009).

Under anaerobic conditions, more readily available electron acceptors must be depleted before methanogenesis can commence (van Hulzen et al., 1999). Therefore, methanogenesis depends on temperature, as increasing temperatures increase the rate of C mineralization, then increase rates of depletion of more readily available electron acceptors, subsequently increasing rates of methanogenesis (van Hulzen et al., 1999). Each of these stages have been observed to have Q_{10} values of 1.1-2, and the overall Q_{10} value considering all stages together (mineralization, depletion of electron acceptors, methanogenesis) has been observed in experiment to be 2.9-3.6 (van Hulzen et al., 1999).

Freeze-thaw events are related to significant GHG emissions (Groffman et al., 2006; Holst et al., 2008; Groffman et al., 2009). These freeze-thaw events are common in the spring and fall, where they influence several microbial and physical properties in the soil. Freezing will redistribute the water content in the soil and force changes in the soil structure, potentially concentrating nutrients in certain areas as well as making available previously inaccessible nutrients and promoting microbial activity (Holst et al., 2008; Groffman et al., 2006; Groffman et al., 2009). Freezing temperatures may limit plant activity and uptake of nutrients, leaving these nutrients to be used by soil microbes (Groffman et al., 2006). Non frost resistant roots and microbes can be killed, leaving an excess of nutrients for biologic processes upon thawing (Groffman et al., 2006; Holst et al., 2008; Groffman et al., 2009). These freeze thaw processes have shown particular significance for N_2O emissions in temperate grasslands and forests, where freeze-thaw related N_2O emissions sometimes account for 50% of the annual budget (Groffman et al., 2009).

1.4.3 Nutrient Availability:

These GHG controlling microbiological reactions require nutrients in the forms of C and N (Oertel et al., 2016). These nutrients are naturally present and cycled in the soil, but are often added via application of fertilizer or manure in agricultural contexts (Oertel et al., 2016). N availability is considered a significant controlling factor for denitrification and nitrification, where a decreasing C/N ratio generally promotes increasing denitrification/nitrification rates and N_2O/NO emissions (Pilegaard et al., 2006). With sufficient N availability at C/N ratios less than 15-20, other environmental factors such as moisture and temperature gain more importance in controlling N_2O emissions (Pilegaard et al., 2006). At C/N ratios greater than 30, denitrification rates and N_2O emissions have been observed to decrease (Pilegaard et al., 2006).

CO_2 and CH_4 emissions chiefly via soil respiration and methanogenesis will tend to increase as the C/N ratio increases (Oertel et al., 2016). Under anoxic conditions, higher N contents in the soil may decrease rates of, or prevent methanogenesis by increasing the redox potential of the soil (providing other, more readily available electron acceptors) and promoting N_2O/N_2 emissions (Serrano-Silva et al., 2014). With sufficient C available, increasing N content can lead to increased rates of soil respiration with greater sensitivity to soil moisture content, and a lesser sensitivity to soil temperature (Peng et al., 2010).

1.4.4 Soil Structure:

Soil structure (porosity, permeability, and bulk density) plays a role in controlling fluid transport, and thus the availability of reactants for GHG producing/consuming biological processes as well as the emission of their products (Oertel et al., 2016; Li et al., 2017). With greater permeability, aeration and replenishment of the soil with atmospheric gases will be promoted (Brassard et al., 2016). With increased porosity and variability of pore sizes, more habitat will be provided, and microorganism growth will be promoted (Li et al., 2017). Increased porosity will also increase water holding capacity of the soil, stabilizing changes in soil water content and making transitions from aerobic to anaerobic conditions less frequent (Brassard et al., 2016). For these reasons, soils with greater porosity and permeability along with associated aeration and water holding capacity will promote aerobic biologic processes such as

methanotrophy, nitrification, and respiration rather than anaerobic processes such as methanogenesis and denitrification (Li et al., 2017; Brassard et al., 2016).

1.5 TEMPORAL TRENDS IN SOIL GAS PRODUCTION, CONSUMPTION, TRANSPORT, AND EMISSIONS

The biological processes described which control GHG behaviour all depend on temporally variable soil and environmental parameters. Soil moisture and temperature will vary on diurnal to seasonal timescales, causing temporal variations in the GHG controlling biological processes and thus temporal variations in GHG soil concentrations and emissions (Vidon et al., 2015; Jacinthe et al., 2015; Parkin, T. B., 1987; Jarecke et al., 2016; McClain et al., 2003; Subke et al., 2018).

1.5.1 Long-Term Trends:

Seasonal trends in moisture content (and oxygen availability) and temperature have been observed to influence soil GHG production, consumption, and transport. There exist consistent observations of increased CH_4 emissions (or decreased CH_4 uptake) during the wet winter and autumn periods in temperate forest soils (Gukland et al., 2009; Christiansen et al., 2012; Baah-Acheamfour et al., 2016). CH_4 fluxes in a temperate forest in central Ontario, Canada showed uptake rates increasing with decreasing moisture content from June to September (Wang et al., 2013). This agrees with numerous studies demonstrating increased soil respiration rates (and CO_2 emissions) in the summer (with higher temperatures and lower soil moisture content) compared to the colder and wetter months (Almagro et al., 2009; De Carlo et al., 2019; Amadi et al., 2016; Wang et al., 2021). In some cases, soil desiccation during summer droughts can limit the soil respiration process, where precipitation events would trigger a rapid rebound of respiration rates (Almagro et al., 2009; Vidon et al., 2014).

Several studies of temperate and agriculturally adjacent environments have observed the lack of significant seasonal trends in N_2O emissions (Christiansen et al., 2012; Amadi et al., 2016; Du et al., 2006; Ying et al., 2009; Vidon et al., 2014). Commonly, N_2O emissions are observed to be more sensitive to specific events rather than seasonal changes in soil moisture and temperature, where spring thaw, or significant precipitation events, for example, provoke elevated N_2O emissions (Amadi et al., 2016; Lemke et al., 1998). However, seasonal trends are still observed in some cases, where largest N_2O emissions can be seen during warm summer months (Baah-Acheamfour et al., 2016; Morishita et al., 2007). Although soils normally behave as net N_2O sources, winter has been observed to bring on negative surface N_2O fluxes in some cases (Du et al., 2006). In tropical environments, nitrification rates have been observed to be higher during the dry season, while denitrification rates and N_2O emissions are greatest during the wet season/periods (Kachenchart et al., 2012).

1.5.2 Short-Term Trends:

A significant portion of the studies examining seasonal trends in GHG emissions from soil use surface chambers that are sampled at intervals that vary from weekly to monthly (Gukland et al., 2009; Christiansen et al., 2012; Baah-Acheamfour et al., 2016; Almagro et al., 2009; De Carlo et al., 2019; Amadi et al., 2016; Ying et al., 2009; Lemke et al., 1998; Morishita

et al., 2007; Kachenchart et al., 2012). These studies provide general understanding of sub-annual changes in soil gas surface fluxes by interpolation and the assumption that these changes are relatively constant between sampling. However, studies have shown that GHG emissions that occur over only a few days, or only within a small area can drastically alter the total flux results for the entire study period (Vidon et al., 2015). These periods or areas of increased GHG emission are deemed "hotspots" or "hot moments", usually brought on during relatively rapid changes in soil hydrology, and these rapid changes are often enhanced in riparian zones (Parkin, T. B., 1987; Vidon et al., 2015; Jacinthe et al., 2015; Jarecke et al., 2016; McClain et al., 2003).

A study of surface GHG emissions from a riparian buffer zone in Indiana included roughly 170 surface flux measurements over the course of a year and a half (Jacinthe et al., 2015). One of these measurements was recorded after a significant precipitation event within a topographic depression, and the inclusion or exclusion of its CH_4 emission value from the mean annual CH_4 flux determines whether the soil behaved overall as a source or a sink (Jacinthe et al., 2015). Other studies have observed similar hot moments, where CH_4 uptake rates decreased after rain events and elevated soil moisture levels, followed by CH_4 uptake rates increasing gradually upon soil moisture decrease (Subke et al., 2018). Another study of GHG emissions from a riparian buffer zone in North Carolina sampled several surface flux chambers 6 times over the course of a 4 day period (Vidon et al., 2015). From this, they discovered that short term variations in GHG flux over relatively constant soil temperature and moisture can be of similar magnitude to spatial variations in GHG fluxes (Vidon et al., 2015). A study at a rehabilitated riparian zone in Ohio examined the relationships between soil O_2 and soil GHG concentrations and surface emissions over relatively short time frames (Jarecke et al., 2016). This study highlighted rapid intake of atmospheric O_2 following soil water drainage after elevated moisture contents and depleted O_2 concentrations (Jarecke et al., 2016). In this study, greater O_2 depletion correlated with greater CO_2 and N_2O soil concentrations and surface fluxes, and upon O_2 recharge with drainage, CO_2 soil concentration and surface fluxes decreased with these changes occurring within <48 hours (Jarecke et al., 2016). However, correlation was not observed between O_2 concentrations and N_2O or CH_4 emissions (Jarecke et al., 2016). By examining O_2 in relation to soil GHGs, the mechanisms driving hotspots and hot moments can be better understood (Jarecke et al., 2016). With N_2O emissions chiefly being related to specific events (precipitation, freeze-thaw, fertilizer application), often times a significant proportion of N_2O emissions can be attributed to hotspots and hot moments (Groffman et al., 2009; Amadi et al., 2016; Lemke et al., 1998).

As well as hotspots and hot moments, regular daily variations in GHG behaviour exist. A study analyzing soil CO_2 concentration profiles every 2 hours over the course of 3 years in a grassland in central Switzerland observed diurnal correlations between CO_2 concentration and temperature, dependent on moisture content (Flechard et al., 2007). During wet periods, CO_2 concentrations were highest in the late afternoon, and lowest in the early morning, positively correlated with soil temperature (Flechard et al., 2007). During dry periods, CO_2 concentrations were highest in the early morning, and lowest in the late afternoon, inversely correlated with soil temperature (Flechard et al., 2007). Similarly, in a temperate coniferous forest, CO_2 emissions were lowest midday, and peaked around 20:00 (Subke et al., 2018). Diurnal hysteresis has been

observed between out of phase soil CO_2 concentration and soil temperature, dependent on soil water content (Riveros-Iregui et al., 2007). Photosynthetically active radiation (PAR) reaches a maximum earlier in the day than temperature (Riveros-Iregui et al., 2007). As autotrophic respiration responds to PAR, and heterotrophic respiration responds to soil temperature, hysteresis is developed between CO_2 concentration and temperature (Riveros-Iregui et al., 2007). This hysteresis is most pronounced in wetter seasons where there is an imbalance between CO_2 production and diffusion, and is diminished during dry seasons (Riveros-Iregui et al., 2007).

The variability in results seen in the studies on short-term GHG behaviour in soil shows that there is value in site specific, high time resolution field data collection. Paired soil GHG and soil physical parameter data at high time resolutions will build on our understanding of the environmental conditions under which soil is a net source or a net sink. It is crucial to understand these processes at the sub-daily temporal level in order to accurately represent GHG behaviour at larger temporal and spatial scales, and to make accurate climactic predictions and soil management recommendations.

Studies examining GHG emissions from soil will often focus on surface fluxes (Gukland et al., 2009; De Carlo et al., 2019; Christiansen et al., 2012; Baah-Acheamfour et al., 2016; Amadi et al., 2016; Morishita et al., 2007; Ying et al., 2009; Kachenchart et al., 2012; Vidon et al., 2015), on one GHG of interest (Gukland et al., 2009; Almagro et al., 2009; De Carlo et al., 2019; Lemke et al., 1998; Du et al., 2006; Riveros-Iregui et al., 2007; Flechard et al., 2007), and on seasonal trends, sampling at intervals spanning from weekly to bimonthly (Gukland et al., 2009; Almagro et al., 2009; De Carlo et al., 2019; Christiansen et al., 2012; Baah-Acheamfour et al., 2016; Amadi et al,. 2016; Lemke et al., 1998; Morishita et al., 2007; Ying et al., 2009; Kachenchart et al., 2012). With evidence of hot moments significantly influencing a soil's net flux (Vidon et al., 2015; Jacinthe et al., 2015), and evidence of regular diurnal variations in flux (Riveros-Iregui et al., 2007; Dong et al., 2000; Flechard et al., 2007), there is a need for high time resolution sampling in order to capture GHG variations at all temporal scales. With few studies examining soil gas concentration profiles along with surface emissions, transport processes are assumed, and the correlation between soil gas production, consumption, transport, and surface emissions in field studies is often overlooked.

1.6 PURPOSE

Continuous soil gas concentration profile and surface flux data of N_2O, CO_2, CH_4, and O_2 along with soil moisture, temperature, atmospheric pressure, and precipitation data were collected at a high time resolution (on average, every four hours) over the entire agronomic season. This information was paired with physical soil data, including particle size distribution and porosity. By collecting data from this array of parameters at this time resolution, we aim to gain insight into how regular and irregular short-term processes play a role in overall soil GHG surface fluxes, how these processes and emissions vary between the shoulder and bank microenvironments of an arborous riparian zone, and how the roles and importance of soil gas controlling parameters vary throughout the agronomic season. By examining surface fluxes as well as subsurface gas concentrations of multiple GHGs along with O_2, valuable information can be gained pertinent to soil gas production, consumption, and transport, and how these gases and their controlling processes interact and influence one another. With concurrent high time resolution monitoring of these parameters over an agronomic season, comparisons can be made between the efficacy of different time resolution sampling programs, and the validity of lower time resolution sampling can be assessed. By studying these processes in CTD managed agricultural riparian zones specifically, more accurate predictions for GHG emissions from agriculture can be pursued, and better recommendations for agricultural ditch management practices can be made in the future.

2 SITE DESCRIPTION

Field observations were collected from privately owned agricultural land located in Embrun, Southeastern Ontario, within the South Nation Watershed (fig. 1). This agricultural land has been subject to several Agriculture and Agri-Food Canada (AAFC) investigations since 2004, first as part of the "Watershed Evaluation of Beneficial Management Practices" (WEBs) program, and, beginning in 2013, as part of the Agriculture Greenhouse Gases Program (AGGP). During the AGGP program, agricultural fields and their adjacent riparian zones were studied and compared based on their riparian vegetation, ditch management/intervention, and drainage management system. The general area is underlain by the poorly drained (slope of <1%) Bainsville soil series (composed of a succession of marine sediment derived clay and silty sands) (Wicklund & Richards, 1962; Government of Canada, 2013).

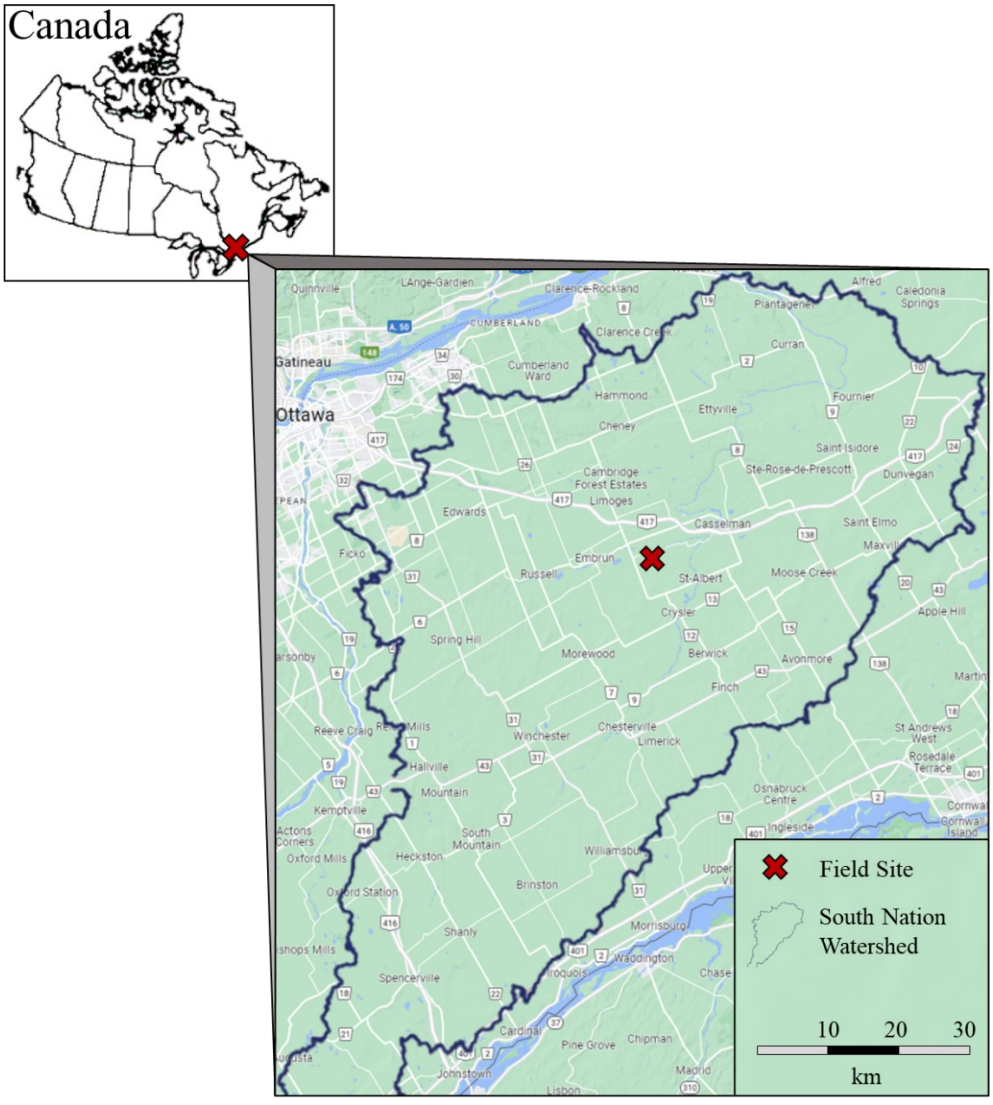

Figure 1: South Nation Watershed (outlined in blue), and the location of the field site (background image from Google Maps).

This specific field study was performed on the northern side of the old growth forested control site (WEBs site 11) riparian zone. The vegetation is dominated by tall trees, with an understory composed of shrubs and grasses (fig. 2). Foliage progresses to its densest by late May (fig. 2 A, B), through June, July, and August (fig. 2 C), before trees begin to shed their leaves through September and October (fig 2 D, E). Between October 18th and October 29th 2022, the south side of the drainage ditch was completely cleared of vegetation, and the vegetation on the north side was thinned (fig. 2 F). As a result, the soil was left overlain by roughly 5-10 cm of woody mulch. The ditch is typically dry throughout the summer and fall, but water depths reached roughly 30 cm in early May and November (fig. 2 A, F). Drainage from this site is managed by a CTD system. During the agronomic season of 2021, forage/hay (including clover and alfalfa) was the main crop being harvested on the field of WEBs site 11. In 2020, soy and forage were grown in rotation. Sampling was focused at two locations within this riparian zone: the shoulder and the bank. The shoulder is located 1 metre from the edge of the agricultural field, where the riparian vegetation begins. The bank is located 4.5 metres from the edge of the field, downslope (0.45 metres lower in elevation than the field), and 2.0 metres from the centre of the drainage ditch (fig. 3). There is greater tree canopy coverage at the bank location.

Both the shoulder and bank soils can be described as humic gleysols with thick topsoil layers and deeper gleyed layers (fig. 4 A, B). However, as a result of differences in elevation, vegetation, and disturbance (where the bank was disturbed in the construction of the drainage ditch), there are differences in the soil profiles and physical properties between the shoulder and bank. The topsoil reached 22 cm depth at the shoulder, and 17 cm at bank. There are thinner and more numerous roots at the bank, resulting in a higher root density (focused from 20 to 55 cm depth) compared to the shoulder, where fewer and thicker roots exist. Both locations have a clay rich horizon. This horizon exists from 22-35 cm depth at the shoulder (directly below the topsoil), and from 55-65 cm depth at the bank (table 1). Overall, the shoulder location has higher porosity, and a larger proportion of silt and clay sized sediment compared to the bank (table 1).

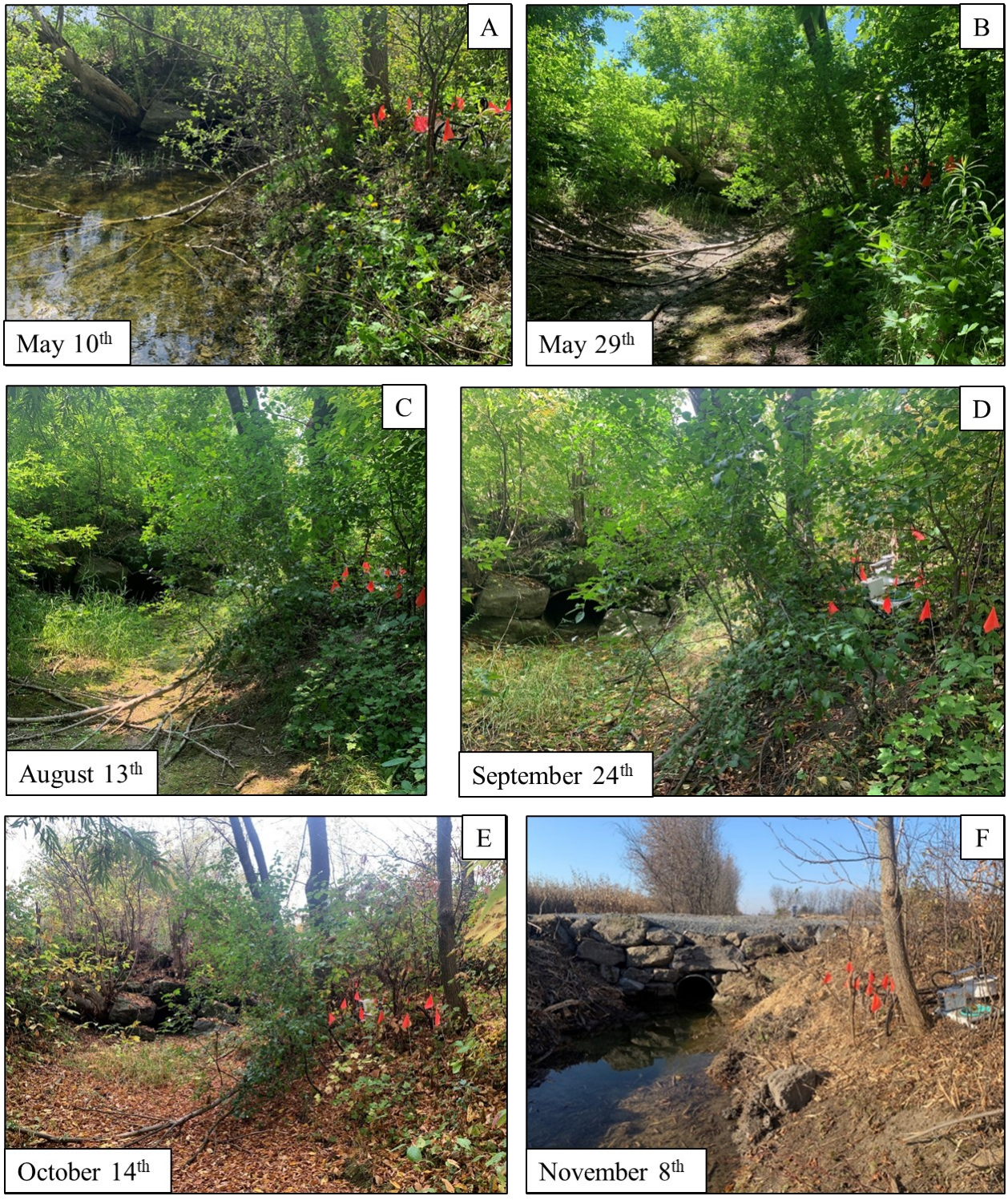

Figure 2: Site 11 throughout the study period (May-November). Bank sample points shown on the right (North) slope, marked with orange flags

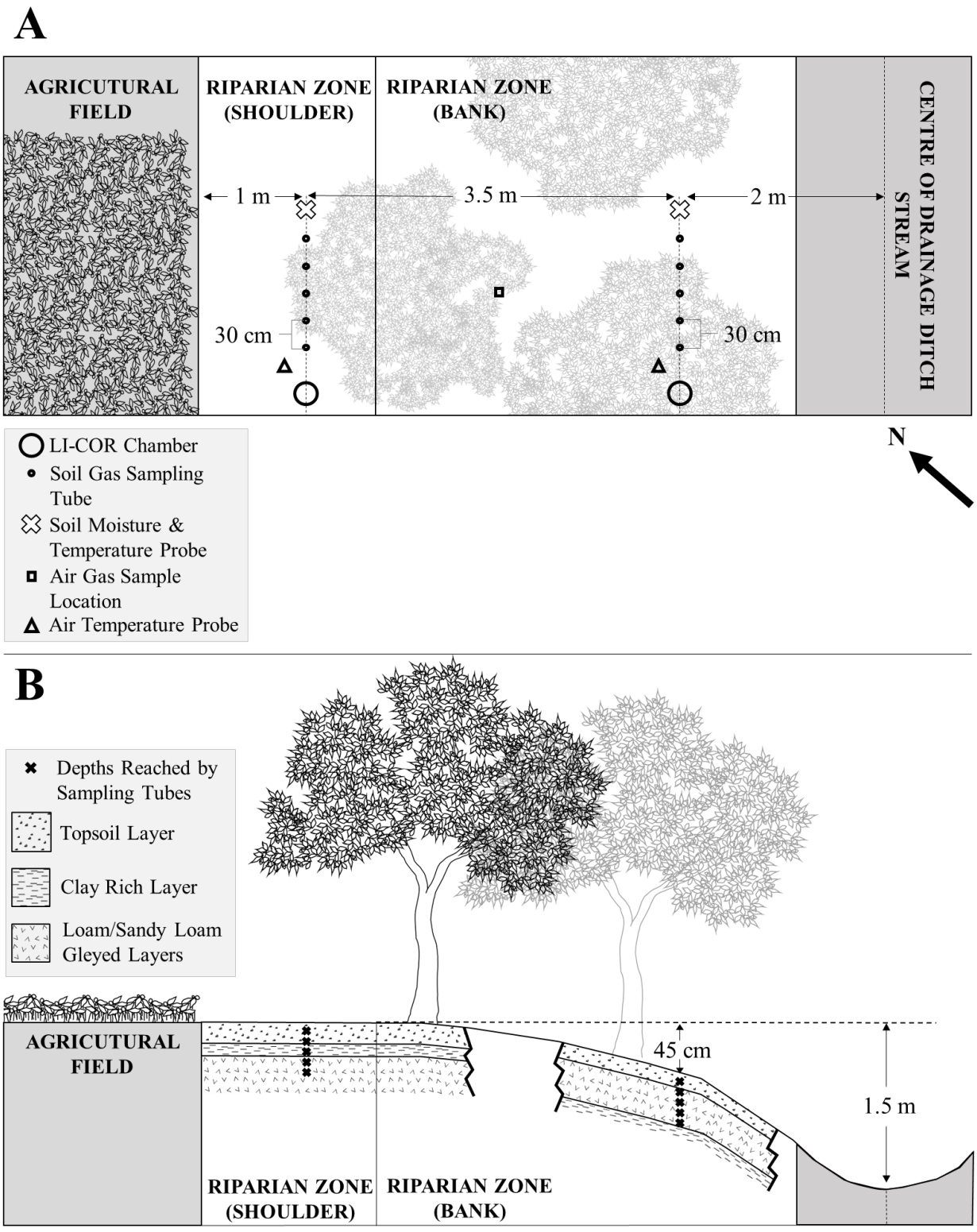

Figure 3: A) Plan view schematic of sampling equipment and its position in the riparian zone relative to the agricultural field. B) Cross-section schematic of sampling equipment and sampling point positions relative with depth in the soil profile.

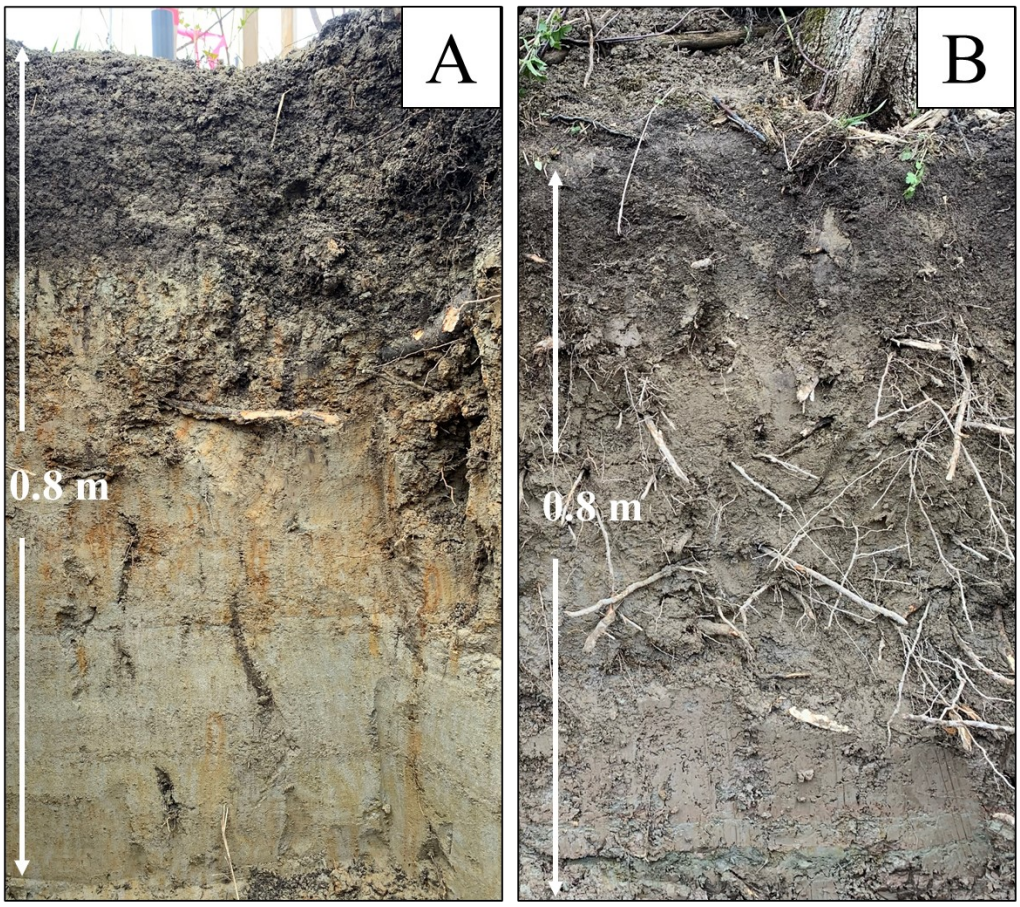

Figure 4: A) Shoulder soil profile. B) Bank soil profile

Location	Depth Range (cm)	% Sand	% Silt	% Clay	Texture	Porosity
Shoulder	0-22	25.7	48.3	26	Loam	60.59
	22-35	5.2	62.9	31.9	Silty clay loam	39.44
	35-45	45	42.3	12.7	Loam	41.82
	45-55	37.1	46.1	16.8	Loam	42.94
	44-65	73.9	17.9	8.1	Sandy loam	43.40
Bank	0-17	30.1	45.7	24.2	Loam	50.08
	17-25	45.8	36.7	17.5	Loam	38.48
	25-35	66.6	22.5	10.8	Sandy loam	40.53
	35-45	66.5	22.9	10.6	Sandy loam	36.73
	45-55	59.5	25.6	14.9	Sandy loam	37.52
	55-65	7.8	35.1	57.1	Clay	51.12

Table 1: Particle size distribution, texture classification, and porosities of soils from 0-65 cm depth at both the shoulder and bank locations.

3 METHODS

3.1 EXPERIMENTAL DESIGN:

High temporal resolution soil gas concentrations, as well as soil gas surface flux data were collected along with high resolution soil temperature, soil moisture content, and air temperature data from the riparian zone adjacent to WEBs site 11 from May 7th until November 25th, 2021. From October 18th until November 1st, the sampling system was temporarily uninstalled while ditch management took place. During this period, the south side of the drainage ditch was cleared of vegetation, the vegetation on the north side was thinned, and a new culvert was installed (fig. 2 F). The automated gas sampling system, housed within a closed utility trailer, collected soil gas samples from the drainage ditch shoulder and bank, from depths ranging from 10 to 50 cm, as well as surface flux samples, where each sample was analyzed in the field for CH_4, CO_2, N_2O, and O_2. A time resolution of 4 hours between sample cycles was generally achieved, with a total of over 24,500 gas samples collected and analysed.

Two rows of five ¼" diameter, stainless steel sampling tubes were installed for collection of subsurface soil gas samples. One row was located on the shoulder (1 m from the edge of the field) on the north side of the riparian zone. The other row was located on the northern bank/slope of the riparian zone, 4.5 m from the edge of the field, and 2 m from the centre of the drainage ditch (fig. 3). In each row, the tubes, spaced 30 cm apart, reached depths of 10, 20, 30, 40, and 50 cm. A LI-COR 8100-104 Opaque Long-Term Chamber was installed adjacent to each row of sampling tubes on 10 cm diameter PVC collars and embedded 10 cm into the soil to measure soil gas surface fluxes. The chamber systems covered a soil surface area of 317.8 cm^2 and have a total chamber volume of 4076.1 cm^3 (LICOR Environmental, 2022).

Samples were drawn from the sampling tubes and chambers through 1/8" ID LDPE tubing and a hydrophobic filter (GENIE 120) by a diaphragm pump (Parker model # A.1F17N1.G12VDC). Sample selection through a series of solenoid valves (STC Valve model # 3V1-1/8), and pump timing, were controlled by a Campbell Scientific CR1000 datalogger (fig. 5). Based on the volume of tubing associated with each sample path, a pump time was determined that would draw the least amount of gas required to purge the volume of tubing and minimize disturbances to the natural soil gas system, while providing a sufficient volume of gas to acquire quality data representing gas concentrations at a specific moment in time. With tubing lengths ranging from 7.40 m to 11.32 m, and a pump rate of 462.5 mL/min, pump times ranged from 45 to 60 seconds. The datalogger program would prompt the sampling and analysis of first the shoulder sampling tubes (10 through 50 cm), followed by the bank sampling tubes (10 through 50 cm), before 5 shoulder chamber samples and 5 bank chamber samples. A closed loop existed within the chamber sampling paths, where, while purging the lines and gas chromatograph (GC) sample loop, the sample would be recirculated back into the chamber to maintain natural flux behaviour/chamber concentrations over time, following an automated closed dynamic chamber method (Rochette et al., 1997, Oertel et al., 2016). After the chamber samples, an air sample as well as two calibration samples would be analysed, completing one sampling cycle. The air sample tube was located midway between the shoulder and bank sampling rows and was suspended 20 cm above the soil surface. The first calibration gas was

composed of 5% CO_2, 10 ppm CH_4, 10 ppm N_2O, and 94.998% N_2, and the second calibration gas was composed of 3% CO_2, 0.1 ppm CH_4, 0.1 ppm N_2O, and 96.99998% N_2.

Soil gas samples were directed to an SRI 860C GC. CO_2, CH_4 and N_2O were separated on two 2-metre long, 1/8" outer diameter, Hayesep-D packed coil columns and directed to a Flame Ionization Detector (FID; CO_2 and CH_4) and an electron capture detector (ECD; N2O). O_2 was separated with a 2.4 m long ArgoTek packed coil column, and analysed on a Thermal Conductivity Detector (TCD). Results were analyzed using SRI PeakSimple chromatography software.

Soil temperature and moisture content were measured with two 6 segment GroPoint Profile probes. Each was installed in-line with, and 30 cm from, a gas sampling equipment row (one on the shoulder, the other on the bank) (fig. 3). These probes reached depths of 90 cm, with six moisture reading locations, each representing the volumetric water content over a specific depth range (0-15, 16-30, 31-45, 46-60, 61-75, and 76-90 cm). Temperature readings were from the four specific depths of 15, 30, 60, and 75 cm. Moisture and temperature data was collected from the shoulder and bank simultaneously every 10 minutes, controlled and stored by a GroPoint Bluetooth datalogger.

Air temperature was measured next to the gas chambers beginning on July 1st on both the shoulder and bank by Campbell Scientific 109-L Air Temperature Sensors suspended 10 cm from the soil surface (fig. 3). Connected directly to the Campbell Scientific CR1000 datalogger, air temperature from both the shoulder and the bank was recorded every 10 minutes. Precipitation and barometric pressure data was collected every 15 minutes by a rain gauge and a DigiBP SDI-12 barometric pressure sensor as part of a fixed all weather Forest Technology System (FTS) located roughly 2 km east of the study site.

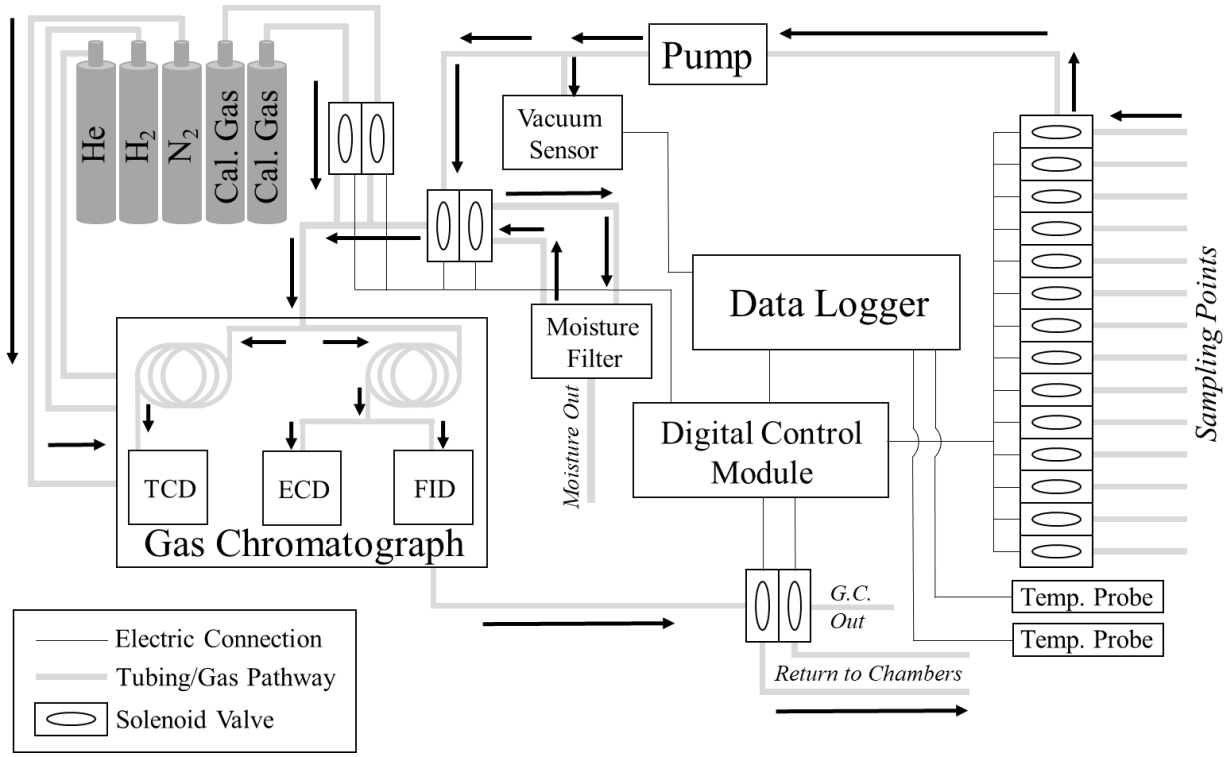

Figure 5: Schematic showing electrical and gas flow organization of automated sampling system. "Cal. Gas" gas cylinders represent calibrations gases.

3.2 SURFACE FLUX CALCULATIONS:

With five gas samples collected at 10-minute intervals from the LI-COR chambers, CH_4, CO_2, N_2O, and O_2 surface fluxes were calculated based on changing concentration over time within the chamber using the equation (derived from Rochette & Hutchinson (2005)):

$$F_{sur,i} = \frac{\partial c}{\partial t} \times \frac{V}{A} \times M_{mi}/V_m \qquad (11)$$

where $F_{sur,i}$ represents the mass flux of analyte i in g m^{-2} s^{-1}, and is determined based on the change in concentration of i over time ($\frac{\partial c}{\partial t}$), the volume of the chamber headspace (V), the surface area of soil exposed to the closed chamber (A), the molecular mass of gas i (M_{mi}), and the molecular volume of air (V_m) at specific and variable chamber temperature and barometric pressure. A positive $F_{sur,i}$ value represents transport from the soil to the atmosphere (upward), while a negative $F_{sur,i}$ value represents transport from the atmosphere into the soil (downward). The temperature used to determine the molecular volume was the air temperature associated with the first of the five chamber samples in a cycle, although the temperature generally varied by less than 1°C over a chamber sample cycle.

3.3 SOIL SAMPLES:

On May 4th, 2022, soil pits were dug, exposing soil profiles along the transects (shoulder and bank) on which the soil-gas sampling tubes were installed in 2021. Brass cores with a volume of 90 cm^3 were tamped horizontally into the soil profiles at depth ranges of 0-22, 22-35, 35-45, 45-55, and 55-65 cm on the shoulder, and depth ranges of 0-17, 17-25, 25-35, 35-45, 45-55, and 55-65 cm on the bank. These depth ranges were chosen as to avoid sampling from soil horizon boundaries, and to include the soil-gas sampling depths. The samples were oven dried at 105ºC for 24 hours and weighed. With the dry mass (m) and the volume (V) known, the dry bulk density was determined (equation):

$$Bulk\ Density = \frac{m}{V} \tag{16}$$

Assuming a particle density of 2.65 g/cm^3, the porosity of each sample was calculated (equation):

$$\varphi = \left(1 - (Bulk\ Density - Particle\ Density)\right) * 100 \tag{17}$$

3.4 STATSTICAL ANALYSIS:

Wavelet analyses were performed on the subsurface gas concentration and surface gas flux data using the 'WaveletComp' R package (Rosch & Schmidbauer, 2018). In wavelet analysis, similar to Fourier analysis, harmonic components are compared to the time series in question, and the magnitude of the contribution of these harmonic components to the observed data is quantified (Cazelles et al., 2008). In Fourier analysis, these harmonic components are pure sine or cosine waves with constant amplitudes and periods, and thus when comparing these constant harmonic components to the time series, the comparison results in a function that is not temporally specific (Cazelles et al., 2008). In this wavelet analysis, the time series in question was compared to pure sine or cosine waves multiplied by Gaussian functions (the product of which are Morlet wavelets) (Rosch & Schmidbauer, 2018; Cazelles et al., 2008). Morlet wavelets, when compared to a time series, will then provide temporal specificity as their amplitude and period taper towards zero, useful for non-stationary time series such as the ones collected in this experiment (Cazelles et al., 2008).

In order to use Morlet wavelets (temporally specific) to analyze an entire time series, a "mother" Morlet wavelet is defined and translated through time (t) by a factor of the time parameter (τ), and scaled by a factor s, generating a set of Morlet wavelet "daughters" (Rosch & Schmidbauer, 2018). In the 'WaveletComp' R package, the "mother" wavelet ($\psi(t)$) is defined as (Rosch & Schmidbauer, 2018),:

$$\psi(t) = \pi^{-1/4} e^{i\omega t} e^{-t^2/2} \tag{18}$$

where ω (the angular frequency) is 6 (as is often used in literature) (Rosch & Schmidbauer, 2018). In this Morlet wavelet analysis, the "comparison" between harmonic components and the time series ($x(t)$) is done by convoluting a time series by this set of "daughter" Morlet wavelets according to the following equation (Rosch & Schmidbauer, 2018),:

$$Wave(\tau, s) = \sum_t x_t \frac{1}{\sqrt{s}} \psi^*(\frac{t-\tau}{s}) \quad (19)$$

where * represents the complex conjugate (Rosch & Schmidbauer, 2018).

The varying amplitude of the resulting function over time is squared (and deemed the "power"), and is represented in the wavelet plots (Rosch & Schmidbauer, 2018),:

$$Power(\tau, s) = \frac{1}{s} \cdot |Wave(\tau, s)|^2 \quad (20)$$

where a higher power level represents a stronger periodic component at a certain moment in time (Rosch & Schmidbauer, 2018). Before plotting, these power levels were raised to a power of 0.5 in order to accentuate the differences in the smaller values. Significance of power levels were represented by calculated p-values of 0.05, the null hypothesis being that there is no periodicity (Rosch & Schmidbauer, 2018).

Data was collected for only a segment of the year with varying time intervals between samples (although relatively consistent), and thus the time series were detrended and linearly interpolated before wavelet analysis, as this analysis requires equidistant sampling times, and to focus on periodicity within the time period of the experiment. The time series were detrended only at the scale of the entire study period, as to not remove any natural seasonality within this span. Data collected at 4-hour intervals was linearly interpolated to every hour to ensure equidistant data, and to account for short periods of time where the sampling system required maintenance.

4 RESULTS:

4.1 TEMPERATURE:

Over the study period, the air temperature (shown at depth = 0 cm) measured just above the soil's surface ranged from -9.5°C in the early morning of November 24th to 31°C in the afternoon of August 26th (fig. 6). The range in temperature over time linearly decreased with depth. For example, a temperature range between 8.5°C (November 25th) and 17.7°C (August 29th) was observed at 75 cm depth at the shoulder (fig. 6), compared to a 40.5 °C variation at the surface. Similarly, the air temperature at the bank ranged from -9.3°C in the morning of November 24th to 33°C in the afternoon of August 22nd, and from 9.1°C (November 24th) to 18.5°C (August 29th) at 75 cm depth. (fig. 6). Seasonal trends at both the shoulder and bank show soil temperature at all depths increasing from the beginning of the study period until mid to late August, followed by decreasing temperatures at all depths to their minimum at the end of the study period (fig. 7 C; 8 C). Sub-seasonal trends were also observed. During the overall temperature increase from June to September, temperatures at all depths would oscillate roughly 2.5 to 5°C over 1-3 week periods at both the shoulder and bank. For example, temperatures increased from August 2nd to August 13th/14th before decreasing to a local minimum on August 17th. This resulted in an overall 6.9°C change at 10 cm depth, and a 3.2°C change at 50 cm depth

at the shoulder, where the trend was delayed 8 hours at 50 cm depth. Diurnal temperature trends are present throughout the study period, similar to the long-term trends in that variation was greatest near the surface and dampened and delayed at depth. For example, at the shoulder location in the month of August, temperatures would typically reach daily maximums between 21:00 and 23:00, and minimums between 09:00 and 11:00, with temperature changes of 1-2°C. These diurnal trends are muted past 20 cm depth.

4.2 PRECIPITATION AND BAROMETRIC PRESSURE:

Over the entire study period, there was a total of 535.54 mm of precipitation (fig. 7 A; 8 A). 5.54 mm of this total was contributed in May, 81.13 mm in June, 125.58 mm in July, 55.23 mm in August, 108.49 mm in September, 109.76 mm in October, and 49.81 mm in November. Large and concentrated precipitation events occurred on July 14th (35.49 mm between 00:00 and 04:00), July 20th (39.59 mm between 20:00 and 23:59), August 29th (29.2 mm between 12:00 and 16:00), September 6th (31.83 mm between 16:00 and 20:00), and September 15th (26.07 mm between 04:00 and 08:00). Large, but less concentrated, precipitation events also occurred, common in the fall. For example, from September 22nd to 24th (total of 25.57 mm), October 2nd to 3rd (37.85 mm), and from October 16th to 17th (total of 21.44 mm). Barometric pressure ranged between a minimum of 98.54 kPa on June 21st, and a maximum of 102.41 kPa on November 20th but showed no obvious seasonal or shorter term trends (fig. 7 D; 8 D).

4.3 SOIL MOISTURE:

Soil volumetric moisture content (VMC) at the shoulder ranged from 58.3% to 17.3%, where similar general temporal trends were observed at all depths. VMC generally increased with depth from 10 to 40 cm, and was often lowest at 50 cm with values continuing to increase past this depth (fig. 6). VMC values were typically similar overall at 10 and 50 cm depth, however with much more short-term variation at shallower depths. For example, throughout the study period, the VMC at 10 cm depth ranged from 17.3% to 52.9%, while the VMC at 50 cm depth ranged from 23.5% to 46.2%. VMC at 20, 30, and 40 cm were relatively similar throughout the majority of the study period, consistently within roughly 5% of each other. This depth distribution of VMC was relatively consistent in the spring and summer (fig. 7 B). In late September, however, the VMC at 10 cm increased to approach values similar to those observed at 20, 30, and 40 cm depths. Following the re-instalment of the sampling system in November, the depth distribution of VMC changed, where there was now a roughly 15% range in VMC between 20, 30, and 40 cm, and VMC at 20 cm was now lower than VMC at 10 cm.

All depths show responsiveness to precipitation events, where there are quick increases in moisture content. In general, the magnitude of the moisture content increase in response to precipitation events decreases with depth. At all depths during the month of August, there was minimal short-term variation due to a lack of precipitation events. As a result of this responsiveness to precipitation, VMC from 10 to 40 cm depths reached local maxima in mid-July and mid-September, with a local minimum at the end of the dry season in August (fig. 7 B).

Soil moisture content at the bank location was generally much lower compared to the shoulder, especially from 10 to 40 cm depth, where values ranged from 0.5% to 31.8% at 10 cm

depth, and from 12.1% to 47.7% at 50 cm depth (fig. 6; 8 B). From May 29th until September 14th, moisture content was consistently highest at 50 cm depth, followed by 20 cm, 30 cm, and 40 cm, in decreasing order, where the moisture content at these depths, over this time period all generally decreased (fig. 6; 8 B). Similar to the shoulder, VMC at 10 cm depth was the most variable, and thus would occasionally show the lowest VMC (during June), or the highest VMC in mid-July. The VMC at 10 cm at the bank increases in the fall (late September/early October), as does the VMC at 10 cm at the shoulder (fig. 8 B). Similar to the shoulder, the depth distribution of VMC drastically changed upon reinstallation of the sampling system. Once reinstalled, VMC increased with depth, and showed a much larger range in VMC values than was observed throughout the rest of the study period (ranged from 2.7% at 10 cm to 26.5% at 50 cm).

Short-term VMC increases were also observed throughout the study period at the bank, mainly in response to precipitation events, and consistently decreasing in magnitude with depth. However, there were much fewer responses of soil VMC to the same number of precipitation events at the bank compared to the shoulder (fig. 8 A, B). Where these responses occurred at the bank, they showed less variation compared to the shoulder. For example, moisture content increased from 14.7% on July 20th at 16:06 to 22.3% on July 20th at 17:56 at 10 cm, and from 14.3% on July 19th at 21:46 to 14.6% on July 20th at 18:06 at 50 cm. In mid-November, a rising water table resulted in a short-term increase in VMC, greater in magnitude with depth, contrary to most other short term VMC increases. VMC increased from 4.1% on November 18th at 06:20 to 7.1% on November 18th at 07:50 at 10 cm depth, and from 28.2% on November 18th at 02:00 to 47.7% on November 18th at 12:20 at 50 cm. At this time, the gas sampling tube reaching 50 cm depth was removed as the soil was saturated. Despite less (and dampened) short-term VMC changes at the bank compared to the shoulder, there were still similar long-term trends at the two locations, where local maxima were reached in mid-July and late September/early October, and a local minimum during the dry period in August.

4.4 SOIL-GAS CONCENTRATIONS:

4.4.1 CO_2:

Overall, at both the shoulder and bank, CO_2 concentrations increased with depth (fig. 6). At the shoulder, the concentrations ranged from 0.24% to 2.83%, where all depths followed the same general long-term concentration trends, although typically to a greater magnitude as depth increases (fig. 6; 7 F). These overall, long-term trends result in a concentration peak centred in mid-July (where concentrations reached 1.45% at 10 cm, and 2.83% at 50 cm on July 14th to 15th), bound by two concentration troughs, the first centred at the end of May (where concentrations of 0.30% at 10 cm, and 1.31% at 50 cm on May 29th-30th), and the second centred at the beginning of September (concentrations reaching 0.24% at 10 cm, and 0.72% at 50 cm on September 2nd to 3rd) (fig. 7 F). Following reinstallation of the sampling system in early November, the previously observed concentration gradient with depth became convoluted, where the CO_2 concentrations were highest at 50 cm, followed by (in descending order); 20, 30, 40, and 10 cm. Within this overall CO_2 concentration trend are short-term concentration changes where concentrations typically vary 0.1-0.3% from the long-term trends at frequencies ranging from 1-

11 days, occurring at the same time at all depths, although often to a greater magnitude at depth. One of these short-term variations showed significantly greater variation, where on September 26th, concentrations varied +0.5% at 10 cm, and +0.9% at 50 cm from the long-term trend over an 11 day period. Within this event are three smaller scale variations, varying 0.2-0.4% at frequencies of 3-4 days.

The CO_2 concentrations at the bank ranged from 0.17% to 2.86%, where concentrations at all depths followed similar long-term trends, and depth specific concentrations varied at greater magnitudes as depth increased (fig. 6; 8 F). These long-term trends resulted in CO_2 concentration highs in early June, late July, and late September, and CO_2 concentration lows in early late-May/early-July, mid-August, and the end of November. Despite larger relative variability, these long-term trends are comparable to those observed at the shoulder, where maximums were also reached in late July (1.56% at 10 cm, and 2.86% at 50 cm) and late September (1.02% at 10 cm, and 2.55% at 50 cm), separated by a minimum in mid-August (0.50% at 10 cm, and 0.76% at 50 cm) (fig. 8 F). After reinstallation in early November, concentrations still increased with depth in general from 10 to 50 cm, with the exception that higher concentrations were recorded at 30 cm compared to 40 cm. The short-term trends occurring within these long-term trends occur at the same time at all depths, often at a greater magnitude at depth, typically varying +/- 0.2-0.5% from the long-term trend at frequencies of 2-10 days. Exceptional short-term events occurred on July 31st (+1% variation over 3 days at 50 cm depth) and September 20th (+0.8% variation over 3 days at 50 cm).

4.4.2 O_2:

O_2 concentrations at the shoulder consistently decreased with depth from the beginning of the study period on May 7th until the sampling equipment was temporarily uninstalled on October 18th (fig. 6; 7 G). Long-term term trends were observed to occur over similar time periods at all depths, although typically to a greater magnitude as depth increases, where O_2 concentrations ranged from atmospheric levels (20.9%) to an overall concentration minimum of 17.52%. These long-term trends result in a concentration peak centred in late-August (where concentrations reach atmospheric concentrations at 10 cm, and 20.75% at 50 cm by September 2nd), bound by two concentration troughs, the first of which is centred in mid-July (where concentrations decline to 20.19% at 10 cm, and 19.00% at 50 cm), and the second of which is centred in early-October (where concentrations decline to 20.18% at 10 cm, and 17.52% at 50 cm) (fig. 7 G). During the period following reinstallation in early November, O_2 concentration did not decrease with depth sequentially, but rather decreased in the following general order; 10 cm, 40 cm, 30 cm, 20 cm, 50 cm. Short-term variations in O_2 concentrations showed less consistency compared to CO_2 trends, especially at shallow depths. Similar to long-term trends, the magnitude of these short-term variations increased with depth, where concentrations typically vary +/- 0.2-0.6% at frequencies of 2-8 days. However, from the beginning of September until October 18th, these short-term negative variations increase in magnitude over time, especially at 50 cm depth. Increasing deviations from the long-term trend of -1.4%, -1.75%, -2.25%, and -2.0% were recorded on September 9th, September 18th, September 21st, and October 12th.

O_2 concentrations at the bank also decreased with depth throughout the majority of the study period and ranged from atmospheric levels to an overall minimum of 16.80% at 50 cm depth on October 12th (fig. 6; 8 G). Long-term concentration change events were much greater in magnitude at greater depths. The resulting overall O_2 concentration trend is comparable to that observed at the shoulder, however, with greater variation due to short-term trends. There is a long-term peak centred in early August (where concentrations reach atmospheric concentrations at 10 cm and 50 cm on August 12th) bound by a trough centred in late July (where concentrations declined to 20.18% at 10 cm on July 21st, and to 18.66% at 50 cm on July 22nd) and by a trough centred in early October (where concentrations declined to 20.32% at 10 cm and 16.80% at 50 cm on October 12th) (fig. 8 G). As at the shoulder location, the O_2 concentrations at the bank show short-term variations during these long-term trends. These short-term variations typically vary +/- 0.2-0.4% at frequencies of 2-5 days, occurring at a greater magnitude with depth. Increasing deviations from the long-term trend of -0.75%, -2.2%, and -2.50% were recorded on September 2nd, September 16th, and October 12th (greater short-term variations compared to at the shoulder). At both the shoulder and bank, O_2 concentration differences between depths become greater during short-term concentration decrease events, and lesser during short-term concentration increase events (fig. 7 G; 8 G).

4.4.3 CH_4:

CH_4 concentrations at the shoulder show decreasing concentrations with depth and follow an overall decreasing trend with time from the beginning until the end of the study period, with values ranging from 0.0012 to 1.89 ppm (fig. 6; 7 E). Temporal variations at the scale of weeks/months within this overall concentration decrease are apparent at all depths, although the magnitude of which are dampened as depth increases (fig. 7 E). When the sampling system was reinstalled on November 1st, the trend of decreasing CH_4 concentration with depth had deteriorated, where concentrations at 10, 20 and 30 cm decreased significantly while the concentrations at 40 and 50 cm gradually increased, resulting in 40 cm having the highest CH_4 concentration. These long-term concentration trends resulted in a broad concentration trough spanning from early July until mid-August (where concentrations of 0.66 ppm at 10 cm, and 0.003 at 50 cm were reached), bound by two broad peaks, centred in early June (where concentrations reached 1.67 ppm at 10 cm, and 0.50 ppm at 50 cm) and in early September (where concentrations reached 1.4 ppm at 10 cm, and 0.33 ppm at 50 cm). Within these long-term (scale of months) trends are concentration variations on the scale of days to weeks. These short-term variations in CH_4 concentration at the shoulder were observed to occur at the same time at all depths throughout the study period, and typically show oscillating concentrations, deviating +/- 0.5 ppm at 10 cm depth, and +/- 0.3% at 50 cm depth from the long-term trends at frequencies of 3-10 days.

The CH_4 concentrations at the bank also typically decreased with depth, as well as decreased over time from the beginning of the study period until the sampling system was temporarily uninstalled on October 18th, with values ranging from 0.0013 to 13.5 ppm (fig. 6; 8 E). The concentrations decreased from 0.90 and 0.20 ppm on May 7th to 0.45 and 0.14 ppm on October 18th at 20 and 50 cm depths, respectively (fig. 8 E). The CH_4 concentration at 10 cm depth at the bank, however, remained just below atmospheric concentrations (1.86 ppm) for the

duration of the study period. The resulting general long-term trend shows a peak centred in mid-August with maximums of 1.48 ppm at 10 cm and 0.45 ppm at 50 cm, bound by two broad troughs, centred in mid-July (declining to concentrations of 1.08 ppm at 10 cm and 0.11 ppm at 50 cm) and early October (declining to concentrations of 1.06 ppm at 10 cm, and 0.03 ppm at 50 cm). As at the shoulder, these long-term trends are composed of short-term events, where concentrations also generally vary +/- 0.5 ppm from the long-term trends at frequencies of 3-10 days. Similar to the CH_4 concentrations at the shoulder, there are evident trends in concentration at the bank, undulating over periods of months or weeks, as well as shorter term (periods of days to weeks) changes in concentration.

Two major short-term concentration change events are apparent at the bank, one from mid-May to the beginning of June, and the other from mid-November until the end of the study period (fig. 8 E). The first of these events shows an increase in CH_4 concentrations at all depths, where the magnitude of this increase increases with depth. The concentration at 50 cm depth increased from 0.20 ppm on May 8th to 11.10 ppm on May 26th, whereas the concentration at 10 cm depth increased from 1.20 ppm on May 8th to 1.60 ppm on May 25th. The second event also shows a CH_4 concentration increase at all depths (greatest at 30 cm depth), however, the tube sampling from 50 cm was removed on November 18th, as the water table rose to saturate this depth, and prevent any gas sampling. During this second major event, CH_4 concentrations increased from 0.30 ppm on November 8th to 13.55 ppm on November 19th at 30 cm depth.

4.4.4 N_2O:

N_2O concentration trends with depth at the shoulder were not as consistent as seen with O_2, CO_2, or CH_4, but most often increased in concentration with depth, with concentrations ranging from 0.02 to 1.80 ppm (fig. 6, 7 H). The overall trend is dominated by large magnitude, short-term variation from May until mid-June, and from September until the end of the study period. In between these periods, from mid-June until September, there was relatively little variation overall in concentration at all depths. Still, short-term changes in N_2O concentrations at the shoulder show consistent variations of +/- 0.1-0.5 ppm from the long-term trend at a frequency of 1-2 days. Exceptional short-term variance events occurred in late-September to mid-October, where there were large changes in concentration which took place over the course of days, and occurred at a much larger magnitude at depth. On September 21st-22nd, concentrations varied up to +1.2 ppm from the long-term trend over 3 days, on September 25th, concentrations varied up to +0.9 ppm over 3 days, and on October 12th-13th, concentrations varied up to +0.8 ppm over 8 days, all at 50 cm depth (fig. 7 H).

Similarly, N_2O at the bank showed a general trend of increasing concentrations with depth, with concentrations ranging from 0.01-2.03 ppm (fig. 6, 8 H). Similar to the shoulder, overall trends at the bank were dominated by short-term events, where variation was most frequent and at the highest magnitudes from the end of August until the end of the study period, and where concentration variations were limited from mid-June until the end of August. Consistent short-term concentration changes typically and consistently vary +/-0.1-0.3 ppm at a frequency of 1-2 days at all depths, often accentuated at depth. However, notable short-term events occurred on September 2nd, 17th, and 28th, where concentrations deviated +0.5, +1.30, and

+0.9 ppm from the long-term trend, and on October 11th and November 7th, where concentrations deviated +0.65 and +1.22 ppm, all at 50 cm depth, over 2-6 days (fig. 8 H).

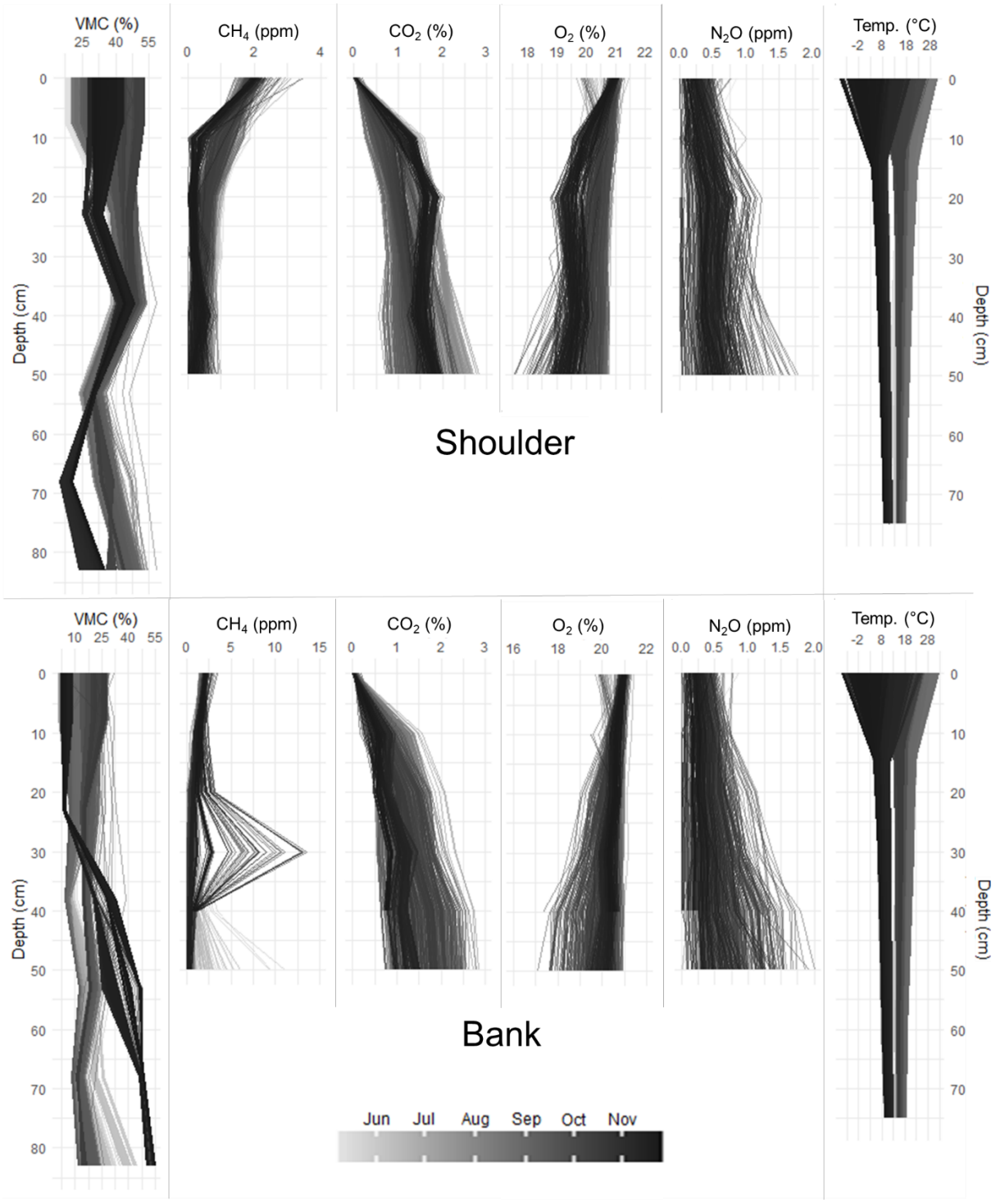

Figure 6: Depth profiles showing VMC, temperature, and gas concentration variation with depth (at 0 (air), 10, 20, 30, 40, and 50 cm) over time, where each line represents one sampling cycle. The gap seen in temperature plot can be attributed to the period of time when the sampling system was temporarily uninstalled (from October 18th to November 1st, a period of relatively rapid temperature change). Gaps in the VMC data can be attributed to the temporary removal of the sampling system as well as significant rainfall events where moisture content changes are fast.

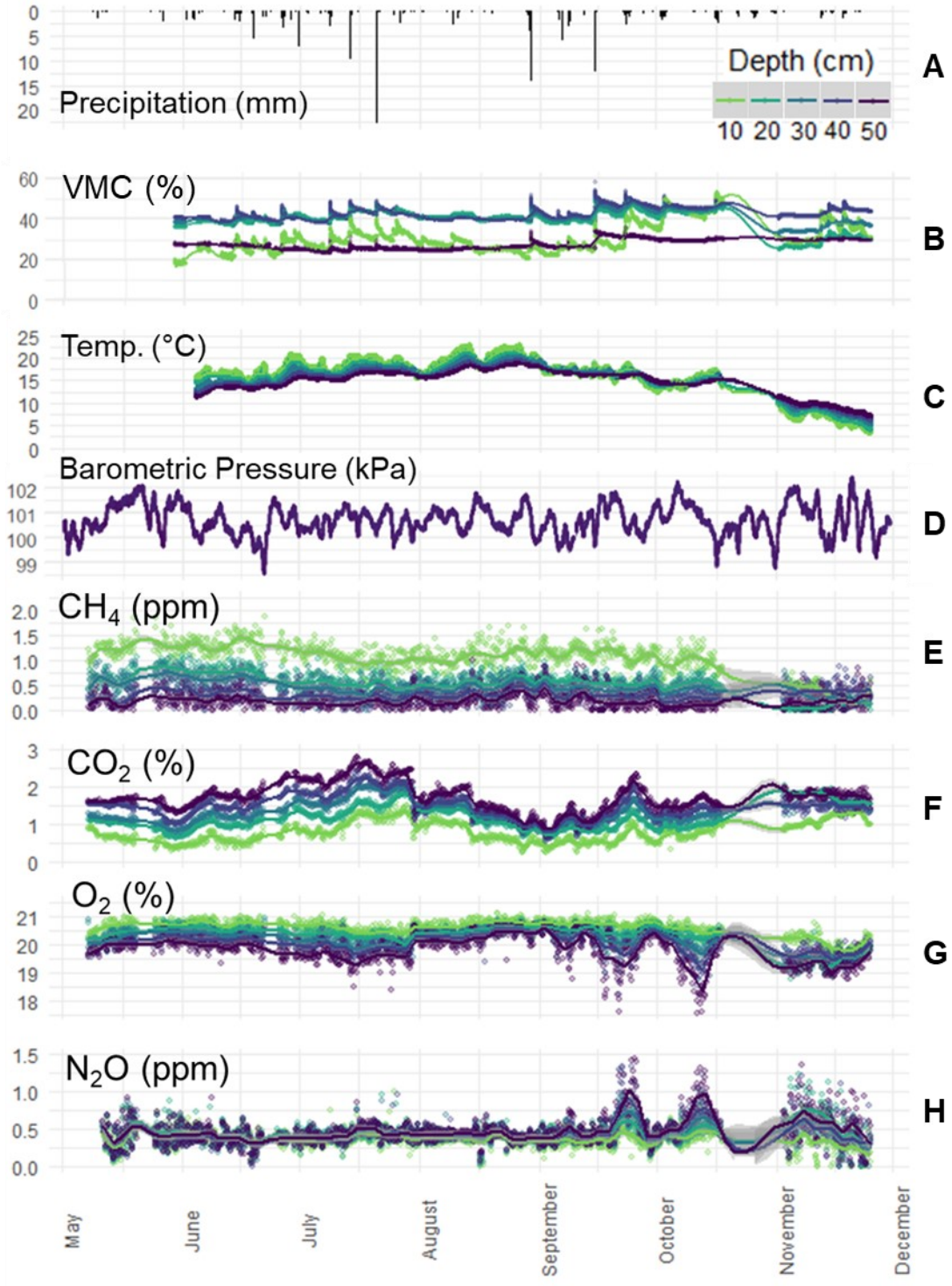

*Figure 7: **Shoulder** location precipitation, soil moisture content, soil temperature, barometric pressure, GHG concentration, and O_2 concentration time series. The points represent the data collected, while the lines show smoothed trends based on LOESS (local polynomial regression fitting) functions, and the grey areas surrounding these trendlines represent the 0.9 confidence interval. The monthly labels indicate the 1st of the month. No data was collected from October 18th to November 1st, as the ditch was being dredged, and vegetation was being cleared.*

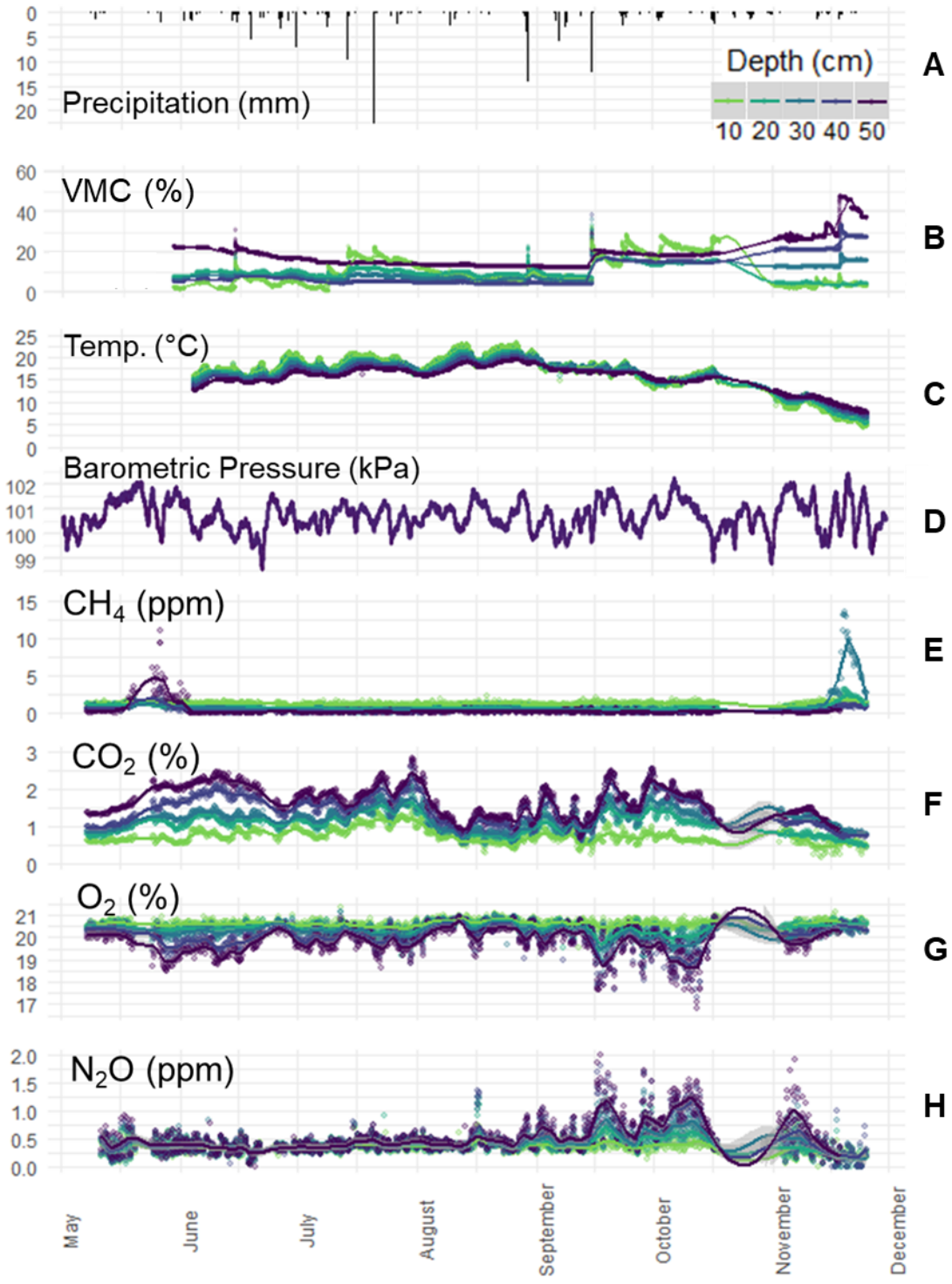

Figure 8: ***Bank*** *location precipitation, soil moisture content, soil temperature, barometric pressure, GHG concentration, and O_2 concentration time series. The points represent the data collected, while the lines show smoothed trends based on LOESS (local polynomial regression fitting) functions, and the grey areas surrounding these trendlines represent the 0.9 confidence interval. The monthly labels indicate the 1st of the month. No data was collected from October 18th to November 1st, as the ditch was being dredged, and vegetation was being cleared.*

4.5 SURFACE FLUXES

4.5.1 CO_2:

CO_2 surface flux values on the shoulder are mainly positive values and range from a maximum negative flux of -48.86 kg ha^{-1} day^{-1} to a maximum positive flux of 282.90 kg ha^{-1} day^{-1}, exhibiting strong long-term trends (fig. 9 E). These long-term trends generate a positive surface flux peak centred in mid-July (where values reached 282.90 kg ha^{-1} day^{-1} (overall maximum positive value) on July 19th), bound by large negative surface flux values in mid-May (reaching -33.59 kg ha^{-1} day^{-1} on May 11th) and mid-September (reaching -48.86 kg ha^{-1} day^{-1} by September 25th). Surface flux values typically vary from these long-term trends +/- 10-50 kg ha^{-1} day^{-1} over sub-daily to daily frequencies. These short-term trends change over time, where during some periods, higher or lower frequency variations will dominate. Occasionally, variation from the long-term trends will occur at exceptionally high magnitudes at near-weekly frequencies. For example, from September 22nd until October 18th, 3 short-term peaks are apparent, where surface flux values reached 197.53, 122.95, and 177.08 kg ha^{-1} day^{-1} on September 25th, October 5th, and October 13th, respectively, with an amplitude of roughly 75-100 kg ha^{-1} day^{-1}.

CO_2 surface fluxes at the bank remained exclusively positive and ranged from 5.02 kg ha^{-1} day^{-1} to 224.71 kg ha^{-1} day^{-1}, also exhibiting strong long-term trends (fig. 10 E). These long-term trends resulted in a trough centred in late August (values reaching 61.54 kg ha^{-1} day^{-1} by August 26th), bound by a peak centred in late July (values reaching 183.34 kg ha^{-1} day^{-1} by July 28th) and a peak centred in mid-September (values reaching 208.97 kg ha^{-1} day^{-1} by September 18th). Short-term trends are present, typically varying +/- 25-50 kg ha^{-1} day^{-1} from the long-term trends at sub-daily to daily frequencies, similar to at the shoulder. At the bank however, the higher magnitude weekly variations are more apparent throughout the study period. For example, during the month of June, there are 5 peaks, all 5-6 days apart, consistently varying roughly +/- 50 kg ha^{-1} day^{-1} from the long-term trend. A similar pattern can also be observed from mid to late July, at the end of which the maximum surface flux values were recorded.

4.5.2 O_2:

O_2 surface fluxes at the shoulder were generally negative, with the largest negative magnitude value being -227.62 kg ha^{-1} day^{-1} (fig. 9 F). However, positive fluxes were also recorded, with an average value of 35.31 kg ha^{-1} day^{-1}, although these positive values may be an artifact of the chamber method. This will be discussed further below. These long-term trends result in a trough (large magnitude, negative values) centred at the end of July/beginning of August (values reaching -183.57 kg ha^{-1} day^{-1} on August 10th), where the surface fluxes were consistently negative (with few exceptions) during July and August, and observed as mainly positive in September (reaching 110.75 kg ha^{-1} day^{-1} by September 20th). Similar to other surface fluxes observed, there are short-term trends varying from the long-term trends at exceptional magnitudes at near-weekly frequencies. For example, from September 25th until October 18th, negative surface flux magnitude highs of -116.95, -79.81, and -88.84 kg ha^{-1} day^{-1} were recorded on September 28th, October 3rd, and October 9th, respectively, with surface fluxes of 68.96 and 93.54 kg ha^{-1} day^{-1} measured between these events, on October 1st and 6th.

O_2 surface fluxes were also chiefly negative at the bank, with values reaching maximum magnitudes of -195.90 kg ha^{-1} day^{-1}, although showed less long-term variation compared to the shoulder (fig. 10 F). Similar to the shoulder, positive values were also recorded, with an average of 17.13 kg ha^{-1} day^{-1}. Surface flux magnitudes consistently and gradually increased from -50.94 kg ha^{-1} day^{-1} on May 8th until October 14th, where values of -109.51 kg ha^{-1} day^{-1} were reached. Surface flux magnitudes then decreased until the end of the study period. Short-term variations with exceptional variations from the long-term trend with near-weekly frequencies are also present. For example, on September 20th and 28th, surface flux magnitude highs of -175.39 and -153.38 kg ha^{-1} day^{-1} were recorded, separated by surface flux magnitude lows of 8.67 and -21.25 kg ha^{-1} day^{-1}, recorded on September 25th and October 1st, respectively.

4.5.3 CH_4:

CH_4 surface fluxes at the shoulder largely remained negative, occasionally becoming positive during relative brief moments in time (fig. 9 G). These values range between a maximum positive flux of $9.0x10^{-3}$ kg ha^{-1} day^{-1} to a maximum negative flux of $-2.3x10^{-2}$ kg ha^{-1} day^{-1}. Long-term trends result in a trough centred in mid-August (where values reached high magnitude negative flux values of $-1.3x10^{-2}$ kg ha^{-1} day^{-1} by August 17th), and a peak centred in mid-September where values reached high magnitude positive values of $2.7x10^{-3}$ kg ha^{-1} day^{-1} by September 19th). From May 12th until May 18th, positive CH_4 surface flux values were more common, reaching a maximum magnitude of $7.7x10^{-3}$ kg ha^{-1} day^{-1} on May 13th. From July 29th until August 30th, surface flux values were all negative, shortly before decreasing in magnitude in the month of September where positive values were once again common, and where an overall maximum positive flux of $9.0x10^{-3}$ kg ha^{-1} day^{-1} was reached on September 18th. These CH_4 fluxes consistently tended to vary +/- 0.005 kg ha^{-1} day^{-1} from the long-term trends at a daily frequency. Occasionally, larger magnitude events would occur, varying near $1.2x10^{-2}$ kg ha^{-1} day^{-1} over 5-7 days. For example, from September 25th, negative surface fluxes increased in magnitude rapidly to $-1.2x10^{-2}$ kg ha^{-1} day^{-1} on September 29th, reached maximum positive values of $2.1x10^{-4}$ kg ha^{-1} day^{-1} by October 3rd, maximum negative values of $-1.4x10^{-2}$ kg ha^{-1} day^{-1} on October 12th, before the negative fluxes decreased in magnitude again until the sampling system was temporarily uninstalled on October 18th.

CH_4 surface fluxes at the bank show similar long-term trends to those observed at the shoulder, with values ranging from a maximum negative flux of $-1.8x10^{-2}$ kg ha^{-1} day^{-1} to a maximum positive flux of $4.4x10^{-3}$ kg ha^{-1} day^{-1} (fig. 10 G). These long-term trends establish a broad trough centred in mid-September (where values reached $-1.3x10^{-2}$ kg ha^{-1} day^{-1} on September 17th) and a peak centred in early June (where values reached $3.2x10^{-3}$ kg ha^{-1} day^{-1} on June 1st). Throughout the study period, surface flux values were chiefly negative. Sporadic positive fluxes were observed from May until the beginning of August, where fluxes remained negative (with two exceptions) until the beginning of October. Surface fluxes tend to vary +/- 0.005-0.01 kg ha^{-1} day^{-1} from these long-term trends over daily to sub-daily frequencies. Similar to the shoulder, there are instances when near-weekly variations are apparent at exceptionally large magnitudes. For example, surface flux values decreased in magnitude from $-1.3x10^{-2}$ kg ha^{-1} day^{-1} on September 16th to $-2.1x10^{-3}$ kg ha^{-1} day^{-1} on September 26th, increased in magnitude to

$-1.3x10^{-2}$ kg ha^{-1} day^{-1} on September 30th before decreasing in magnitude again until the sampling system was temporarily uninstalled.

4.5.4 N_2O:

N_2O surface fluxes at the shoulder remained near zero throughout the study period, ranging from a maximum negative flux of $-9.88x10^{-3}$ kg ha^{-1} day^{-1} to a maximum positive flux of $9.77x10^{-2}$ kg ha^{-1} day^{-1}, with overall positive fluxes (fig. 9 H). These long-term trends resulted in a surface flux peak centred at the end of July and beginning of August (where values reached roughly $5x10^{-3}$ kg ha^{-1} day^{-1}), bound by two troughs, where the net surface fluxes were negative in May (values reaching $-5x10^{-3}$ kg ha^{-1} day^{-1}) and September (values reaching near $-2.60x10^{-3}$ kg ha^{-1} day^{-1}). Within these long-term trends exist short-term trends where surface flux values typically vary up to +/- $5.0x10^{-3}$ kg ha^{-1} day^{-1} at a daily frequency. Occasionally, these daily variations are much larger in magnitude in the positive direction. On July 9th, July 23rd, July 25th, and August 16th, these daily surface changes varied $2.5x10^{-2}$, $3.0x10^{-2}$, $5.5x10^{-2}$, and $9.5x10^{-2}$ kg ha^{-1} day^{-1} from the long-term trend, respectively. During this event on August 16th, maximum positive N_2O surface fluxes were recorded. From the end of July and through September, N_2O surface fluxes showed variation from the long-term trend at a near-weekly frequency. For example, surface flux reached positive maximums of $2.8x10^{-3}$, $3.6x10^{-3}$, and $3.1x10^{-3}$ kg ha^{-1} day^{-1} on August 29th, September 7th, and September 16th, and negative maximums of $-2.2x10^{-3}$, $-3.0x10^{-3}$, and $-1.8x10^{-3}$ kg ha^{-1} day^{-1} on September 2nd, September 13th, and September 19th, giving this weekly pattern an amplitude of roughly $2.67x10^{-3}$ kg ha^{-1} day^{-1}.

N_2O surface fluxes at the bank ranged from maximum negative values of $-1.1x10^{-2}$ kg ha^{-1} day^{-1} to maximum positive values of $9.5x10^{-3}$ kg ha^{-1} day^{-1}, with overall net positive fluxes (fig, 10 H). For the month of May surface fluxes were net negative, decreasing in magnitude to reach chiefly positive values by June, where for the rest of the study period, monthly net surface flux values were positive. From June on, surface flux readings showed a long-term horizontal trend, remaining mainly between 0 and $2.5x10^{-3}$ kg ha^{-1} day^{-1} with no strong variation at the monthly scale. Typical short-term variations are observed, where surface flux values vary +/- $2.5x10^{-3}$ to $5.0x10^{-3}$ kg ha^{-1} day^{-1}. A large magnitude short-term event occurred on August 16th, where surface fluxes reached $9.8x10^{-2}$ kg ha^{-1} day^{-1}. Similar short-term variations at the weekly scale are also present in N_2O at the bank, where surface fluxes reached maximum positive values of $3.1x10^{-3}$ and $3.0x10^{-3}$ kg ha^{-1} day^{-1} on September 20th and September 30th, and a maximum negative value of $-1.0x10^{-3}$ kg ha^{-1} day^{-1} on September 26th. The resulting near-weekly trend thus showed an amplitude of roughly $2.0x10^{-3}$ kg ha^{-1} day^{-1}.

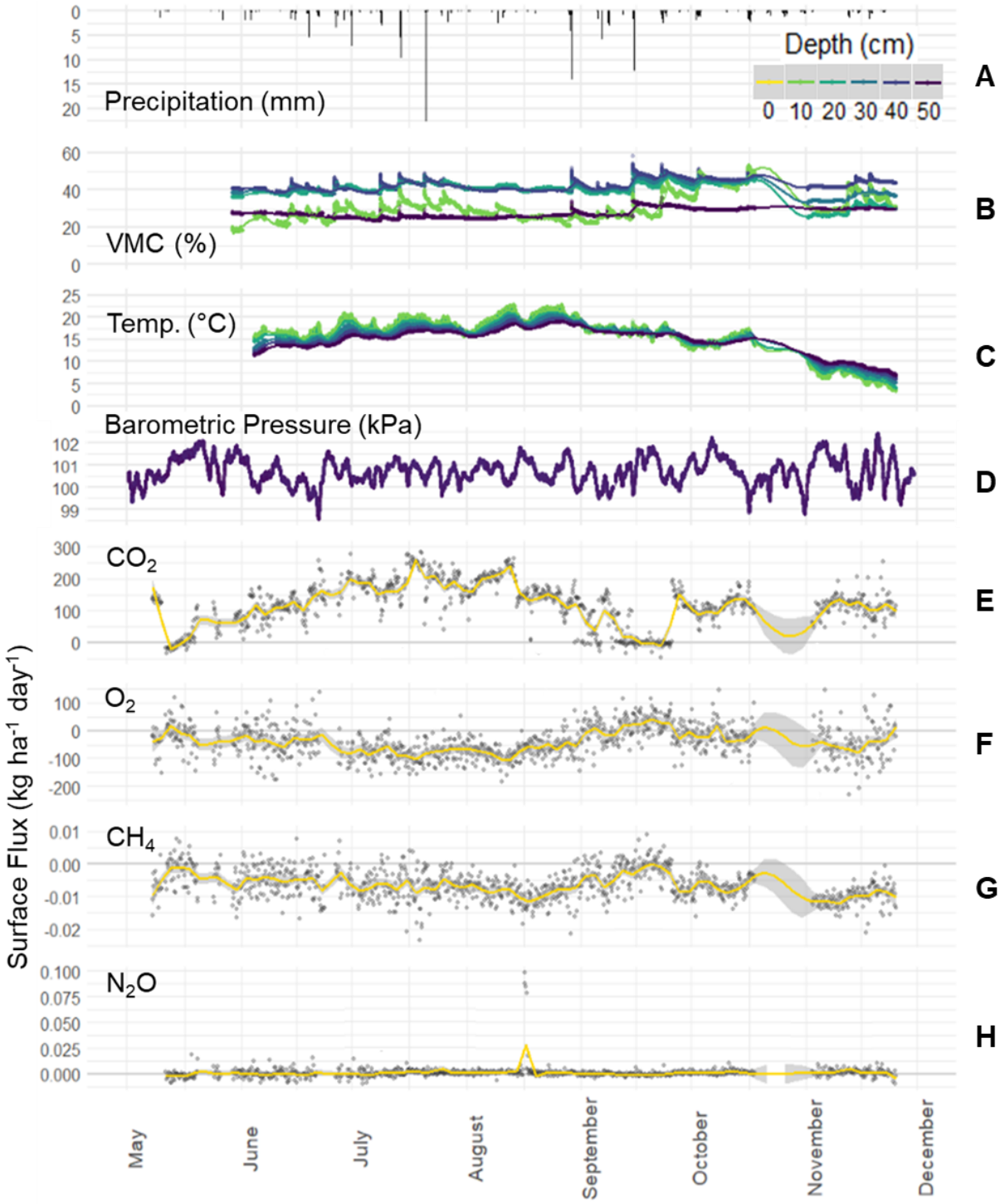

*Figure 9: **Shoulder** location precipitation, soil moisture content, soil temperature, barometric pressure, as well as GHG and O_2 surface flux time series. The points represent the data collected, while the lines show smoothed trends based on LOESS (local polynomial regression fitting) functions, and the grey areas surrounding these trendlines represent the 0.9 confidence interval. The line labelled as "0 cm depth" represent fluxes observed using the chamber method, while the rest of the fluxes were found using the gradient method.*

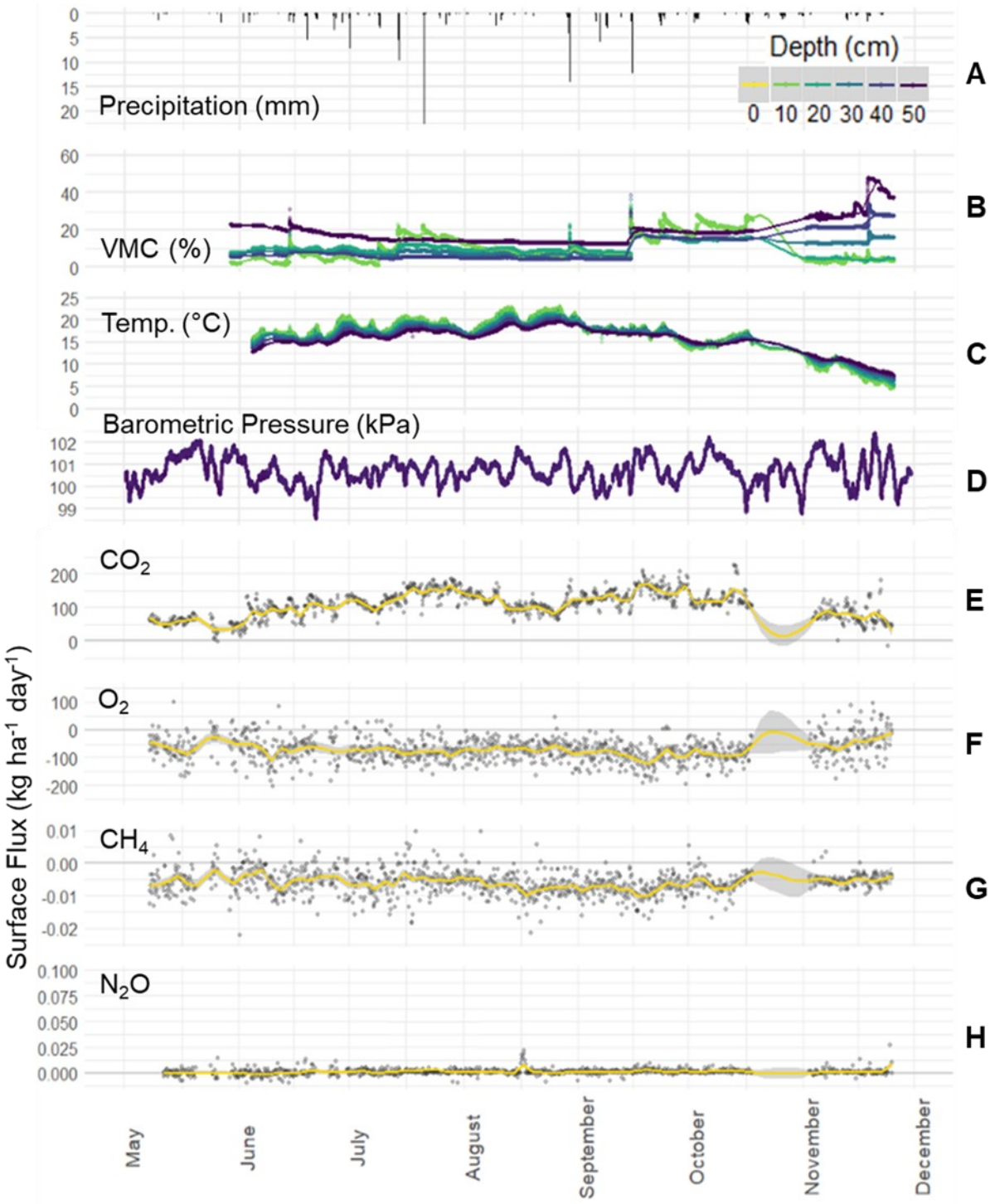

*Figure 10: **Bank** location precipitation, soil moisture content, soil temperature, barometric pressure, as well as GHG and O_2 surface flux time series. The points represent the data collected, while the lines show smoothed trends based on LOESS (local polynomial regression fitting) functions, and the grey areas surrounding these trendlines represent the 0.9 confidence interval. The line labelled as "0 cm depth" represent fluxes observed using the chamber method, while the rest of the fluxes were found using the gradient method.*

5 DISCUSSION

5.1 PHYSICAL DIFFERENCES BETWEEN SHOULDER AND BANK SOILS

Differences in soil structure, root density, nutrient availability, and interaction with the water table will all have influences on the observed subsurface soil gas concentrations and surface emissions. Soil at the bank is very disturbed, with less distinct soil horizons as a result of the construction of the drainage ditch (fig. 4). Still, a clay layer exists at the bottom of the bank profile. A clay layer (silty clay loam) also exists at the shoulder, dividing the organic rich upper horizon from the lower sand/silt dominated loam/sandy loam horizons. Overall, the shoulder soils are composed of greater silt and clay proportions, whereas the bank is dominantly sand from 17-55 cm depth, suggesting a higher permeability at the bank compared to the shoulder. However, the shoulder soils show slightly higher porosities compared to the bank. Based on field observations, a higher root density exists at the bank, where there is a larger proportion of thin roots. Roots at the shoulder are much less prevalent, and, where they exist, are much thicker than the majority of the roots at the bank.

Overall, soil at the bank has a lower soil moisture content compared to the shoulder (fig. 7, 8). Where the canopy, which exists over the bank location, intercepts a proportion of precipitation (Wang et al., 2013), moisture content at the bank often shows responses to precipitation events at a smaller magnitude compared to the shoulder. For example, coinciding with the largest precipitation event in the study period on July 20th, moisture content at 10 cm depth increased 9.7% at the shoulder over 16 hours, and only 6.9% at the bank (fig. 7, 8). Similarly, moisture content decrease (whether from drainage or evapotranspiration) occurs at a slower rate at the bank, where following the precipitation event on July 20th, moisture content at the shoulder decreased 10% at a rate of 0.1%/hour, while moisture content at the bank decreased 7% at a rate of 0.07%/hour. Responses of soil moisture content to precipitation at depths from 20 to 50 cm are much more prevalent at the shoulder compared to the bank, and occasionally, all depths at the bank will show no soil moisture response to precipitation when the shoulder does. The lack of responsiveness of deeper soil layers to precipitation events at the bank is likely due to a combination of factors. For example, the canopy interception will minimize and slow infiltration (Wang et al., 2013), as will the steeper slope at the bank (which may result in a greater proportion of runoff). The moisture content at 50 cm at the bank is consistently higher than those at 20-40 cm depth, likely due to the low permeability, high water retention clay layer that exists from 55-65 cm depth, and proximity to the water table. Despite these differences, the moisture contents at the shoulder and bank follow the same general temporal trends until October 18th. Following reinstallation of the sampling system, moisture contents at depth at the bank were high, while moisture contents at 10 and 20 cm were low. This is likely related to the rising water table supplying soil at depth with moisture content, where the water table rose past 50 cm depth, and the sampling tube reaching this depth had to be removed as available soil gas was replaced with water.

5.2 CONTROLS ON SOIL GAS DEPTH DISTRIBUTION

O_2 concentrations at both the shoulder and bank were generally observed to decrease with depth throughout the study period, while CO_2 exhibited trends of increasing concentrations with depth (fig. 6). Blume et al, at a nearby agricultural riparian zone field site, similarly observed increasing CO_2 concentrations with depth, despite decreasing CO_2 production rates via soil respiration (as a result of labile content availability). These CO_2 concentration profiles were attributed to higher rates of CO_2 transport near the surface, and lower rates as depth increased (Blume, O., 2020; Blume et al., 2022). Soils near the surface at both the shoulder and bank showed higher porosity values and generally lower moisture content values than deeper soils (fig. 6), promoting greater transport rates/fluxes as transport is dependent on porosity/permeability, and moisture content (Blume, O., 2020; Blume et al., 2022; Smith et al., 2018). The observed CO_2 and O_2 concentration profiles are thus the result of greater consumption of O_2 and production of CO_2 near the surface via soil respiration, compensated by the greater transport rates at these shallower depths (fig. 6).

CH_4 concentrations at both the shoulder and bank were typically highest (and near atmospheric levels (1.86 ppm)) at shallow depths and decreased consistently with O_2 concentrations as depth increased, with CH_4 surface fluxes typically being negative (fig. 6, 9, 10). This indicates that the soil is primarily a sink for CH_4, where its concentration profile is dependent on transport processes, reaction rate, and distance from the soil/atmosphere boundary. With O_2 constantly present at the observed depths, methanotrophy is a CH_4 controlling process, consuming CH_4 and producing CO_2, although contributing only minor amounts of CO_2 relative to soil respiration. N_2O concentrations at both the shoulder and bank generally increased with depth as O_2 concentrations decreased (fig. 6). As O_2 becomes limited, and moisture content increases with depth, nitrifying bacteria can reduce NO_2^- (in place of O_2) to NO and N_2O, favouring N_2O as a product as moisture content increases (Oertel et al., 2016; Smith et al., 2018). N_2O can also originate from saturated, anaerobic soils at greater depths than those measured in this study, produced via denitrification and transported to the observed depths.

5.3 SPATIAL VARIABILITY OF SOIL GAS CONTROLS

Using multiple linear regression analysis (MLRA), the dependence and responsiveness of the observed surface fluxes and soil-gas concentrations to temperature, VMC, and barometric pressure over the entire study period (considering only these three variables, simultaneously) was examined. The results showed low adjusted R^2 values overall for surface fluxes, decreasing in the order of CO_2, CH_4, O_2, followed by N_2O at both the shoulder and bank, with negative adjusted R^2 values for N_2O at both locations (low and negative R^2 values implying little dependency of the trend on the variables incorporated in the model) (fig. 11). At the shoulder, adjusted R^2 values of CO_2 and O_2 peaked at 20 cm, generally decreasing with greater depth past this point (with the exception of CO_2 showing higher adjusted R^2 values at 50 cm than at 30 and 40 cm). CH_4 adjusted R^2 values peaked at 10 cm decreasing with depth, and N_2O adjusted R^2 values generally increased with depth overall. At the bank, all gases showed low adjusted R^2 values at 10 cm, with highest values at 20 cm, and overall decreasing trends past this point. From 20 cm to 50 cm, N_2O adjusted R^2 values showed the least amount of variation, only ranging between 0.25 and 0.35.

These adjusted R^2 trends demonstrate that subsurface gas concentrations are overall more responsive to the changing environmental conditions (moisture, temperature, and barometric pressure) at depths ranging from 10 to 20 cm. Low adjusted R^2 values corresponding to surface fluxes (at both the shoulder and bank) and shallow subsurface concentrations (particularly at the bank) may be due to the significant control of a factor other than moisture, temperature, and barometric pressure; perhaps the influence of the atmosphere/soil boundary. Closer to the soil surface, there is the potential for greater soil gas exchange with the atmosphere, and less accumulation or depletion of gasses produced or consumed in the soil (Blume, O., 2020; Blume et al., 2022), thus resulting in seemingly less exaggerated responses of fluxes or concentrations to changing environmental parameters.

Increased responsiveness of GHG controlling microbial processes to changes in temperature and moisture content (demonstrated by high adjusted R^2 values, particularly at the bank at 20 cm depth, and between 10 and 20 cm at the shoulder) could be a result of labile organic material availability, where for example, sensitivity of denitrification and soil respiration to moisture content will increase with sufficient nutrient availability, as moisture content promotes nutrient transport as well as prevents microbe water stress (Pilegaard et al., 2006; Peng et al., 2010; Schindlbacher et al., 2004). Similarly, with sufficient moisture content and nutrient availability, microbially mediated reaction rates tend to increase with increasing temperatures (within the ranges seen in this study) (Oertel et al., 2016; Shabaga et al., 2015; Smith et al., 2018; Schaufler et al., 2010; Whalen & Reeburgh, 1996; Abdallah et al., 2009).

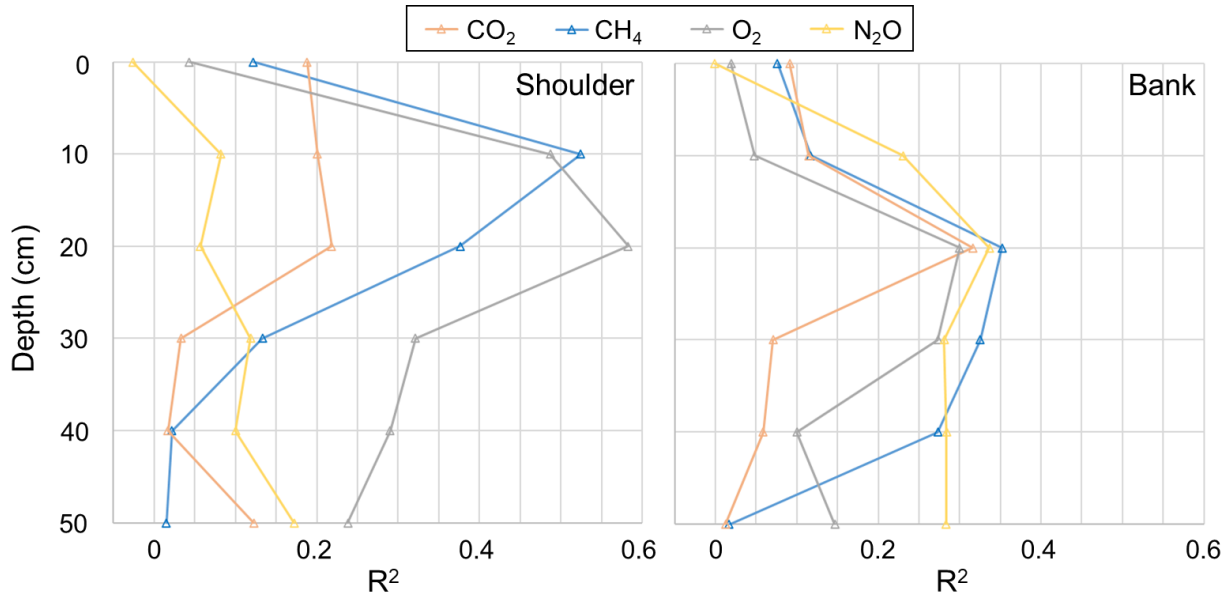

Figure 11: Comparison of MLRA adjusted R^2 values with depth and location (shoulder and bank) when considering soil VMC, temperature, and barometric pressure influences on soil gas concentrations.

The distribution of VMC, temperature, and barometric coefficients resulting from this MLRA demonstrates the variability of the relative control of these parameters on soil gas (fig. 12). With differences in the combination of soil structure, moisture content, nutrient availability, proximity to the surface, and temperature with depth (and between the shoulder and bank), there are differences in sensitivity of soil gas variation to these parameters. For example: barometric pressure contributions were greatest (highest magnitude MLRA coefficients) at the bank, at depth, for O_2 and N_2O specifically, with strong negative values for O_2 and strong positive values for N_2O; temperature and barometric pressure elicit stronger responses of soil [CH_4] at 30 cm at the bank; and barometric pressure coefficients for CO_2 increased in magnitude with depth at both the shoulder and bank, yet these coefficients were positive at the bank, and negative at the shoulder.

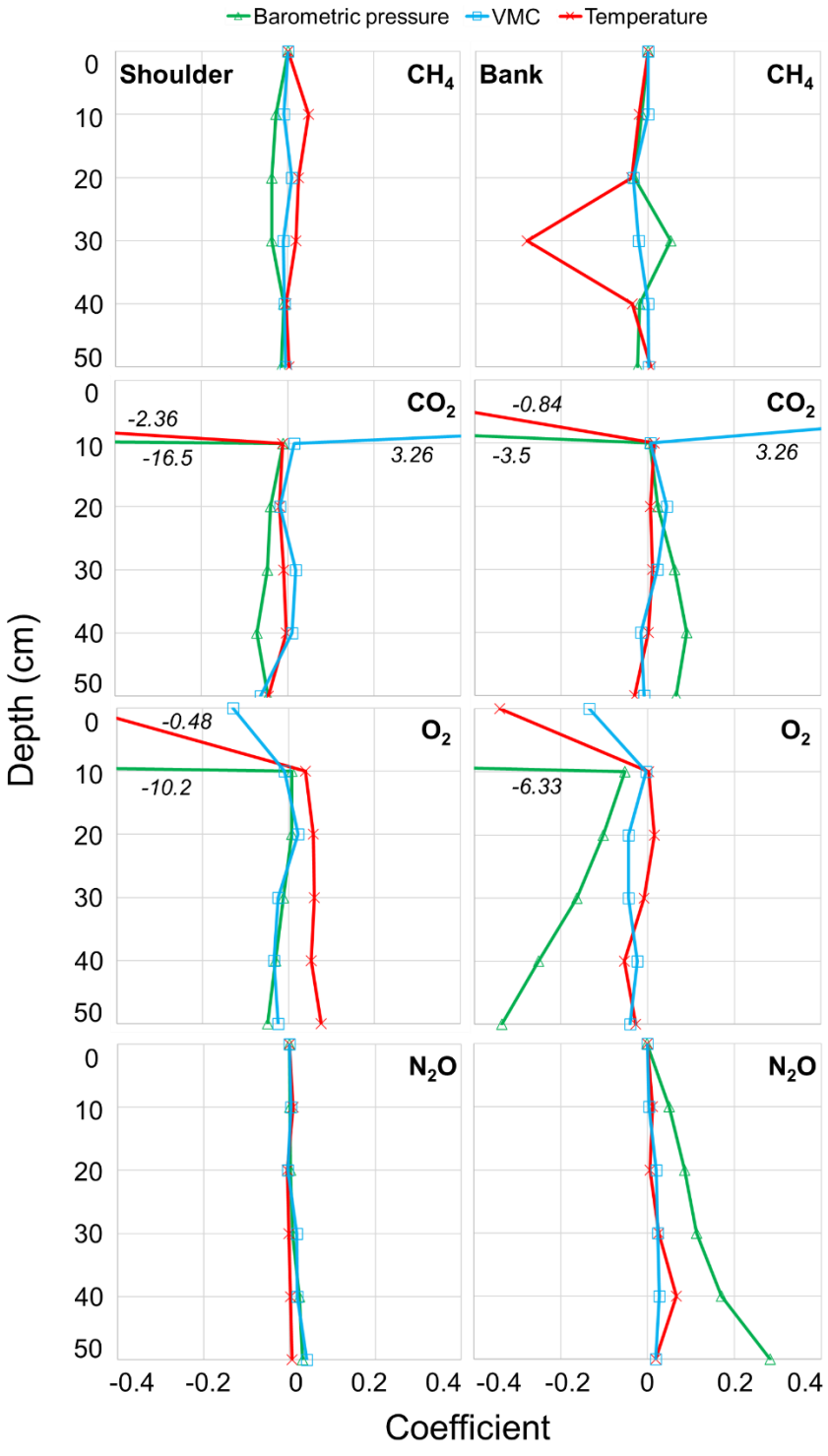

Figure 12: Spatial variation in coefficients of temperature, VMC, and barometric pressure in terms of subsurface gas concentration (from 10 to 50 cm depth) and surface fluxes (represented at depth = 0 cm) as result of MLRA. Where surface flux coefficients surpass the bounds of the plots, their values are labelled next to their lines.

5.4 TEMPORAL VARIABILITY OF SOIL GAS

5.4.1 Long-term variability:

Long-term trends in soil concentrations and surface fluxes generally agree with the current literature. Increased CH_4 emissions occur during wet periods likely due to increased production in anaerobic conditions (Gukland et al., 2009; Christiansen et al., 2012; Baah-Acheamfour et al., 2016), and coincide with elevated subsurface concentrations (fig. 7, 8, 9, 10). CH_4 influxes tend to increase in magnitude while moisture content decreases in dry periods (Wang et al., 2013), where in this case, influxes were greatest in August, coinciding with high subsurface concentrations. Similarly, under dry conditions in August where uptake and replenishment of soil with atmospheric CH_4 might be occurring, O_2 influx magnitudes are greatest, and soil [O_2] at all depths approach atmospheric levels. CO_2 emissions and subsurface concentrations were high in late July before decreasing drastically in August. High soil temperatures paired with low soil moisture (to a certain limit), as seen in August, have been observed to increase soil respiration productivity (Almagro et al., 2009; De Carlo et al., 2019; Amadi et al., 2016; Wang et al., 2021). However, the moisture content in August may be low enough to be limiting and impede soil respiration, resulting in the decreasing trends in subsurface concentration and surface flux in the same month (Vidon et al., 2014). Seasonal variation in N_2O emissions at both the shoulder and bank is weak (most notably at the bank) as is occasionally observed (Amadi et al., 2016; Lemke et al., 1998). However, seasonal peaks in emissions (most notable at the shoulder) were observed during the summer, as is also occasionally observed (Baah-Acheamfour et al., 2016; Morishita et al., 2007). Large peaks in soil [N_2O] from September onwards are not matched by surface emissions, even coinciding with influxes in September.

5.4.2 Short-term variability:

Throughout these overall long-term trends, short-term variations in soil gas concentrations and surface emissions of CO_2, O_2, CH_4, and N_2O are prevalent. Soil [CO_2] showed short-term variations of up to 2% (at 50 cm depth), over time periods ranging from 16 hours to 7 days. These variations were often accompanied by changes in CO_2 surface flux rates, ranging from 25 kg ha^{-1} day^{-1} to 190 kg ha^{-1} day^{-1} over time periods ranging from 4 hours to 7 days. Despite differences in rates of these short-term variations, they were consistent throughout the entire study period. During the wet periods (from June to July and from September to November), short-term increases in soil [CO_2] were typically 0.5-1% (at 50 cm depth) over 1-3 days, and were matched by increases in CO_2 surface emissions of 25-150 kg ha^{-1} day^{-1}. The fastest changes in soil [CO_2] were events during the dry period (specifically at the shoulder) where concentrations decreased 1-1.5% (at 50 cm) over 16-24 hours, matched by 75-150 kg ha^{-1} day^{-1} decreases in surface emissions. The fastest change in CO_2 surface emissions occurred on September 25th at the shoulder, where emissions rose 190 kg ha^{-1} day^{-1} over ~4 hours. Similar to the long-term trends, soil [O_2] and O_2 surface fluxes typically follow opposite trends to CO_2 at short time periods. Soil [O_2] short-term variations of up to 3% occurred over time periods as short as 16 hours while surface fluxes varied up to roughly 50 kg ha^{-1} day^{-1} over periods as short as 24 hours. The largest changes in soil [O_2] were observed from September until mid-October,

where concentrations would decrease 1% to 3% (at 50 cm) over 1 to 10 days, with intermittent increases of similar magnitude towards atmospheric levels. Both soil [O_2] and [CO_2] showed more frequent large magnitude, short-term variations at the bank compared to the shoulder.

Short-term variations in soil [CH_4] were relatively consistent throughout the study period (compared to CO_2 and O_2), with changes of 0.1-0.25 ppm occurring over 1-5 days (at 50 cm depth), and with more frequent variation near the surface. These short-term variations were strongest from late July until early September during the dry period where concentrations would show a ~0.25 ppm spike every 6-10 days. Similar to soil [CH_4], CH_4 surface fluxes show relatively consistent short-term variation, at magnitude from roughly 0.005 kg ha^{-1} day^{-1} to 0.01 kg ha^{-1} day^{-1} over 2-5 days. The two most notable variations in soil [CH_4] occurred at the bank, where concentrations increased 10.9 ppm (at 50 cm) in May, and 13.25 ppm (at 30 cm) in November, over 18 and 11 days, respectively. These two major events did not result in any major changes in surface fluxes. The largest changes in soil [N_2O] occurred from September until mid-October, where concentrations increased 0.5 to 1.3 ppm over 3 to 8 days at 50 cm depth at irregular intervals (with 3 to 17 days in between peaks).

5.5 TEMPORAL VARIABILITY OF SOIL GAS CONTROLS

5.5.1 Role of barometric pressure during dry season:

With significant increases in barometric pressure, upward soil-gas movement and effluxes can be inhibited, and the importance of the advective component of transport can increase, where a high proportion of air filled pore space during dry periods amplifies these effects (Forde et al., 2019; Laemmel et al., 2017; Maier et al., 2012). On July 30th, barometric pressure increased from 99.85 kPa to 100.55 kPa and on August 14th, barometric pressure increased from 100.50 kPa to 101.21 kPa (fig. 13; 14). These increases in barometric pressure coincided with decreases in CO_2 surface efflux (effluxes decreased from 925 to 527 kg ha^{-1} day^{-1} on July 30th, and from 208 to 121 kg ha^{-1} day^{-1} on August 14th), decreases in O_2 and CH_4 surface influx magnitudes, as well as rapid soil [CO_2], [CH_4], and [O_2] changes towards atmospheric levels, where soil [CO_2] at 50 cm dropped 1.27% over 16 hours on July 30th, and 0.95% over 24 hours on August 13th-14th at the shoulder (fig. 13, 15). These rapid changes in soil gas concentrations and surface fluxes at the shoulder occurred over modest decreases in temperature (2.6ºC at 10 cm, 0.1ºC at 50 cm) and moisture content (1.12% at 10 cm, and 0.21% at 50 cm) (fig. 13).

Other studies have observed changes in GHG fluxes over relatively constant moisture and temperature (Vidon et al., 2015). However, with no accompanying barometric pressure data, the cause for these flux variations was unclear. In this case, the effects of increasing barometric pressure (enhanced by the low moisture content during this dry season) likely contributes to downward advection, supplying the soil with atmospheric gas and inhibiting effluxes. A diffusive component of the overall transport will still exist (upward for CO_2, and downward for O_2), although inhibited, as the typical concentration gradients of increasing [CO_2] and decreasing [O_2] with depth remain, only at smaller magnitudes. The decreases in CO_2 surface effluxes measured using the chamber method are likely only fractions of the true decreases in effluxes, as atmospheric pressure influences on surface fluxes are likely suppressed when measuring using

the chamber technique, leading to an underestimation of the magnitude of the total surface flux variations (Maier et al., 2012).

Responses of CO_2 and O_2 to changing barometric pressure are also present at the bank location. However, where there is an abrupt change in all soil gas concentrations towards atmospheric levels at the shoulder on July 30th, there is an abrupt increase in CO_2 concentrations and a decrease in O_2 concentrations at the bank (fig. 14). Similar to the shoulder, though, these increases in pressure still coincide with a decrease in the magnitude of CO_2 effluxes and O_2 influxes. This suggests that the changes in barometric pressure can be causing a change in soil gas transport in multiple directions. An increase in barometric pressure will similarly inhibit surface effluxes from both the shoulder and bank. However, differences in soil structure, topographic position, and proximity to the ditch and saturated conditions exist between the shoulder and bank. These differences might result in differences in subsurface gas behaviour induced by the same efflux inhibiting increase in barometric pressure. Where this increase in pressure can cause advective transport of atmospheric gas into soil at the shoulder, soil-gas displaced by this event must be transported elsewhere, potentially causing high soil [CO_2] to be measured at the bank location. This difference in responses to changes in barometric pressure at the shoulder and bank continues throughout the study period (as seen in the difference in signs MLRA pressure coefficients between the shoulder and bank (fig. 12)).

Following the initial event on July 30th, the bank shows consistent and gradual changes in soil gas concentrations, trending towards atmospheric levels, where eventually (by August 12th), subsurface CO_2 and O_2 had converged to similar values at all depths (fig. 14). Where moisture content is lower overall at the bank compared to the shoulder, it is possible that soil respiration is inhibited (where it has been observed that poorly drained soils are known to bear higher CO_2 production rates (Jacinthe et al., 2015; Jacinthe et al., 2003)), and transport is promoted (in addition to the increased transport at the bank based on the physical soil structure). Soils with greater permeability and air filled pore spaces (such as the sandier, drier soils at the bank (above 50 cm depth)) are more sensitive to changes in atmospheric pressure (Maier et al., 2012), resulting in more variable subsurface concentrations overall. At the shoulder, the higher moisture content and less efficient soil gas transport allows for larger magnitude, more abrupt changes in concentration, where there is greater resistance to environmental changes until a threshold is surpassed.

The complexity of the effects of changes in barometric pressure on soil gas concentrations and surface fluxes is also reflected in N_2O behaviour following the event on August 14th, where different responses were observed at the shoulder and bank, both days after the changes observed in O_2 and CO_2. On August 16th, unprompted by changes in moisture content and temperature, soil [N_2O] at the shoulder rapidly decreased to $7.0x10^{-2}$ ppm at 40 cm, and soil [N_2O] at the bank rapidly increased to 1.35 ppm at 40 cm (fig. 15, 16). However, both of these rapid concentration changes corresponded to rapid increases in N_2O surface fluxes; up to $9.77x10^{-2}$ kg ha^{-1} day^{-1} at the shoulder, and $1.7x10^{-2}$ kg ha^{-1} day^{-1} at the bank.

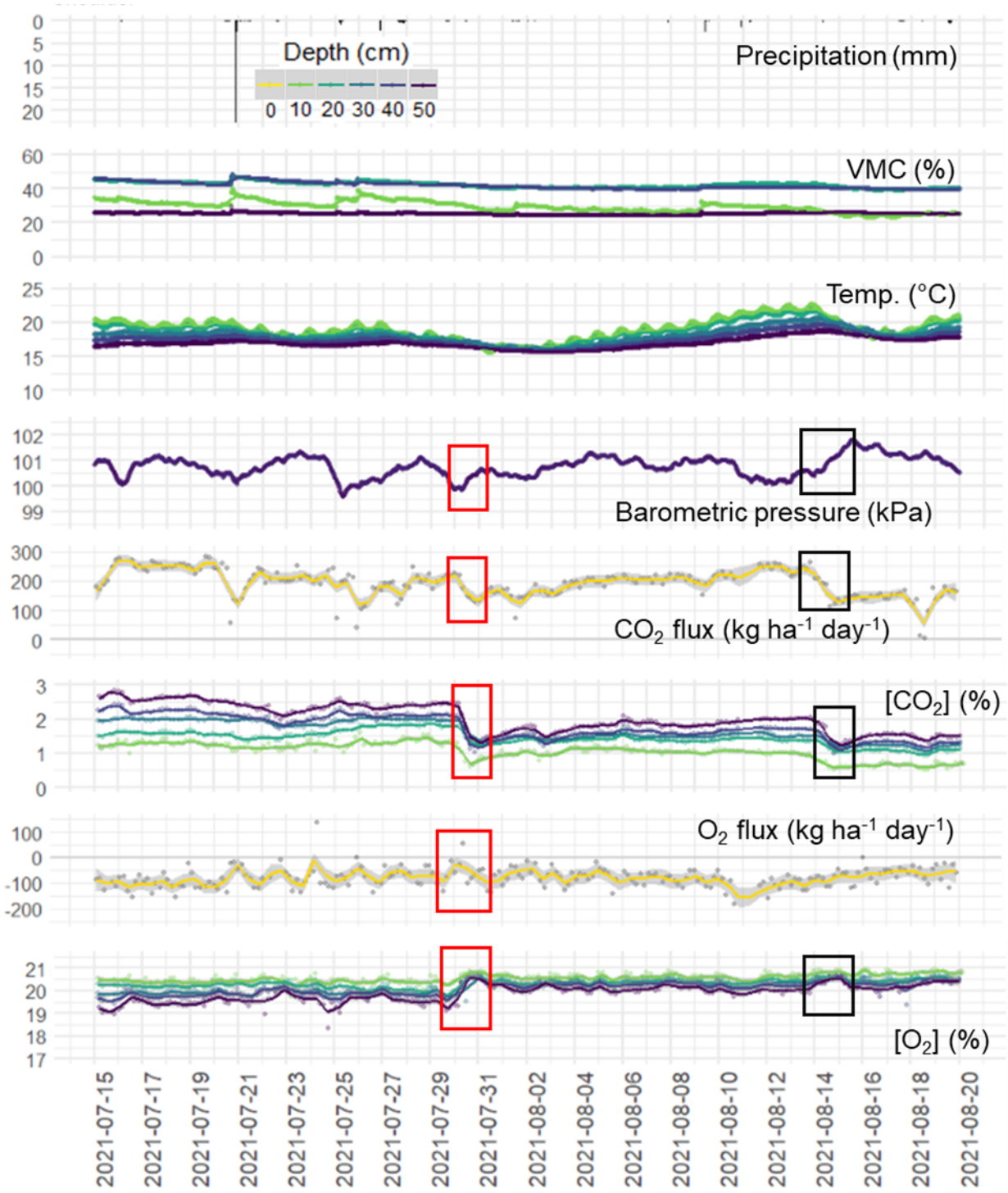

*Figure 13: **Shoulder** CO_2 and O_2 soil gas concentrations and chamber method surface fluxes along with barometric pressure and soil moisture and temperature during dry period. The points represent the data collected, while the lines show smoothed trends based on LOESS (local polynomial regression fitting) functions, and the grey areas surrounding these trendlines represent the 0.9 confidence interval. The boxes highlight the events described above; where red denotes the events related to the barometric pressure changes on July 30th, and black denotes the events related to the barometric pressure changes on August 14th.*

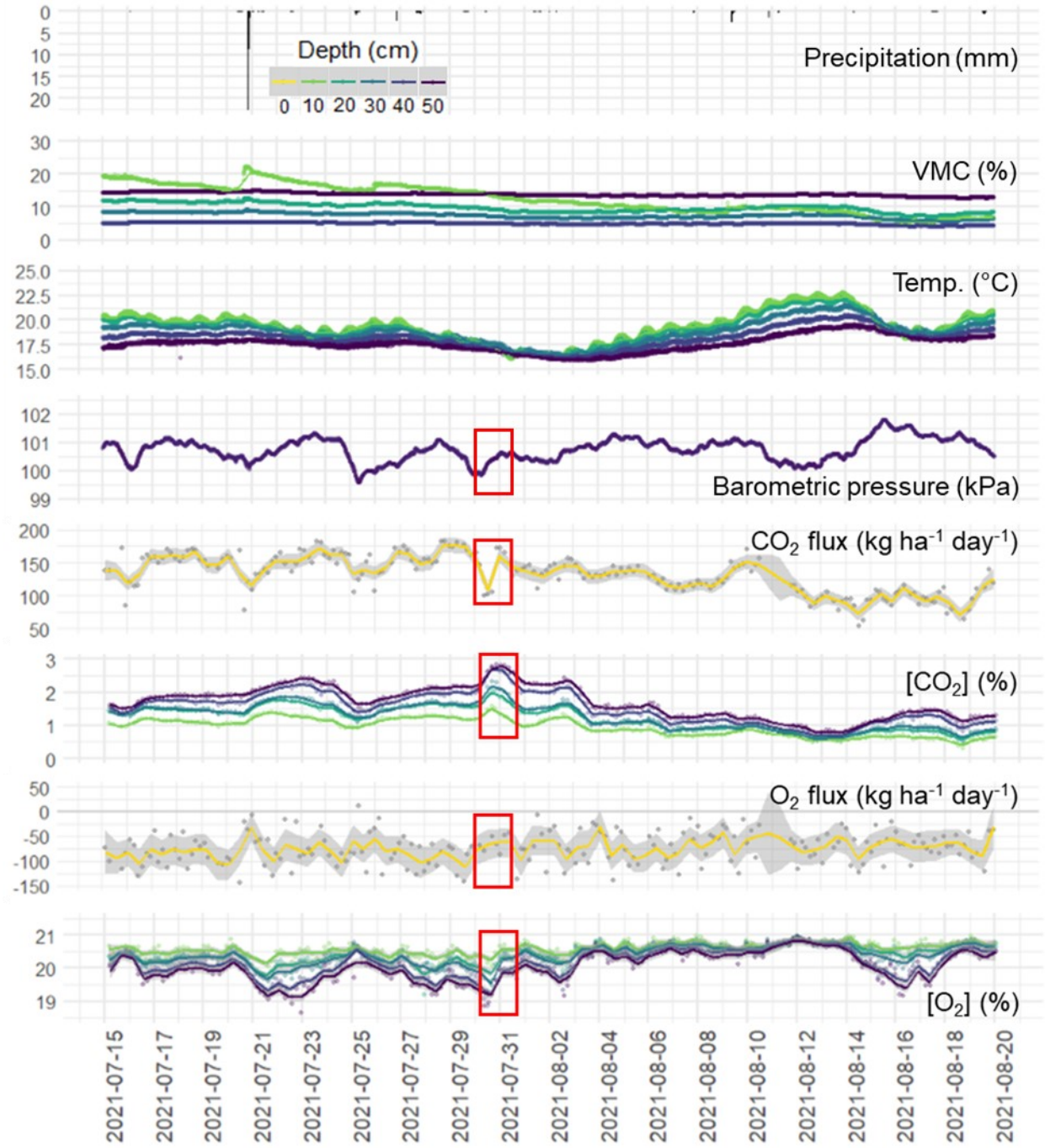

Figure 14: ***Bank*** *CO_2 and O_2 soil gas concentrations and chamber method surface fluxes along with barometric pressure and soil moisture and temperature during dry period. The points represent the data collected, while the lines show smoothed trends based on LOESS (local polynomial regression fitting) functions, and the grey areas surrounding these trendlines represent the 0.9 confidence interval. The red boxes highlight the events described above, related to the barometric pressure changes on July 30th*

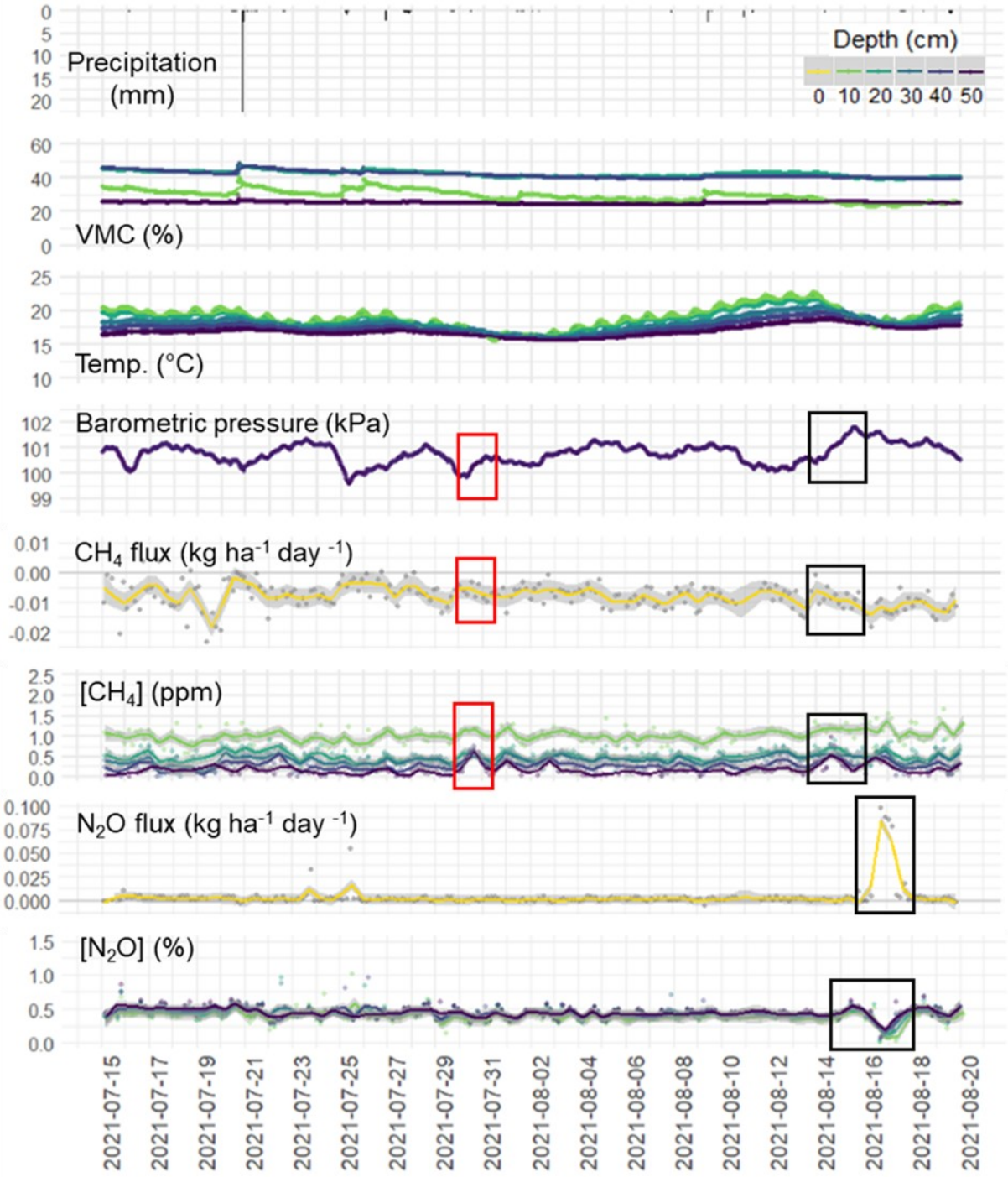

*Figure 15: **Shoulder** CH_4 and N_2O soil gas concentrations and chamber method surface fluxes along with barometric pressure and soil moisture and temperature during dry period . The points represent the data collected, while the lines show smoothed trends based on LOESS (local polynomial regression fitting) functions, and the grey areas surrounding these trendlines represent the 0.9 confidence interval. The boxes highlight the events described above; where red denotes the events related to the barometric pressure changes on July 30th, and black denotes the events related to the barometric pressure changes on August 14th.*

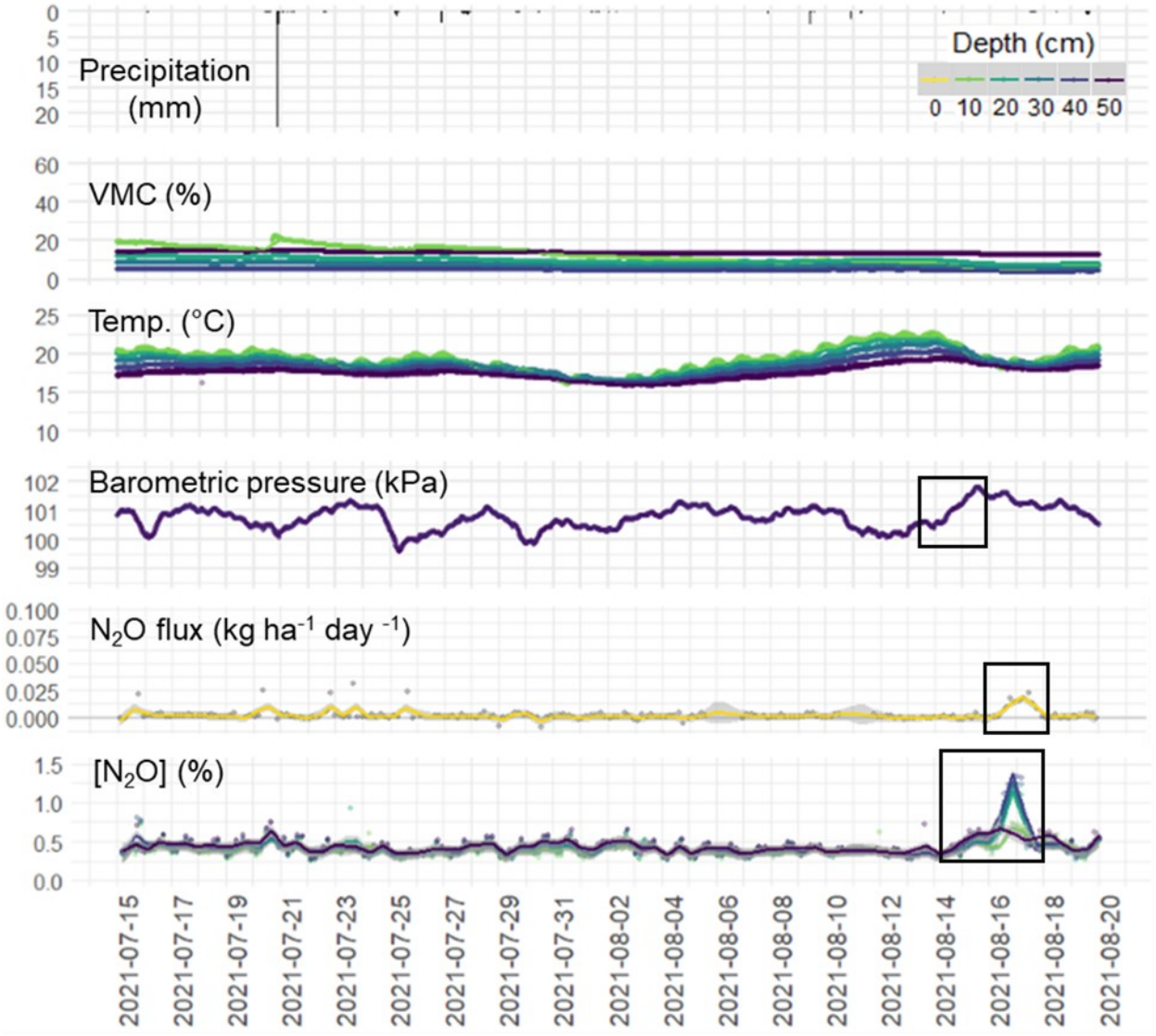

*Figure 16: **Bank** N_2O soil gas concentrations and chamber method surface fluxes along with barometric pressure and soil moisture and temperature during dry period . The points represent the data collected, while the lines show smoothed trends based on LOESS (local polynomial regression fitting) functions, and the grey areas surrounding these trendlines represent the 0.9 confidence interval. The black boxes highlight the events described above, related to the barometric pressure changes on August 14th.*

5.5.2 Temporal variability of the role of soil moisture:

The effects of short-term moisture content variation (hours to days) can vary depending on the overall environmental factors under which they occur. Following dry periods, pulses of soil moisture increase following precipitation events can cause rapid revitalization of soil respiration (Slessarev & Schimel, 2020; Borken & Matzner, 2009; Unger et al., 2010; Schindlbacher et al., 2004; Groffman et al., 2009). Under higher average moisture content conditions, short-term moisture content increases can inhibit exchange of gas between the soil and atmosphere for multiple days, allowing for the accumulation of subsurface CO_2, followed by its abrupt release from the surface. Based on location within a riparian zone, a rising water table will have different effects on soil gas production and transport. Soils with different soil structures (porosity and permeability) can respond differently to these short-term variations in soil moisture.

With water stress and inhibition of microbial activity during dry periods (Borken & Matzner, 2009; Schindlbacher et al., 2004), dead microbial cells can accumulate along with a proportion of any organic material that is added to the soil during these dry periods (Borken & Matzner, 2009). Similar to freeze-thaw events, dry-wet cycles can also induce physical changes in the soil structure, freeing up organic material (Unger et al., 2010; Groffman et al., 2009). Following re-wetting after a dry period, a pulse of elevated CO_2 production and emission is often observed within hours (Birch effect), whereby renewed moisture content will revitalize the microbial community, and promote temporary elevated soil respiration in the presence of this moisture content and accumulated/freed organic material (Slessarev & Schimel, 2020; Borken & Matzner, 2009; Unger et al., 2010).

Following the dry season in early to mid-August where precipitation was sparse, temperatures were high, and moisture was low, more frequent considerable (> 5 mm/hour) precipitation events began at the end of August (fig. 17). The first of these precipitation events occurred on August 28th-30th, where rapid increases in soil moisture content (~10% VMC increase over 28 hours) corresponded to decreases in soil [O_2] (~0.30% at 50 cm) as well as increases in soil [CO_2] (~0.35% at 50 cm) at the shoulder (fig. 17). The changes in soil gas concentration were accentuated at depth, and peaks in soil [CO_2] at 10 and 50 cm depths lagged behind the moisture content peaks by 12 and 16 hours, respectively. Along with these changes in soil gas concentration, there was an 88 kg ha^{-1} day^{-1} increase in CO_2 surface emissions and a 42 kg ha^{-1} day^{-1} increase in the magnitude of O_2 influx where the peaks/troughs in surface fluxes lagged behind the peak in moisture content by roughly 18 hours. Thus, reintroduction of sufficient moisture content appears to have revitalized soil respiration, resulting in rapid CO_2 production, O_2 consumption, and temporarily elevated CO_2 emissions. However, the introduction of moisture content also likely plays a role in displacing O_2, contributing to diminished soil [O_2].

Following the initial re-wetting event, subsequent precipitation events contributed to the overall increasing moisture content. Similar precipitation events to that of August 28th-29th occurred on September 5th and 8th. The magnitude of the CO_2 surface flux reached decreased over the course of these events, with the greatest change in surface flux magnitude occurring with the event on September 5th (fig. 17). The differences in CO_2 emission rates and magnitudes between these three re-wetting events are possibly a result of multiple factors: a larger wetting

event can result in greater physical redistribution of organic material, resulting in a larger respiration pulse (Lado-Monserrat et al., 2014); increased moisture content can limit gas transportation, allowing for accumulation; and the amount of CO_2 released after a wetting event can decrease with increasing number of recently previous events (Fierer & Schimel, 2002).

During these rewetting events, soil [CH_4] followed similar trends to those of soil [O_2], although at a smaller relative magnitude, increasing towards atmospheric levels following precipitation events, with changes accentuated at depth (fig. 18). For example, depleted O_2 concentrations increased from 19.55% on September 8th to 20.76% by September 10th at 40 cm depth, while CH_4 concentrations increased from 0.095 ppm to 0.59 ppm over the same time period, at the same depth (fig. 17, 18). Similar to O_2, CH_4 influxes increased in magnitude during these periods of depleted soil gas concentrations. For example, CH_4 surface influxes increased in magnitude from $1.15x10^{-3}$ kg ha^{-1} day^{-1} on September 6th to $1.18x10^{-2}$ kg ha^{-1} day^{-1} on September 8th (fig. 18). Increasing soil [CH_4] cooccurring with increases in soil [O_2], as well as the nature of CH_4 and O_2 influxes supports the concept of methane's main source being transport from the surface (along with O_2). Consumption of CH_4 via methanotrophy will also contribute to decreasing O_2 concentrations and increasing CO_2 concentrations, although to a lesser degree compared to soil respiration.

Peaks in subsurface [N_2O] occur along with the peaks in soil [CO_2] brought on by these wetting events. For example, from September 8th to 9th, CO_2 concentrations increased from 1.18% to 1.44% at 40 cm depth, while N_2O concentrations increased from 0.38 ppm to 0.60 ppm (fig. 17, 18). Soil [N_2O] increasing with soil [CO_2] suggests that deficiencies in O_2, brought on by displacement via increased moisture content as well as by consumption via soil respiration and methanotrophy, can promote production of N_2O via nitrification (and potential production of N_2O via denitrification at saturated and anaerobic locations - either microsites, or at greater depths (Smith et al., 2018; Schindlbacher et al., 2004; Wen et al., 2016)). However, the changes in soil [N_2O] were only correlated with small changes in N_2O surface fluxes. For example, N_2O surface fluxes increased from ~0 on September 10th to $1.14x10^{-3}$ kg ha^{-1} day^{-1} on September 11th in response to the subsurface concentration increase on September 8th-9th (fig. 18). This correlation between soil [N_2O] changes and the lack of large changes in N_2O surface emissions suggests that N_2O might be consumed as it is produced and transported through the soil, potentially where anaerobic microsites allow for anaerobic denitrification (producing N_2 from N_2O) (Wen et al., 2016), or where reactions with minerals in the soil might occur (Chapuis-Lardy et al., 2007).

As many precipitation events are often paired with low atmospheric pressure, it is important to note the potential influence of barometric pumping as well as the aforementioned rewetting effects on CO_2 emissions. For example, during the rewetting event from August 28th-30th, there was a corresponding drop in atmospheric pressure from 101.72 kPa to 99.95 kPa (fig. 17, 18). This drop in pressure associated with the precipitation event and soil rewetting may have accentuated the CO_2 surface emissions. Similarly, the increase in subsurface concentrations of CO_2 and N_2O can be a result of the combination of increased production, as well as low barometric pressure drawing up soil gas from greater depths (where soil [CO_2] and soil [N_2O] are higher, and soil [O_2] is lower).

Where the bank is composed of more permeable soils with overall lower average moisture contents, its subsurface concentrations are more sensitive to the combination of short-term changes in transport mediating factors such as changes in soil moisture, prompted by these wetting events, and barometric pressure. As a result, the bank subsurface concentrations show more short-term variance (fig. 19). With fewer precipitation events resulting in increased moisture content at the bank compared to the shoulder, changing barometric pressure has more of an influence here on subsurface concentrations and surface fluxes. For example, there are no peaks in moisture content at the bank associated with the precipitation events on September 5th and 8th (fig. 19).

Increased moisture content at the shoulder is observed to drastically inhibit gas exchange between the soil and atmosphere for over a week, following a large precipitation event on September 15th, resulting in accumulation of soil [CO_2], depletion of soil [O_2], and elevated soil [N_2O]. On September 15th, soil moisture content rose 3.9% per hour to 37.5% at 10 cm and remained at an average of 31.84% while CO_2 surface emissions decreased and remained near zero with little variation until September 25th at the shoulder (fig. 17). While CO_2 diffusive surface fluxes remained stagnant from September 15th to 25th, CO_2 subsurface concentrations steadily increased $1.77x10^{-3}$%/hour to 1.05% at 10 cm, and $3.85x10^{-3}$%/hour to 2.07% at 40 cm (fig. 17). Similarly, soil [N_2O] increased from 0.32 ppm on September 15th to 1.09 ppm on September 25th at 40 cm at the shoulder (fig. 18).

During this overall accumulation of CO_2 and depletion of O_2, there can be a discrepancy in the magnitude of short-term subsurface replenishment with atmospheric gas between O_2 and CO_2. O_2 diffusive surface influxes during this 10 day period from September 15th to 25th had decreased in magnitude, and were often observed as positive (effluxes), where these measured positive fluxes are likely an artifact of the chamber method which does not adequately take advective fluxes into account (Maier et al., 2012) (fig. 17). While O_2 diffusive surface fluxes were low, soil [O_2] generally decreased, where this gradual decrease in soil concentration occurs with short periods of sharp decrease and increase (fig. 17). For example, within the overall decreasing trend from September 15th to September 25th, soil [O_2] at 40 cm decreased at a rate of $3.3x10^{-2}$%/hour to 17.98% from September 15th to 17th, immediately followed by an increase at a rate of $5.5x10^{-2}$%/hour to 20.57% by September 18th. This was then followed by a similar event, reaching its minimum soil [O_2] by September 21st. Corresponding with these rapid increases in soil [O_2] are increases in the magnitude of O_2 influxes and increases in barometric pressure. Corresponding to the depleted soil [O_2] levels are relatively low barometric pressures, peaks in soil [N_2O], and small peaks in soil [CO_2] within the overall steady soil [CO_2] and [N_2O] increases (fig. 17, 18). The large increases in O_2 and relatively small CO_2 decreases during these events in September suggests a potential difference in response to transport influencing factors between CO_2 and O_2. On September 25th, efficient soil gas transport resumed, resulting in an abrupt increase in CO_2 surface emissions from 3.44 kg ha^{-1} day^{-1} at 15:02 to 190.70 kg ha^{-1} day^{-1} at 19:02, and the return of soil gas concentrations to levels observed prior to September 15th, where soil [CO_2] decreased from September 25th until October 2nd at a rate of $3.9x10^{-3}$%/hour to 0.5% at 40 cm.

Drastic changes in subsurface [CH_4] were observed at the bank in May and November, but were not observed at the shoulder, likely due to the difference in proximity to a rising water

table (fig. 8). Although no moisture content data exists for the event in May, the event in November corresponds with the large increase in moisture content (accentuated at depth) associated with the rising water table. Soil [CH_4] at 30 cm rose from 2.5 ppm to 13.5 ppm over 41 hours from November 18th to 19th while moisture content increased 4.3%, [CO_2] decreased 0.14%, and [O_2] increased 0.3% at 30 cm depth (fig. 8). On November 18th the tube sampling from 50 cm was removed due to saturation at this depth. From its peak on November 19th, soil [CH_4] at 30 cm decreased much more gradually following the abrupt increase, reaching concentrations of 2.7 ppm by November 25th. CH_4 effluxes and production are known to be related to water table depth, where emissions are greater with a shallower water table (Itoh et al., 2008; Jacinthe et al., 2015). However, in this case, CH_4 surface fluxes remained inward despite elevated soil [CH_4] (fig. 10).

The CH_4 pulse could be a result of rapid transport of CH_4 produced at unobserved depths, where ebullition can rapidly transport CH_4 produced at depth towards the surface at a rate greater than that of oxidation (Smith et al., 2018, Serano-Silva et al., 2014). Physical soil properties can trap this CH_4 pulse at shallow depths (30 cm) where it is more gradually consumed by methanotrophy in the presence of higher levels of labile organic matter and O_2, or subsequently gradually transported elsewhere. Atmospheric pressures increased from 99.92 kPa on November 18th to 101.94 kPa on November 19th, while the soil [CH_4] was increasing. These increasing pressures would act against the upward transport of CH_4.

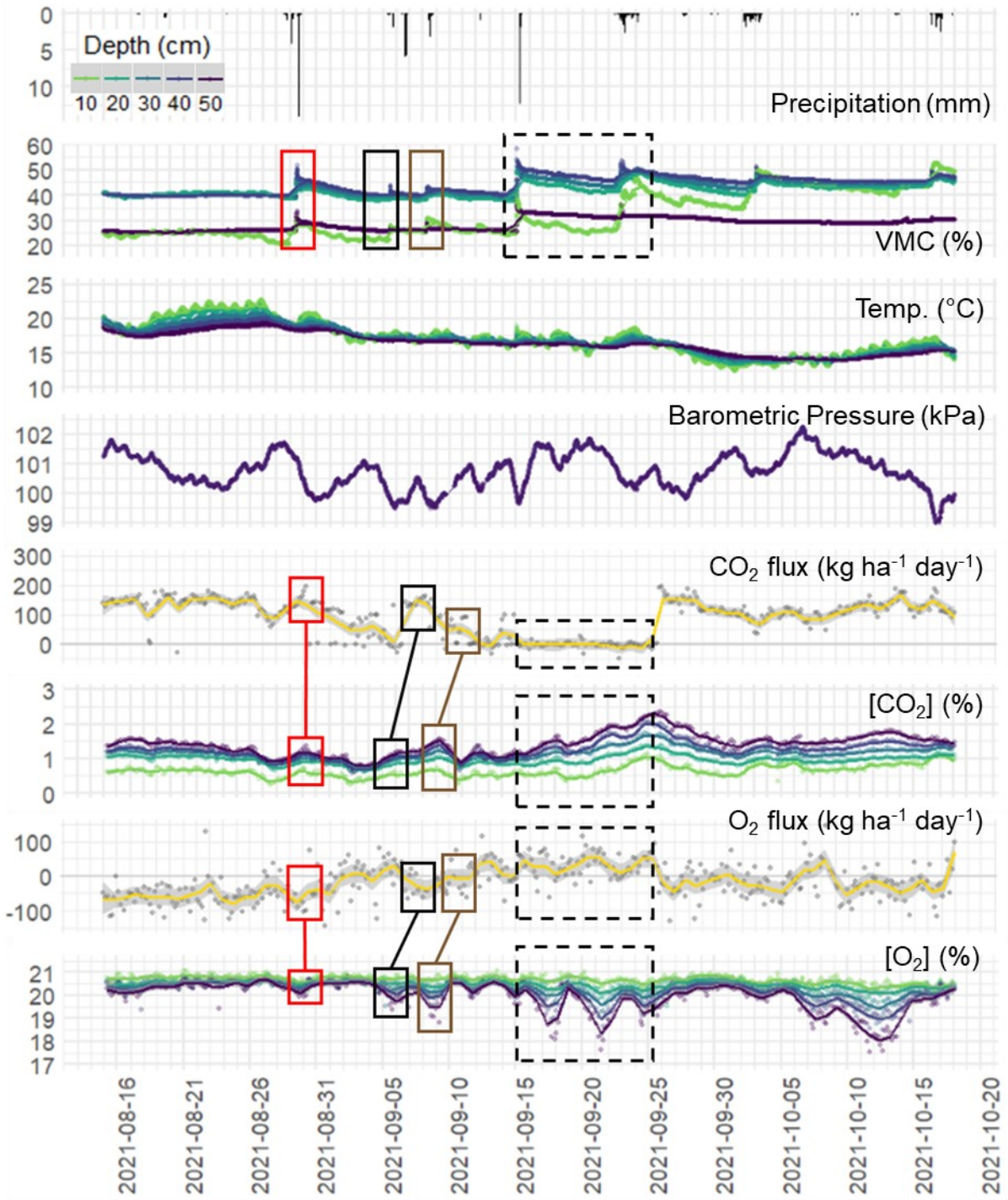

*Figure 17: **Shoulder** CO_2 and O_2 soil gas concentrations and chamber method surface fluxes along with barometric pressure and soil moisture and temperature during rewetting period. The points represent the data collected, while the lines show smoothed trends based on LOESS (local polynomial regression fitting) functions, and the grey areas surrounding these trendlines represent the 0.9 confidence interval. Boxes and connecting lines show events described above; where red denotes the events related to the August 28th- 30th wetting event, black denotes the September 5th wetting event, brown denotes the September 8th wetting event, and the dashed box denotes the period from September 15th-25th where surface fluxes are inhibited*

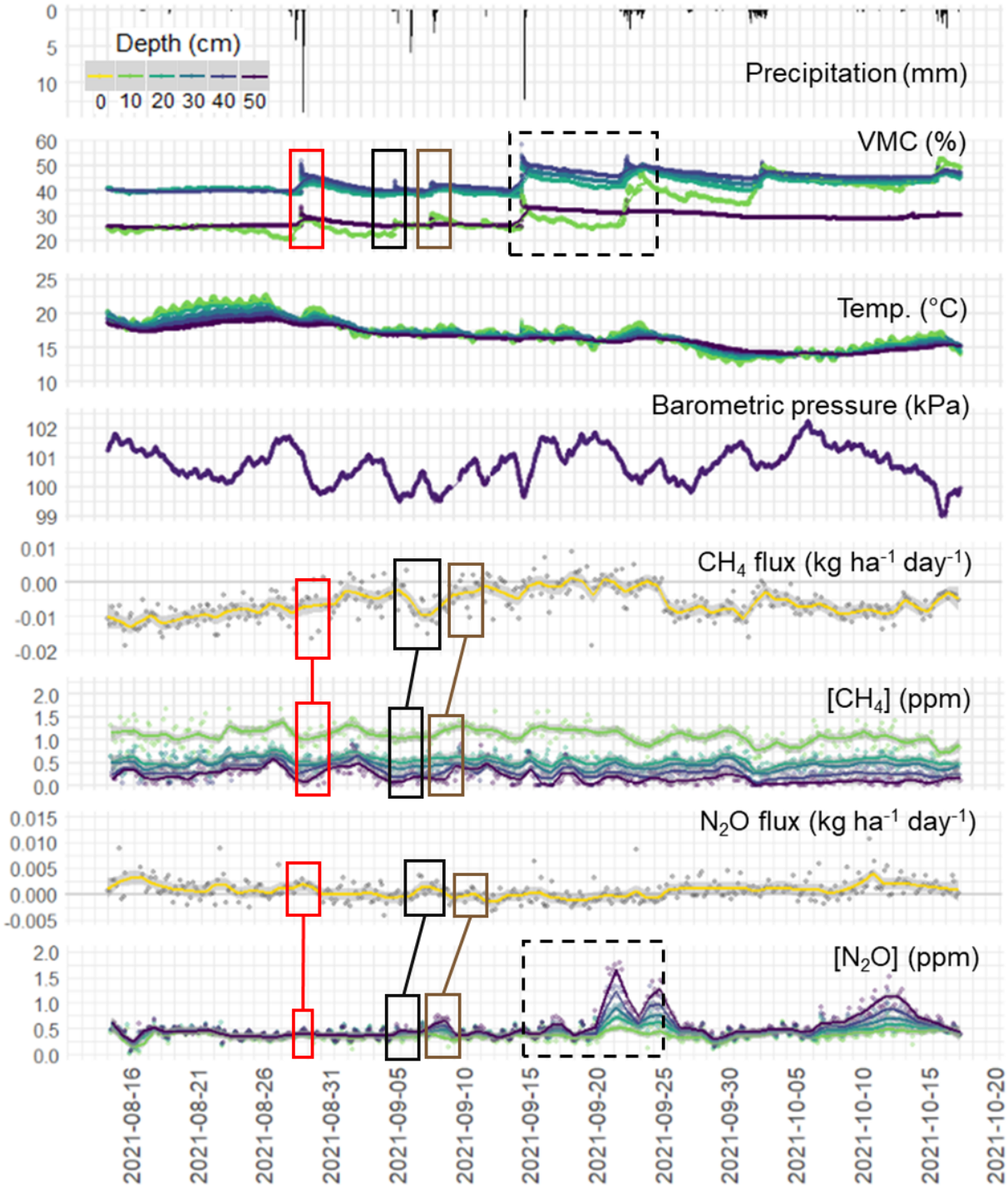

*Figure 18: **Shoulder** CH_4 and N_2O soil gas concentrations and chamber method surface fluxes along with barometric pressure and soil moisture and temperature during rewetting period. The points represent the data collected, while the lines show smoothed trends based on LOESS (local polynomial regression fitting) functions, and the grey areas surrounding these trendlines represent the 0.9 confidence interval. Boxes and connecting lines show events described above; where red denotes the events related to the August 28th- 30th wetting event, black denotes the September 5th wetting event, brown denotes the September 8th wetting event, and the dashed box denotes the period from September 15th-25th where surface fluxes are inhibited*

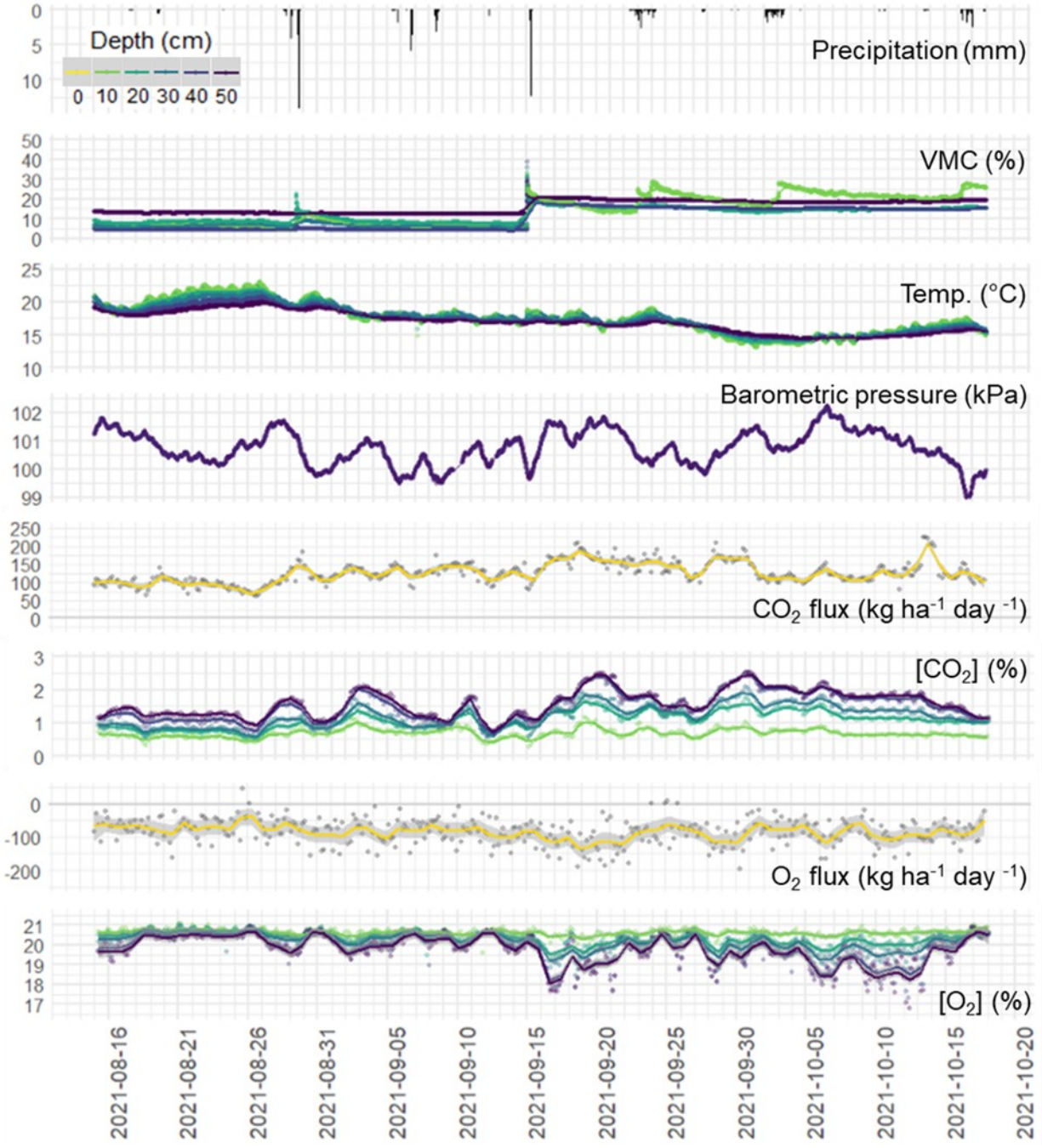

*Figure 19: **Bank** CO_2 and O_2 soil gas concentrations and chamber method surface fluxes along with barometric pressure and soil moisture and temperature during rewetting period. The points represent the data collected, while the lines show smoothed trends based on LOESS (local polynomial regression fitting) functions, and the grey areas surrounding these trendlines represent the 0.9 confidence interval.*

5.5.3 Role of temperature in diurnal variation:

Differences in production rates at the diurnal scale have been observed to be the result of photosynthetically active radiation triggering the autotrophic component of soil respiration, reaching a maximum earlier in the day compared to temperature, which the heterotrophic component of soil respiration primarily responds to, creating diurnal variations in the balance between transport and production (Riveros-Iregui et al., 2007). Examples of this short-term hysteresis at the shoulder location are highlighted in fig. 20, and show different behaviours depending on depth, average temperature, and moisture content. At each depth, the magnitude of the soil [CO_2] change within a diurnal hysteresis pattern will increase with increasing moisture content (Riveros-Iregui et al., 2007). As depth increases, these hysteresis loops change shape as temperature changes are dampened; as inhibited transport promotes CO_2 concentration changes, uncompensated by transport rates as seen near the surface; and as the lag between photosynthetically active radiation and temperature increases with distance from the surface (Riveros-Iregui et al., 2007).

At 10 cm depth, the hysteresis loops commonly occur over one to two days, and show significant soil [CO_2] variation (as well as temperature variation) over this short time period (for example, a concentration range of 0.11%, and a temperature range of 1.2ºC was observed from July 4th at 03:00 to July 5th at 03:00) (fig. 20). At 40 and 50 cm, these hysteresis loops more often span a longer time period (often two to three days) and show a larger ratio of change in soil [CO_2] to change in temperature, where, for example, a 0.32% soil [CO_2] change was observed over a 0.23ºC temperature change at 40 cm depth (from July 15th at 15:14 to July 17th at 20:30). At all depths, hysteresis loops span longer periods of time in September and October, when moisture contents were greatest, and few clear hysteresis loops were observed in August, where soil moisture was relatively low and there were few precipitation events.

These hysteresis loops typically show clockwise trends, where autotrophic respiration dominates during the increasing trend of soil [CO_2] with temperature, and where heterotrophic respiration dominates during the decreasing trend of CO_2 with temperature. Counter-clockwise hysteresis loops, as observed by Parkin & Kaspar (2003) and Xiaolu et al. (2020), were occasionally seen at all depths. At 10, 20, 30, and 50 cm depths at the shoulder location, a large counter-clockwise hysteresis loop spanning September 22nd-26th was observed (fig. 21). A vast majority of the hysteresis loops observed at 20 cm depth also travelled counter-clockwise, where these counter-clockwise patterns may be indication of less significant contributions from autotrophic respiration (Riveros-Iregui et al., 2007). The gleyed clay layer which exists directly below the 20 cm sampling tube may inhibit autotrophic respiration, where it has been observed that a negative correlation exists between soil clay content and soil autotrophic respiration (Xiaolu et al., 2020). The event from September 22nd to 26th corresponds to a rewetting event, potentially indicating changes in autotrophic respiration capability with increased soil moisture content.

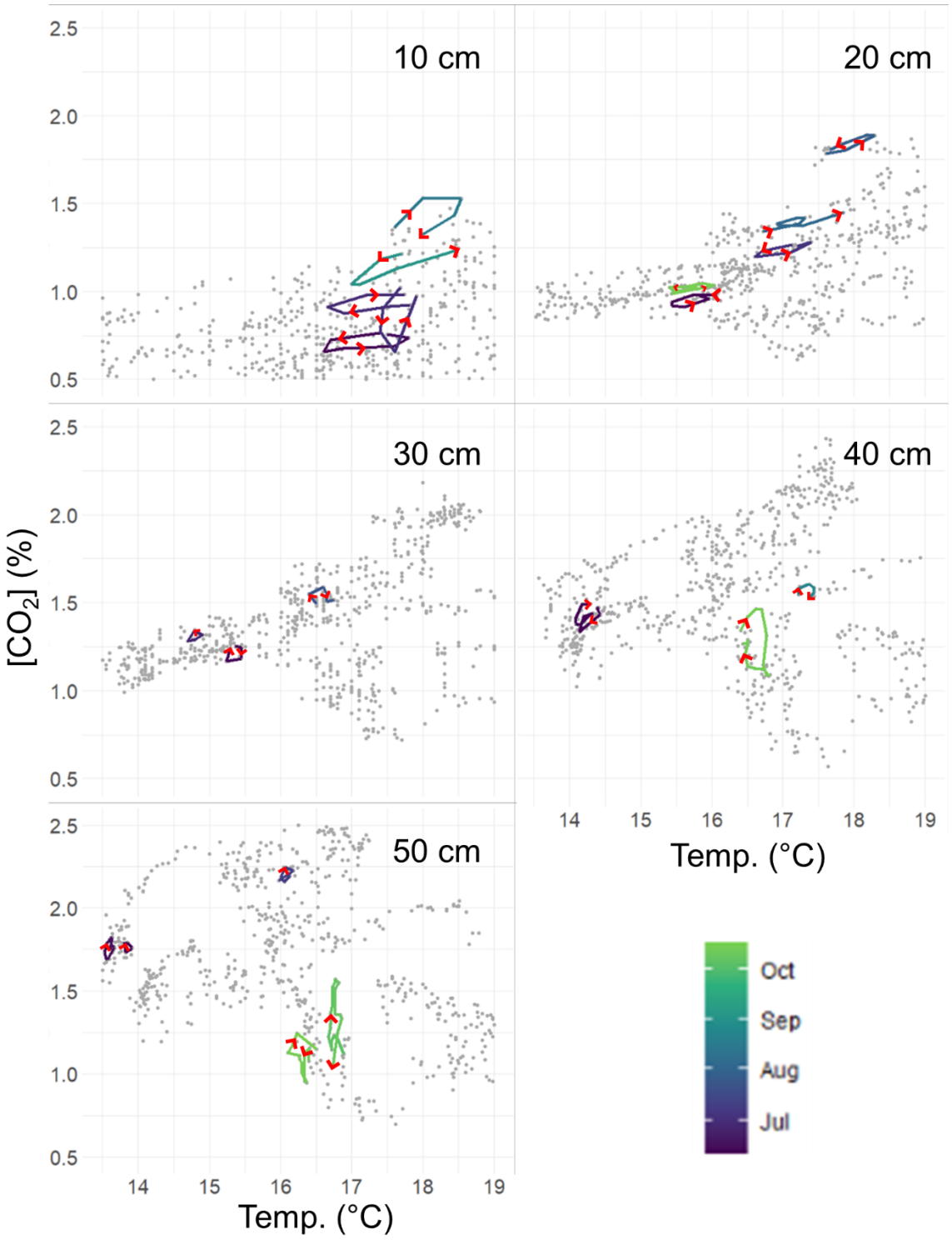

*Figure 20: Hysteresis patterns highlighted at all depths at the **shoulder** by coloured lines with red arrows denoting the passage of time. Grey points represent the entire dataset collected.*

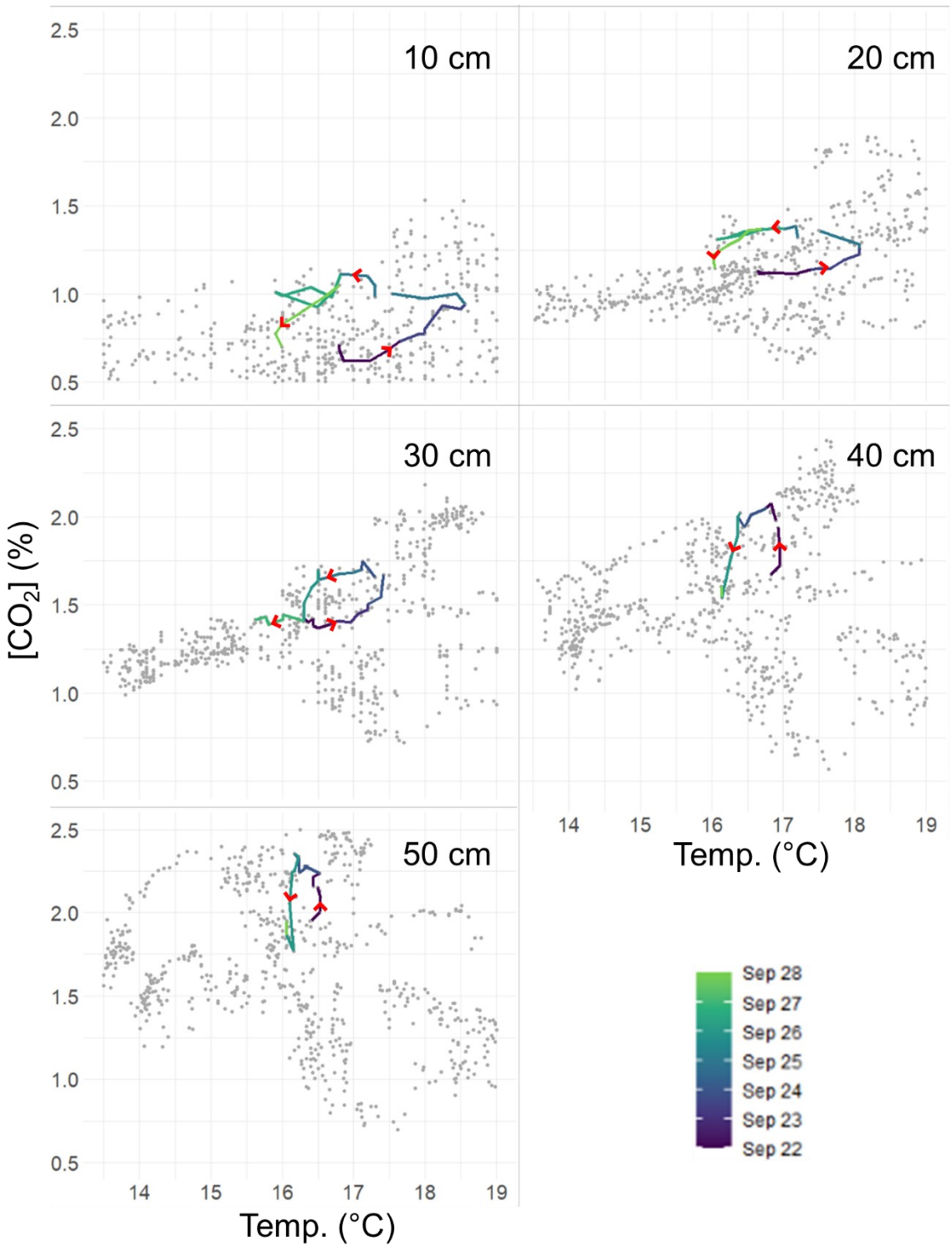

*Figure 21: Counter-clockwise CO_2 hysteresis with temperature at all depths at the **shoulder**. Similar to figure 20, grey points represent the entire dataset collected, and hysteresis is highlighted by coloured lines with red arrows to denote the passage of time.*

5.6 SIGNIFICANCE OF TEMPORAL SCALES

Wavelet analysis of subsurface gas concentrations and surface fluxes over time at the shoulder and bank helps highlight and compare the significance and contribution of long and short-term trends to the overall time series observed. At both the shoulder and bank, soil [CO_2] showed the strongest long-term trends compared to the other gases, at periods of 3-6 months (~2,000 to 4,000 hours), likely due to the dependency of soil [CO_2] on seasonal variations in moisture content (fig. 22, 23). The lack of a strong seasonal trend in soil [O_2] compared to soil [CO_2] displays a difference in production/consumption and transport between the two gases. Although O_2 generally displays a mirrored trend to that of CO_2, there is a discrepancy between the production/accumulation of CO_2 and the consumption of O_2, where soil O_2 is replenished at a faster rate than CO_2 can be transported to the surface. This dampens any seasonal trend in soil [O_2] that would be expected based on the seasonal trend in soil [CO_2] production and accumulation.

More power exists in soil [CO_2] trends at the bank at the mid to short-term scale (roughly 64 to 512 hour (2.5 to 21 day) periods) compared to the shoulder, especially in the rewetting period from September to October, where these periods gain more power as depth increases (fig. 22, 23). The higher power at these mid to short-term periods at the bank is a result of the drier, more permeable soils at the bank being more sensitive to, and showing quicker and higher amplitude responses to, changes in moisture and barometric pressure. This power is amplified with depth from September to October, as the balance between increased soil respiration and decreased gas transport brought on by increased moisture content during these wetting events results in a concentration variation of a greater magnitude at depth. Similarly, soil [O_2] at depth showed the most power during this rewetting period at both the shoulder and bank. This is when the greatest O_2 deficiencies were observed (due to the combination of increased soil respiration productivity and inhibited gas transport), and thus the greatest rates of replenishment. The magnitudes of the deficiencies and subsequent replenishment were exaggerated at the shoulder (and at depth) due to increased moisture content and limited transport, and thus these events hold more relative power compared to at the bank (and compared to shallower depths, also due to the larger difference between atmospheric gas and soil gas at depth).

The powerful seasonal trends in soil [CO_2] also manifests in surface fluxes, still bearing more power at the shoulder compared to the bank (fig. 22, 23). However, there are no apparent regular diurnal patterns in CO_2 surface fluxes at the shoulder or the bank (no consistent power at this time scale), where significance is only given to brief moments in surface fluxes at these short timescales. These brief moments of ‘powerful’ surface flux are less frequent but carry more power at the shoulder, as the soil properties and exposure to moisture content changes potentially allows for greater soil respiration, as well as the accumulation of soil CO_2 and thus greater contributions to the atmosphere over short periods of time upon release by changing conditions. Similarly, O_2 influxes are more consistent over time, where the power is spread out over a larger number of events.

With respect to CH_4 and N_2O subsurface concentrations and surface fluxes, short-term trends carry the most power at both the shoulder and bank (fig. 22, 23). The most powerful trends associated with soil [N_2O] from 10 to 20 cm depth at both the shoulder and bank occur at periods ranging from 16 to 32 hours, with the greatest power in May and November while water table levels were high. As depth increases, more power is attributed to trends at periods ranging from 32 hours to 21 days, specifically in September and October, when moisture contents were high and soil [O_2] was low, contributing to the production and accumulation of soil [N_2O].

Similar trends in power to those in soil [N_2O] were observed in soil [CH_4] at the shoulder, where the most power was attributed to periods ranging from 8 to 64 hours in shallow soils, and as depth increased, periods up to 11 days gained power. At shallower depths (10-30 cm), the events carrying the most power were the rapid influx events associated with changes in barometric pressure under dry conditions in mid-August, at periods from 16-32 hours. At greater depths (50 cm), however, the power of these dry period influxes diminished, and rapid CH_4 increases related to drainage/drying following the first rewetting event carry the most power at periods from 32-64 hours (in early September). At the bank, the soil [CH_4] pulses related to the rising water table in May and November overpower any of the other short-term events in the wavelet analysis. Both soil [N_2O] and soil [CH_4] show powerful mid to long-term variations at depth related to seasonally wet conditions (potentially due to increased anaerobic production), and show powerful shorter-term variations associated with changes in soil gas transport, whether due to a rising water table (which will potentially induce increased anaerobic production as well as influence transport), or barometric pressure influences during the dry season (CH_4).

The most powerful CH_4 and N_2O surface flux events do not correspond to the most powerful subsurface concentration events. Where it is understood that a significant proportion of N_2O and CH_4 emissions can be a result of short-term events (hotspots/moments), it is important to note the ability of processes in the soil to dampen or prevent emissions related to subsurface concentration increases at the scale observed in this study (Amadi et al., 2016; Lemke et al., 1998; Groffman et al., 2009). CH_4 surface fluxes showed more power at longer time periods (up to 11 days) at both the shoulder and bank compared to N_2O, which most consistently showed the highest power at diurnal time periods (16-32 hours). Powerful variations in CH_4 and N_2O surface fluxes occurred in mid-July, related to significant precipitation events, when soil-gas transport is inhibited. These variations occurred at 32-64 hour periods at the shoulder, and 16-32 hour periods at the bank, demonstrating a more rapid recovery of permeable bank soils to changing soil moisture content.

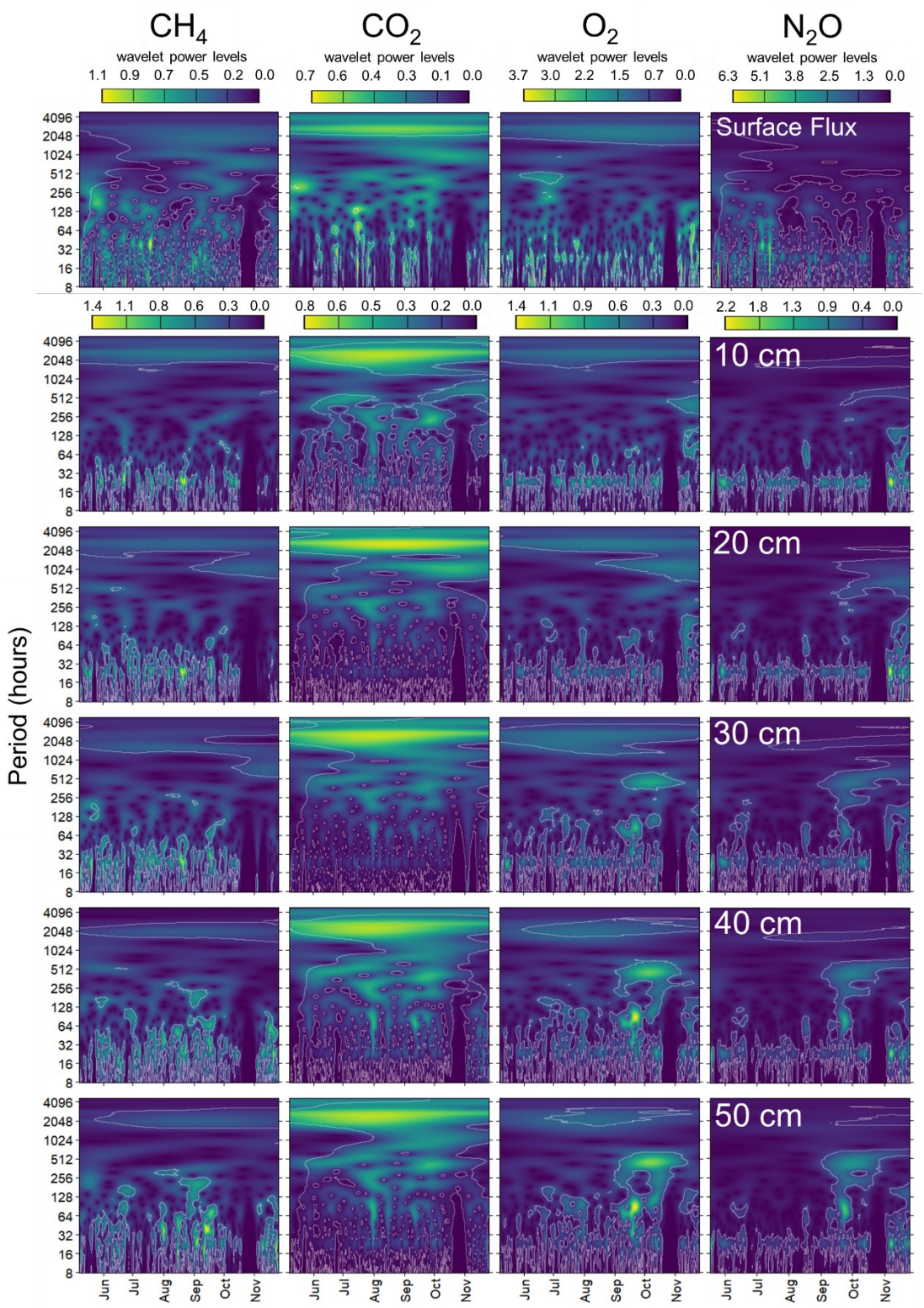

*Figure 22: Wavelet analysis of subsurface gas concentrations (at all depths) and surface fluxes over the entire study period at the **shoulder**, showing relationship between power of certain periodic trends over time. Grey lines represent where the p-value = 0.05, the null hypothesis being that there is no periodicity.*

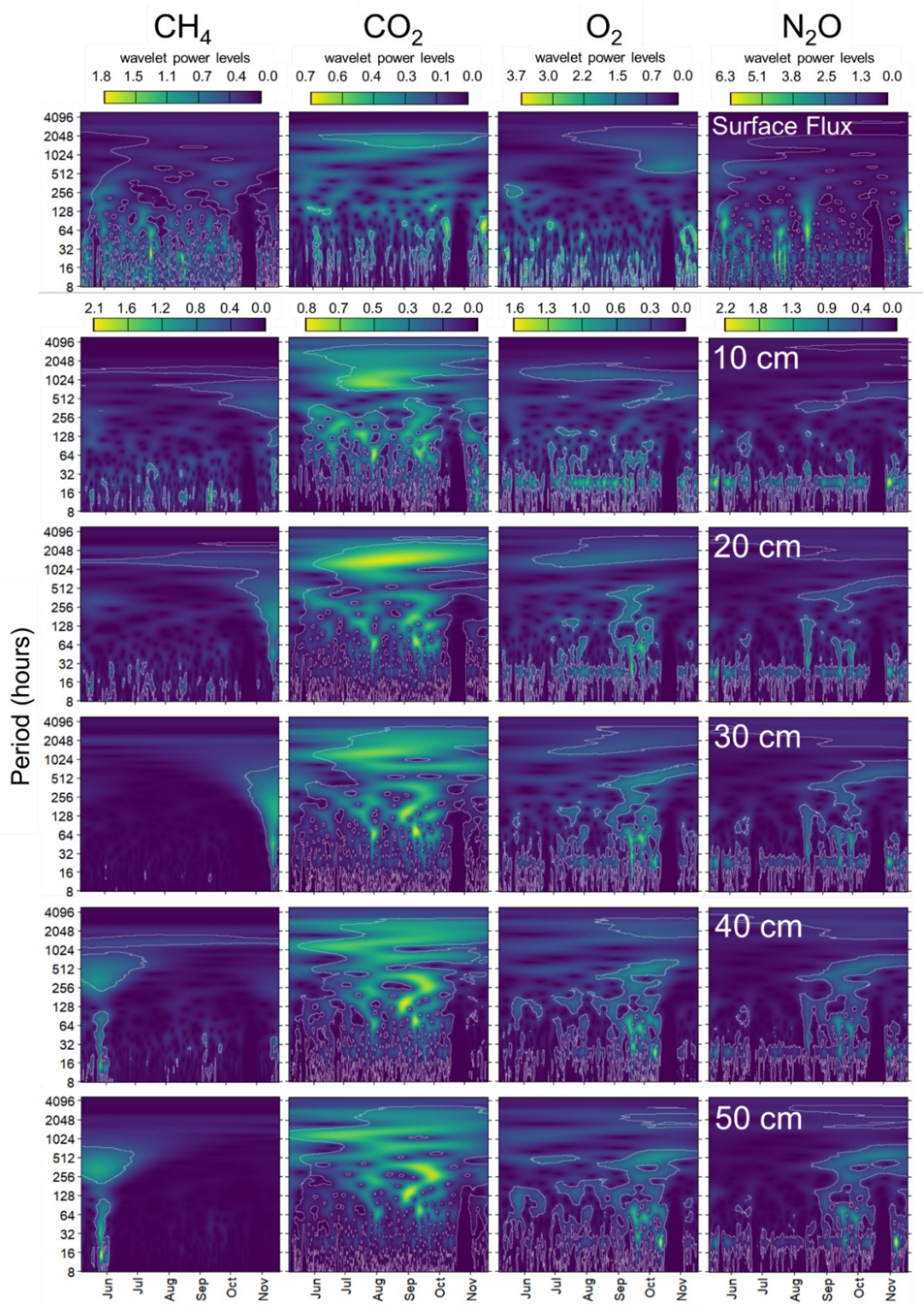

*Figure 23: Wavelet analysis of subsurface gas concentrations (at all depths) and surface fluxes over the entire study period at the **bank**, showing relationship between power of certain periodic trends over time. Grey lines represent where the p-value = 0.05, the null hypothesis being that there is no periodicity.*

5.7 SIGNIFICANCE OF TRANSPORT PROCESSES

It is evident that the balance which exists between the array of soil GHG controlling parameters changes over the agronomic season, variably influencing significant short-term subsurface concentration changes and surface flux events. The importance of considering gas transport when aiming to understand short-term variations in soil gas is highlighted in this study in measuring barometric pressure, moisture content, and subsurface gas concentrations along with the surface fluxes. Many soil GHG studies attribute surface fluxes directly to GHG production, neglecting complex and temporally sensitive subsurface gas concentrations and transport. For example, high time resolution studies have observed variations in GHG surface fluxes over relatively constant temperature and moisture content, and attributed these variations to biogeochemical variations or miniscule soil moisture variations, as barometric pressure and subsurface gas concentration measurements were absent (Vidon et al., 2015). This study is able to make the connection between soil gas concentration and surface flux variations (over relatively constant soil moisture and temperature), and changes in barometric pressure, exaggerated during the dry season.

Previous studies that have taken subsurface concentrations of O_2 and GHGs into account along with GHG surface fluxes, have observed short-term increases in soil [O_2] correlated with decreases in soil [CO_2] and [N_2O], as well as increases in CO_2 surface fluxes, similar to what was observed in this study during the wet periods following supressed CO_2 surface emissions (on September 25th) (Jarecke et al., 2016). Jarecke et al. attributed these events to changes in soil transport processes associated with soil drainage. However, during the dry period in August, we observed a decrease in CO_2 emissions associated with the soil [O_2] increases, and were able to attribute these changes to increases in barometric pressure, where such scenarios and explanations are absent in previous studies.

Other high time resolution studies have focused on CH_4 emissions while measuring water table dynamics (Jacinthe et al., 2015). Jacinthe et al. found that water table depth was the dominant control on CH_4 emissions, where flooding events (high water table) correlated with increased emissions. Occasionally, however, flooding events would not correspond with increased CH_4 emissions, leading the authors to believe that, in these cases, oxidation consumes soil [CH_4] before it is emitted, but lacked the subsurface gas concentration measurements to confirm this theory. Our observations strengthen their argument, where large measured increases in soil [CH_4] do not always correspond to surface emissions, and would occur when water table levels were high. Smaller short-term changes in CH_4 surface fluxes observed in this study also agree with the literature, where influx rates increase as moisture content decreases (similar to O_2), due to promoted aeration (Subke et al., 2018).

Our observations agree with other studies showing that N_2O emissions and subsurface concentration trends are mainly controlled by short-term events (Amadi et al., 2016; Lemke et al., 1998). However, our data shows the frequency and magnitude at which soil [N_2O] can vary without resulting in large increases in surface emissions. Our data also provides evidence of the largest N_2O emissions occurring during the dry season (rather than spring or fall freeze thaw events, when they are often observed (Groffman et al., 2009; Amadi et al., 2016; Lemke et al.,

1998)), unprovoked by drastic changes in soil moisture or temperature, potentially influenced by changing soil gas dynamics triggered by changes in barometric pressure.

5.8 CONTRIBUTIONS OF SHORT-TERM EVENTS TO OVERALL EMISSIONS

Both the shoulder and bank, overall, were CH_4 sinks, and sources of CO_2 and N_2O. The bank was responsible for sequestering 1.16 g CH_4/m^2, and emitting 19.51 kg CO_2/m^2 and 44.05 mg N_2O/m^2, while the shoulder was responsible for sequestering 1.20 g CH_4/m^2, and emitting 20.77 kg CO_2/m^2 and 235.37 mg N_2O/m^2 (over the entire study period). Despite more frequent, high magnitude, short-term variations in surface fluxes at the shoulder compared to the bank, total CO_2 emissions were similar from both locations. This suggests that the differences in temporal trends are largely due to differences in soil gas transport rather than overall soil gas production, and thus do not result in differences in total CO_2 efflux over the study period. Soil gas transport is more efficient at the bank, where diffusion through gas (rather than through water) is more common, allowing for rapid diffusive exchange of gases between the soil and atmosphere and thus less frequent drastic surface flux variations. With higher moisture content and lower permeability at the shoulder, there are more frequent and prolonged events where soil gas transport is inhibited, followed by higher magnitude, rapid release of accumulated soil gas.

This variation is important to consider when measuring soil gas over time. If surface flux was measured biweekly, as is often done in long-term or seasonal studies, the actual variation which exists can easily lead to a range of interpolated total flux values. By selecting sample cycles from this study 14 days apart, linearly interpolating between them, and offsetting the simulated starting sampling date by 24 hours over 8 iterations, 8 simulations of biweekly sampling field programs have been created. The results show a larger range of overall emissions from the shoulder compared to the bank due to the higher variability in surface fluxes (fig. 24). The emissions calculated based on high-time resolution data show CH_4 emissions within the range of simulated sums (within Q_1 and Q_3 at the bank, and within the overall max. and min. at the shoulder), and CO_2 emissions generally higher than the simulated sums (fig. 24). High time resolution sampling will capture CO_2 emission pulses associated with increased production and wetting events, or associated with rapid release of accumulated CO_2. If biweekly sampling happens to capture one of these frequent short-term elevated CO_2 emission events, then the overall emissions might be overestimated, as seen in the outlier in fig. 24. However, if these short-term events are missed, then overall emissions might be underestimated. N_2O showed the most variation based on these biweekly sampling simulations, where N_2O emissions are heavily dependent on irregular short-term events, as seen in the wavelet analysis (fig. 22, 23).

These simulated sampling programs showed a significant range in overall flux sums, but the actual, high time resolution values are within, or close to, these ranges. Simulated biweekly CO_2 sampling resulted in total sums ranging from -28% to +5% of the high time resolution sampling sum at the shoulder, and from -15% to -2.5% at the bank (fig. 24). CH_4 biweekly simulations resulted in surface influxes ranging from +34% to -4.6% at the shoulder, and +17% to -22% at the bank. N_2O simulations showed the most variation, from -99% to +99% of the high time resolution sampling at the shoulder, and up to +1,163% at the bank (fig. 24). Thus, relatively reasonable estimates of CO_2 and CH_4 surface fluxes could be acquired based on a

biweekly sampling program, yet the more sporadic nature of N_2O surface fluxes and lack of seasonal trends make the actual contributions to the atmosphere difficult to capture at this biweekly sampling resolution.

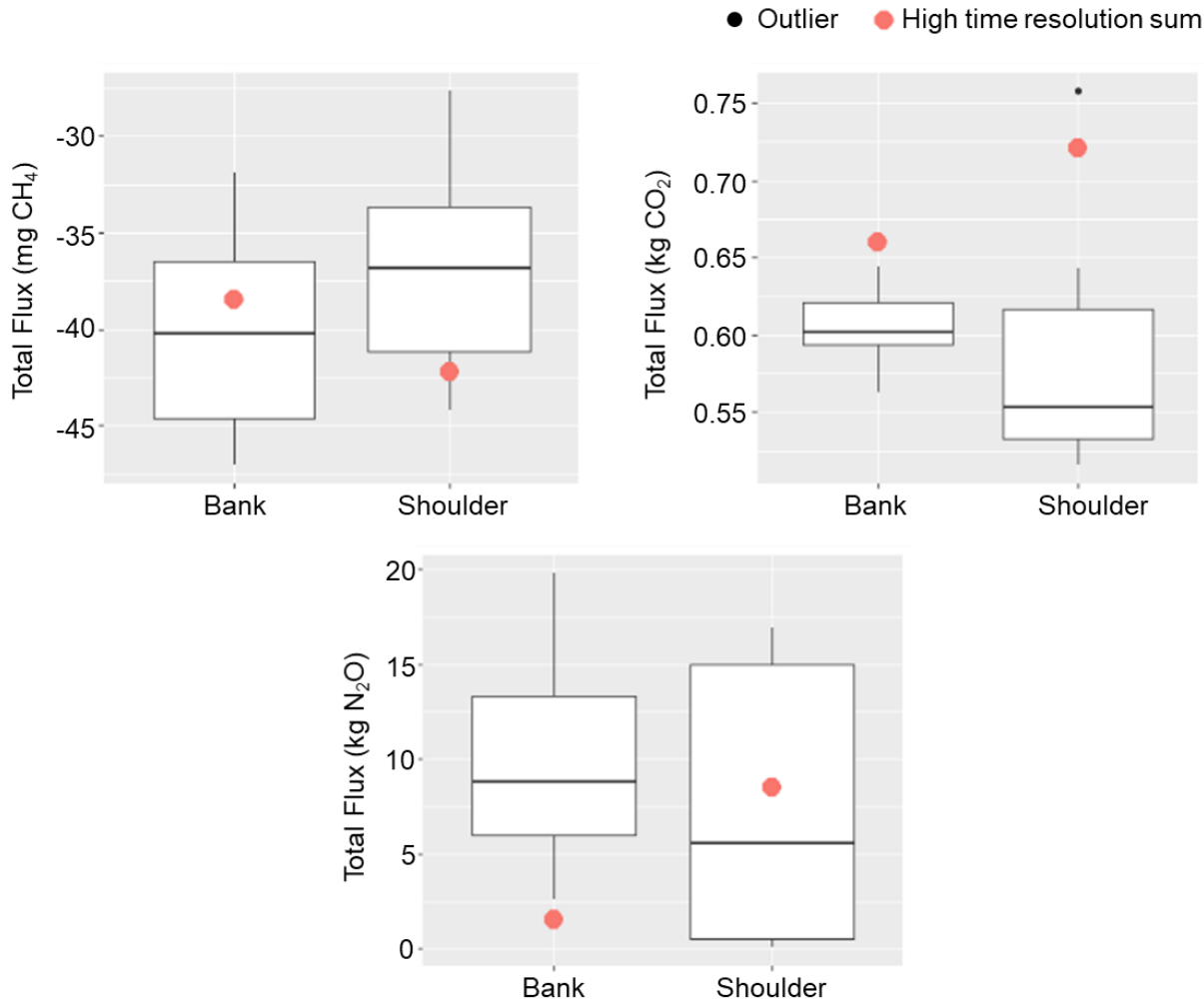

Figure 24: Box and whisker plots (showing the 25th percentile (Q_1) and the 75th percentile (Q_3) as the lower and upper bounds of the boxes); the median (Q_2) as the horizontal line within the box; and the maximum and minimum shown at the ends of the vertical lines) comparing the range of biweekly sampling simulation surface flux sums (of CO_2, CH_4, and N_2O) to the surface flux sums calculated based on high time resolution chamber method sampling performed in this study.

6 CONCLUSIONS

The shoulder and bank locations contributed comparable total CO_2 and CH_4 surface emissions over the entire period, where soils were an overall sink for CH_4, and a source of CO_2. Wavelet analysis of CO_2, CH_4, O_2, and N_2O surface fluxes showed seasonal trends were most powerful and significant for CO_2, with the highest emissions during periods of high moisture content. However, irregular short-term events held the most power overall for all gases. Several different types of short-term events (where significant subsurface gas concentration variations can occur over 12 to 65 hours) caused by soil gas production, consumption, and/or transport exist, and often result in changes in surface fluxes.

Rapid increases in soil moisture content will promote soil respiration productivity as well as inhibit soil gas transport, leading to accentuated accumulation of CO_2 and depletion of O_2. Decreasing moisture content following these events (via drainage or evapotranspiration) results in rapid changes in transport, where pathways for rapid diffusion through gas rather than water are more prevalent, and soil gas pressure changes caused by these drying processes can promote influx of atmospheric gas. Inhibited transport via increased moisture content can reach a point where CO_2 surface fluxes remain near zero (for ~10 days in this case) in unsaturated conditions. During these periods of inhibited transport, replenishment of O_2 to the soil from the atmosphere can still occur (associated with changes in barometric pressure), able to maintain soil $[O_2] >$ 16.5%, thus not inhibiting soil respiration. Rapid release of accumulated CO_2 upon reinstatement of transport processes in this case resulted in a 185 kg/ha/day increase in CO_2 emissions over 4 hours. During dry periods, changes in atmospheric pressure can result in rapid replenishment of soil with atmospheric gases (these events taking place over <24 hours), unprompted by changes in soil moisture or temperature. Moments of rapid soil $[CH_4]$ variation are most often associated with changes in pressure (whether changes in soil pressure or atmospheric pressure) where concentrations increase towards atmospheric levels. However, where there is a rising water table, rapid transport of CH_4 produced at greater, anaerobic depths (at concentrations roughly 25x of what was typically observed) can reach the unsaturated zone. In this case, these massive transport events did not reach the surface due to inhibited transport, and CH_4 was gradually consumed (and potentially gradually transported elsewhere) in these near-surface, oxidized conditions. Soil $[N_2O]$ can increase rapidly (up to 1.5 ppm over 36 hours) following precipitation events and increased moisture content, as well as decreased atmospheric pressure, where this pressure change can play a role in causing upward advection of N_2O produced in deeper anaerobic conditions.

The same controls on subsurface gas production, consumption, and transport of moisture content, temperature, and changes in barometric pressure exist at the shoulder and bank, but differences in soil structure and vegetation results in varying responses to these controlling factors. The bank soils are sloped, and better sheltered by the tree canopy, resulting in fewer and dampened short-term increases in moisture content caused by precipitation events. The bank soil is also disturbed, and composed of a higher fraction of sand, resulting in greater permeability. These differences cause the bank to be well drained, and drier overall. This makes the bank more responsive to variations in atmospheric pressure compared to the shoulder, where this sensitivity

to pressure bears the greatest control over N_2O and O_2 at depth. This sensitivity to atmospheric pressure at the bank results in more frequent and drastic short-term variations in subsurface gas concentrations, where transport is not limited by moisture content to the same degree as the shoulder (which shows overall more gradual changes in subsurface concentrations, controlled by production, accumulation and consumption followed by less frequent, but still abrupt, changes in transport).

These differences in subsurface gas behaviour result in differences in temporal variation in surface fluxes. With a more constant and efficient exchange between bank soil and the atmosphere, largely controlled by advective transport and changes in barometric pressure, diffusive surface fluxes show variation at lower magnitudes at the short-term scale compared to the shoulder. The accumulation and release of gases at the shoulder, largely dependent on moisture content inhibiting efficient diffusion results in more drastic seasonal and short-term trends in surface fluxes compared to the bank, due to the higher clay and silt fraction (lower permeability) inhibiting drainage, as well as the increased exposure to abrupt increases in moisture content as there is less protection from the tree canopy. Despite these differences in short and long-term temporal trends, the shoulder and bank show comparable total fluxes over the entire study period, where the bank is responsible for sequestering 1.16 g CH_4/m^2, and emitting 19.51 kg CO_2/m^2, while the shoulder was responsible for sequestering 1.20 g CH_4/m^2, and emitting 20.77 kg CO_2/m^2 over the entire study period. However, the bank was only responsible for emitting 44.05 mg N_2O/m^2, while the shoulder was responsible for emitting 235.37 mg N_2O/m^2, potentially attributed to greater moisture content at the shoulder resulting in a greater density of anaerobic, N_2O producing microsites.

Simulated biweekly sampling over a range of start dates using linear interpolation resulted in ranges in total GHG fluxes. These simulated flux sums varied as much as +1,163% from the high time resolution total of N_2O at the bank, +34% of CO_2 at the shoulder, or as low as -2.5% of CO_2 at the bank. Overall, the simulated total flux ranges were largest at the shoulder, due to the more drastic changes in surface fluxes compared to the bank.

6.1 IMPLICATIONS

By concurrently sampling soil temperature, soil moisture content, and barometric pressure along with soil gas concentrations and surface emissions at a high time resolution, we were able to show how the roles and importance of soil gas controlling parameters vary over time under differing overall environmental conditions. By measuring barometric pressure and subsurface gas concentrations specifically, valuable insights were able to be made regarding the transport component of soil gas behaviour and emissions, which is often neglected in experimental designs. The role of short-term variations in moisture content and barometric pressure in contributing rapid changes in soil gas concentrations or surface emissions varies depending on the season and overall soil moisture content during which these events take place. For example, significant short-term events are often related to changes in barometric pressure, exaggerated in dry soils; and wet periods (in the fall in this case) can lead to inhibited surface fluxes, accumulation of CO_2, and its subsequent large and rapid release. This study highlights the

importance of considering transport processes, by which both of these significant short-term events are strongly influenced.

With overall environmental conditions varying spatially (as well as temporally), differences in short and long-term trends exist between the shoulder and bank. Despite these differences in temporal trends, similar overall CO_2 and CH_4 emissions were measured from the shoulder and bank. The similarity in surface fluxes should be considered in the evaluation of ditch management BMPs, and the role of an arborous riparian microecosystem in contributing to a GHG emission budget.

The presence of variable short-term changes in surface emissions gives rise to the potential of over, or underestimated emissions if a lower sampling resolution is applied. For example, CO_2 flux overestimations will be made if a large rapid efflux event is captured, and underestimations will be made if a majority of these events are missed. Although high time resolution sampling allows for more accurate results, less frequent sampling might be suitable if selective sampling (ex. during and following precipitation events), or short-term simulations are incorporated into the sampling program. However, the presence of barometric pressure influences on surface fluxes must be considered when using the chamber method, as this method likely neglects a proportion of advective flux.

The wide array of field observations collected at a high time resolution during this study, including subsurface concentrations and surface fluxes of multiple gases simultaneously, provides a valuable and unique dataset for calibration of reactive transport models. Models can incorporate this dataset to investigate potential outcomes associated with agricultural practices, i.e., dredging activities, and varying climate conditions while striving towards a better understanding of the processes controlling GHG emissions.

6.2 FUTURE RECOMMENDATIONS

With the importance of pressure driven advective fluxes on short-term soil-gas behaviour in question, high time resolution monitoring of water table dynamics and windspeed difference between the shoulder and bank along with the parameters measured in this study would provide valuable insights into this pressure driven transport component. Similarly, 2-D transport of soil gas driven by these pressure fluctuations should be further investigated, where the same barometric pressure changes at two proximal locations do not result in the same responses of subsurface gas concentrations. It would also prove useful to measure these parameters over an entire year, where significant water table fluctuations and freeze-thaw events might occur further into the spring and fall. In measuring these parameters at the same location, following ditch dredging and vegetation removal, the effects arborous vegetation in riparian zones on soil GHG behaviour can be studied further.

To understand the balance between soil-gas production, consumption, and transport, the discrepancy between soil [O_2] and soil [CO_2] during wet periods should be investigated further. During dry periods, changes in barometric pressure result in large variations in both soil [CO_2] and soil [O_2] toward atmospheric concentrations. However, during wet periods, barometric

pressure changes elicit only small changes in soil [CO_2], while [O_2] shows much greater sensitivity.

7 REFERENCES:

Abdalla, M., Jones, M., Smith, P., & Williams, M. (2009). Nitrous oxide fluxes and denitrification sensitivity to temperature in Irish pasture soils. Soil Use and Management, 25(4), 376–388. https://doi.org/10.1111/j.1475-2743.2009.00237.x

Almagro, M., López, J., Querejeta, J.I., & Martínez-Mena, M. (2009). Temperature dependence of soil CO 2 efflux is strongly modulated by seasonal patterns of moisture availability in a Mediterranean ecosystem. Soil Biology & Biochemistry, 41(3), 594–605. https://doi.org/10.1016/j.soilbio.2008.12.021

Amadi, C.C., Van Rees, K. C. J., & Farrell, R. E. (2016). Soil–atmosphere exchange of carbon dioxide, methane and nitrous oxide in shelterbelts compared with adjacent cropped fields. Agriculture, Ecosystems & Environment, 223, 123–134. https://doi.org/10.1016/j.agee.2016.02.026

Amos, R. T., Mayer, K. U., Bekins, B. A., Delin, G. N., & Williams, R. L. (2005). Use of dissolved and vapor-phase gases to investigate methanogenic degradation of petroleum hydrocarbon contamination in the subsurface. Water Resources Research, 41(2), W02001–n/a. https://doi.org/10.1029/2004WR003433

Aponte, C., Marañón, T., & García, L. V. (2010). Microbial C, N and P in soils of Mediterranean oak forests: influence of season, canopy cover and soil depth. Biogeochemistry, 101(1/3), 77–92. https://doi.org/10.1007/s10533-010-9418-5

Arora, K., Mickelson, S. K., Helmers, M. J., & Baker, J. L. (2010). Review of Pesticide Retention Processes Occurring in Buffer Strips Receiving Agricultural Runoff. Journal of the American Water Resources Association, 46(3), 618–647. https://doi.org/10.1111/j.1752-1688.2010.00438.x

Baah-Acheamfour, M., Carlyle, C. N., Lim, S.-S., Bork, E. W., & Chang, S. X. (2016). Forest and grassland cover types reduce net greenhouse gas emissions from agricultural soils. The Science of the Total Environment, 571, 1115–1127. https://doi.org/10.1016/j.scitotenv.2016.07.106

Baskerville, M., Bazrgar, A., Reddy, N., Ofosu, E., Thevathasan, N., Gordon, A. M., & Oelbermann, M. (2021). Greenhouse gas emissions from riparian zones are related to vegetation type and environmental factors. Journal of Environmental Quality, 50(4), 847–857. https://doi.org/10.1002/jeq2.20250

Blume, O. (2020). Greenhouse Gas Production and Transport Within Tile Drained Agriculture (Master's Thesis, Carleton University, Ottawa, Ontario).

Blume, O., Guitard, E., Crann, C., Orekhov, M., Amos, R., Clark, I., Lapen, D., Blowes, D., Ptacek, C., Craiovan, E., & Sunohara, M. (2022). Relationships between carbon age and CO2 efflux in agricultural and drainage ditch soils using the thermonuclear bomb pulse. Vadose Zone Journal. Early View. https://doi.org/10.1002/vzj2.20208

Boone, R. D., Nadelhoffer, K. J., Canary, J. D., & Kaye, J. P. (1998). Roots exert a strong influence on the temperature sensitivity of soil respiration. Nature (London), 396(6711), 570–572. https://doi.org/10.1038/25119

Borin, M., Passoni, M., Thiene, M., & Tempesta, T. (2010). Multiple functions of buffer strips in farming areas. European Journal of Agronomy, 32(1), 103–111. https://doi.org/10.1016/j.eja.2009.05.003

Borken, W. & Matzner, E. (2009). Reappraisal of drying and wetting effects on C and N mineralization and fluxes in soils. Global Change Biology, 15(4), 808–824. https://doi.org/10.1111/j.1365-2486.2008.01681.x

Brassard, P., Godbout, S., & Raghavan, V. (2016). Soil biochar amendment as a climate change mitigation tool: Key parameters and mechanisms involved. Journal of Environmental Management, 181, 484–497. https://doi.org/10.1016/j.jenvman.2016.06.063

Brewer, P. E., Calderón, F., Vigil, M., & von Fischer, J. . (2018). Impacts of moisture, soil respiration, and agricultural practices on methanogenesis in upland soils as measured with stable isotope pool dilution. Soil Biology & Biochemistry, 127, 239–251. https://doi.org/10.1016/j.soilbio.2018.09.014

Butterbach-Bahl, K., Baggs, E. M., Dannenmann, M., Kiese, R., & Zechmeister-Boltenstern, S. (2013). Nitrous oxide emissions from soils: how well do we understand the processes and their controls? Philosophical Transactions. Biological Sciences, 368(1621), 1–13. https://doi.org/10.1098/rstb.2013.0122

Cazelles, B., Chavez, M., Berteaux, D., Ménard, F., Vik, J. O., Jenouvrier, S., & Stenseth, N. C. (2008). Wavelet Analysis of Ecological Time Series. Oecologia, 156(2), 287–304. https://doi.org/10.1007/s00442-008-0993-2

Chambers and Accessories for the LI-8100A. (2022). LI-COR Environmental. (n.d.). Retrieved from https://www.licor.com/env/products/soil_flux/LI-8100a

Chapuis-Lardy, L., Wrage, N., Metay, A., Chotte, J. L., & Bernoux, M. (2007). Soils, a sink for N2O? A review. Global Change Biology, 13(1), 1–17. https://doi.org/10.1111/j.1365-2486.2006.01280.x

Christiansen, J.R., Gundersen, P., Frederiksen, P., & Vesterdal, L. (2012). Influence of hydromorphic soil conditions on greenhouse gas emissions and soil carbon stocks in a Danish temperate forest. Forest Ecology and Management, 284, 185–195. https://doi.org/10.1016/j.foreco.2012.07.048

Cole, L. J., Stockan, J., & Helliwell, R. (2020). Managing riparian buffer strips to optimise ecosystem services: A review. Agriculture, Ecosystems & Environment, 296, 106891–. https://doi.org/10.1016/j.agee.2020.106891

Crabbé, P., Lapen, D. R., Clark, H., Sunohara, M., & Liu, Y. (2012). Economic benefits of controlled tile drainage: Watershed Evaluation of Beneficial Management Practices, South Nation River basin, Ontario. Water Quality Research Journal, 47(1), 30–41. https://doi.org/https://doi.org/10.2166/wqrjc.2012.007

De Carlo, N.D., Oelbermann, M., & Gordon, A. M. (2019). Carbon dioxide emissions: Spatiotemporal variation in a young and mature riparian forest. Ecological Engineering, 138, 353–361. https://doi.org/10.1016/j.ecoleng.2019.07.036

Dong, Y., Zhang, S., Yuchun, Q., Chen, Z., & Geng, Y. (2000). Fluxes of CO2, N2O and CH4 from a typical temperate grassland in Inner Mongolia and its daily variation. Chinese Science Bulletin, 45(17), 1590–1594. https://doi.org/10.1007/bf02886219

Du, R., Lu, D., & Wang, G. (2006). Diurnal, seasonal, and inter-annual variations of N2O fluxes from native semi- arid grassland soils of inner Mongolia. Soil Biology & Biochemistry, 38(12), 3474–3482. https://doi.org/10.1016/j.soilbio.2006.06.012

Dutaur, L., & Verchot, L. V. (2007). A global inventory of the soil CH4 sink. Global Biogeochemical Cycles, 21(4), GB4013–n/a. https://doi.org/10.1029/2006GB002734

ECCC. (2021). National Inventory Report 1990–2019: Greenhouse Gas Sources and Sinks in Canada. Retrieved from https://publications.gc.ca/collections/collection_2021/eccc/En81-4-1-2019-eng.pdf

Evans, R. O., Skaggs, R. W., & Giiliam, J. W. (1995). Controlled Versus Conventional Drainage Effects on Water Quality. Journal of Irrigation and Drainage Engineering, 121(4), 271–276.

Fang, C., Smith, P., & Smith, J. U. (2006). Is resistant soil organic matter more sensitive to temperature than the labile organic matter? Biogeosciences, 3(1), 65–68. https://doi.org/10.5194/bg-3-65-2006

Fierer, N. & Schimel, J. P. (2002). Effects of drying-rewetting frequency on soil carbon and nitrogen transformations. Soil Biology & Biochemistry, 34(6), 777–787. https://doi.org/10.1016/S0038-0717(02)00007-X

Flechard, C. R., Neftel, A., Jocher, M., Ammann, C., Leifeld, J., & Fuhrer, J. (2007). Temporal changes in soil pore space CO 2 concentration and storage under permanent grassland. Agricultural and Forest Meteorology, 142(1), 66–84. https://doi.org/10.1016/j.agrformet.2006.11.006

Forde, O. N., Cahill, A. G., Beckie, R. D., & Mayer, K. U. (2019). Barometric-pumping controls fugitive gas emissions from a vadose zone natural gas release. Scientific Reports, 9(1), 14080–14089. https://doi.org/10.1038/s41598-019-50426-3

Gilliam, J. W., Skaggs, R. W., & Weed, S. B. (1979). Drainage Control to Diminish Nitrate Loss from Agricultural Fields1. Journal of Environmental Quality, 8(1), 137. https://doi.org/10.2134/jeq1979.00472425000800010030x

Global Monitoring Laboratory - Carbon Cycle Greenhouse Gases. (n.d.). Retrieved from https://gml.noaa.gov/ccgg/trends_n2o/

Government of Canada. (2013). Description of soil ONBIVSS~~~A (BAINSVILLE). Retrieved from http://sis.agr.gc.ca/cansis/soils/on/BIV/SS~~~/A/description.html

Gregorich, E. G., Rochette, P., VandenBygaart, A. J., & Angers, D. A. (2005). Greenhouse gas contributions of agricultural soils and potential mitigation practices in Eastern Canada. Soil and Tillage Research, 83(1 SPEC. ISS.), 53–72. https://doi.org/10.1016/j.still.2005.02.009

Groffman, P. M., Butterbach-Bahl, K., Fulweiler, R. W., Gold, A. J., Morse, J. L., Stander, E. K., Tague, C., Tonitto, C., & Vidon, P. (2009). Challenges to incorporating spatially and temporally explicit phenomena (hotspots and hot moments) in denitrification models. Biogeochemistry, 93(1/2), 49–77. https://doi.org/10.1007/s10533-008-9277-5

Groffman, P.M., Hardy, J. P., Driscoll, C. T., & Fahey, T. J. (2006). Snow depth, soil freezing, and fluxes of carbon dioxide, nitrous oxide and methane in a northern hardwood forest. Global Change Biology, 12(9), 1748–1760. https://doi.org/10.1111/j.1365-2486.2006.01194.x

Guckland, A., Flessa, H., & Prenzel, J. (2009). Controls of temporal and spatial variability of methane uptake in soils of a temperate deciduous forest with different abundance of European beech (Fagus sylvatica L.). Soil Biology & Biochemistry, 41(8), 1659–1667. https://doi.org/10.1016/j.soilbio.2009.05.006

Gumiere, S. J., Le Bissonnais, Y., Raclot, D., & Cheviron, B. (2011). Vegetated filter effects on sedimentological connectivity of agricultural catchments in erosion modelling; a review. Earth Surface Processes and Landforms, 36(1), 3–19. https://doi.org/10.1002/esp.2042

Gundersen, P., Laurén, A., Finér, L., Ring, E., Koivusalo, H., Sætersdal, M., Weslien, J.-O., Sigurdsson, B. D., Högbom, L., Laine, J., & Hansen, K. (2010). Environmental Services Provided from Riparian Forests in the Nordic Countries. Ambio, 39(8), 555–566. https://doi.org/10.1007/s13280-010-0073-9

Hanson, P.J., Edwards, N. T., Garten, C. T., Andrews, J. A., Rustad, L. E., Huntington, T. G., & Boone, R. D. (2000). Separating root and soil microbial contributions to soil respiration; a review of methods and observations. Biogeochemistry, 48(1), 115–146. https://doi.org/10.1023/A:1006244819642

Holst, J., Liu, C., Yao, Z., Bruggemann, N., Zheng, X., Giese, M., & Butterbach-Bahl, K. (2008). Fluxes of nitrous oxide, methane and carbon dioxide during freezing–thawing cycles in an Inner Mongolian steppe. Plant and Soil, 308(1/2), 105–117. https://doi.org/10.1007/s11104-008-9610-8

Hosono, T., Hosoi, N., Akiyama, H., & Tsuruta, H. (2006). Measurements of N2O and NO emissions during tomato cultivation using a flow-through chamber system in a glasshouse. Nutrient Cycling in Agroecosystems, 75(1-3), 115–134. https://doi.org/10.1007/s10705-006-9016-z

IPCC. Climate Change 2013: The Physical Science Basis. Contribution of Working Group I to the Fifth Assessment Report of the Intergovernmental Panel on Climate Change; IPCC: Cambridge, UK; New York, NY, USA, 2013.

Itoh, M., Ohte, N., Koba, K., Sugimoto, A., & Tani, M. (2008). Analysis of methane production pathways in a riparian wetland of a temperate forest catchment, using δ 13 C of pore water CH 4 and CO 2. Journal of Geophysical Research, 113(G3). https://doi.org/10.1029/2007JG000647

Jacinthe, P. A., Groffman, P. M., & Gold, A. J. (2003). Dissolved organic carbon dynamics in a riparian aquifer; effects of hydrology and nitrate enrichment. Journal of Environmental Quality, 32(4), 1365–1374.

Jacinthe, P. A., Vidon, P., Fisher, K., Liu, X., & Baker, M. E. (2015). Soil methane and carbon dioxide fluxes from cropland and riparian buffers in different hydrogeomorphic settings. Journal of Environmental Quality, 44(4), 1080–1090. https://doi.org/10.2134/jeq2015.01.0014

Jäckel, U., Schnell, S., & Conrad, R. (2001). Effect of moisture, texture and aggregate size of paddy soil on production and consumption of CH4. Soil Biology & Biochemistry, 33(7-8), 965–971. https://doi.org/10.1016/S0038-0717(00)00248-0

Jarecke, K. M., Loecke, T. D., & Burgin, A. J. (2016). Coupled soil oxygen and greenhouse gas dynamics under variable hydrology. Soil Biology & Biochemistry, 95, 164–172. https://doi.org/10.1016/j.soilbio.2015.12.018

Kachenchart, B., Jones, D. L., Gajaseni, N., Edwards-Jones, G., & Limsakul, A. (2012). Seasonal nitrous oxide emissions from different land uses and their controlling factors in a tropical riparian ecosystem. Agriculture, Ecosystems & Environment, 158, 15–30. https://doi.org/10.1016/j.agee.2012.05.008

Kayler, Z. E., Sulzman, E. W., Rugh, W. D., Mix, A. C., & Bond, B. J. (2010). Characterizing the impact of diffusive and advective soil gas transport on the measurement and interpretation of the isotopic signal of soil respiration. Soil Biology & Biochemistry, 42(3), 435–444. https://doi.org/10.1016/j.soilbio.2009.11.022

Khalil, M. I., & Baggs, E. M. (2005). CH4 oxidation and N2O emissions at varied soil water-filled pore spaces and headspace CH4 concentrations. Soil Biology & Biochemistry, 37(10), 1785–1794. https://doi.org/10.1016/j.soilbio.2005.02.012

Kuzyakov, Y. (2006). Sources of CO2 efflux from soil and review of partitioning methods. Soil Biology & Biochemistry, 38(3), 425–448. https://doi.org/10.1016/j.soilbio.2005.08.020

Lado-Monserrat, L., Lull, C., Bautista, I., Lidon, A., & Herrera, R. (2014). Soil moisture increment as a controlling variable of the "Birch effect". Interactions with the pre-wetting soil moisture and litter addition. Plant and Soil, 379(1/2), 21–34. https://doi.org/10.1007/s11104-014-2037-5

Laemmel, T., Mohr, M., Schack-Kirchner, H., Schindler, D., & Maier, M. (2017). Direct observation of wind-induced pressure-pumping on gas transport in soil. Soil Science Society of America Journal, 81(4), 770–774. https://doi.org/10.2136/sssaj2017.01.0034n

Le Mer, J., & Roger, P. (2001). Production, oxidation, emission and consumption of methane by soils: A review. European Journal of Soil Biology, 37(1), 25–50. https://doi.org/10.1016/S1164-5563(01)01067-6

Lemke, Izaurralde, R. L., & Nyborg, M. (1998). Seasonal distribution of nitrous oxide emissions from soils in the Parkland region. Soil Science Society of America Journal, 62(5), 1320–1326. https://doi.org/10.2136/sssaj1998.03615995006200050025x

Li, Y., Hu, S., Chen, J., Müller, K., Li, Y., Fu, W., Lin, Z., & Wang, H. (2017). Effects of biochar application in forest ecosystems on soil properties and greenhouse gas emissions: a review. Journal of Soils and Sediments, 18(2), 546–563. https://doi.org/10.1007/s11368-017-1906-y

Liang, L. L., Campbell, D. I., Wall, A. M., & Schipper, L. A. (2018). Nitrous oxide fluxes determined by continuous eddy covariance measurements from intensively grazed pastures: Temporal patterns and environmental controls. Agriculture, Ecosystems & Environment, 268, 171–180. https://doi.org/10.1016/j.agee.2018.09.010

Lloyd, J., & Taylor, J. A. (1994). On the Temperature Dependence of Soil Respiration. Functional Ecology, 8(3), 315–323. https://doi.org/10.2307/2389824

Maier, M., Schack-Kirchner, H., Aubinet, M., Goffin, S., Longdoz, B., & Parent, F. (2012). Turbulence Effect on Gas Transport in Three Contrasting Forest Soils. Soil Science Society of America Journal, 76(5), 1518–1528. https://doi.org/10.2136/sssaj2011.0376

Malchair, S., & Carnol, M. (2009). Microbial biomass and C and N transformations in forest floors under European beech, sessile oak, Norway spruce and Douglas-fir at four temperate forest sites. Soil Biology & Biochemistry, 41(4), 831–839. https://doi.org/10.1016/j.soilbio.2009.02.004

Massman, W. J., (1998). A review of the molecular diffusivities of H2O, CO2, CH4, CO, O3, SO2, NH3, N2O, NO, and NO2 in air, O2 and N2 near STP. Atmospheric Environment (1994), 32(6), 1111–1127. https://doi.org/10.1016/S1352-2310(97)00391-9

Maxwell, R. A., & Coleman, D. C. (1995). Seasonal dynamics of nematode and microbial biomass in soils of riparian-zone forests of the Southern Appalachians. Soil Biology & Biochemistry, 27(1), 79–84. https://doi.org/10.1016/0038-0717(94)00136-O

Mayer, K. U., Frind, E. O., & Blowes, D. W. (2002). Multicomponent reactive transport modeling in variably saturated porous media using a generalized formulation for kinetically controlled reactions. Water Resources Research, 38(9), 13-1-13–21. https://doi.org/10.1029/2001wr000862

McClain, M. E., Boyer, E. W., Dent, C. L., Gergel, S. E., Grimm, N. B., Groffman, P. M., Hart, S. C., Harvey, J. W., Johnston, C. A., Mayorga, E., McDowell, W. H., & Pinay, G. (2003). Biogeochemical Hot Spots and Hot Moments at the Interface of Terrestrial and Aquatic Ecosystems. Ecosystems (New York), 6(4), 301–312. https://doi.org/10.1007/s10021-003-0161-9

Mikkela, C., Sungh, I., Svensson, B. H., & Nilsson, M. (1995). Diurnal variation in methane emission in relation to the water table, soil temperature, climate and vegetation cover in a Swedish acid mire. Biogeochemistry, 28(2), 93–114. https://doi.org/10.1007/BF02180679

Millington, R. J. (1959). Gas Diffusion in Porous Media. Science (American Association for the Advancement of Science), 130(3367), 100–102. https://doi.org/10.1126/science.130.3367.100.b

Molins, S., & Mayer, K. U. (2007). Coupling between geochemical reactions and multicomponent gas and solute transport in unsaturated media; a reactive transport modeling study. Water Resources Research, 43(5), W05435–n/a. https://doi.org/10.1029/2006WR005206

Moore, R. D., Spittlehouse, D., & Story, A. (2005). Riparian microclimate and stream temperature response to forest harvesting: A review. Journal of the American Water Resources Association, 41(4), 813–834.

Morishita, T., Sakata, T., Takahashi, M., Ishizuka, S., Mizoguchi, T., Inagaki, Y., Terazawa, K., Sawata, S., Igarashi, M., Yasuda, H., Koyama, Y., Suzuki, Y., Toyota, N., Muro, M., Kinjo, M., Yamamoto, H., Ashiya, D., Kanazawa, Y., Hashimoto, T., & Umata, H. (2007). Methane uptake and nitrous oxide emission in Japanese forest soils and their relationship to soil and vegetation types. Soil Science and Plant Nutrition (Tokyo), 53(5), 678–691. https://doi.org/10.1111/j.1747-0765.2007.00181.x

Ng, H. Y. F., Tan, C. S., Drury, C. F., & Gaynor, J. D. (2002). Controlled drainage and subirrigation influences tile nitrate loss and corn yields in a sandy loam soil in Southwestern Ontario. Agriculture, Ecosystems & Environment, 90(1), 81–88. https://doi.org/10.1016/S0167-8809(01)00172-4

Nigel, R., Chokmani, K., Novoa, J., Rousseau, A. N., & El Alem, A. (2014). An extended riparian buffer strip concept for soil conservation and stream protection in an agricultural riverine area of the La Chevrotière River watershed, Québec, Canada, using remote sensing and GIS techniques. Canadian Water Resources Journal, 39(3), 285–301. https://doi.org/10.1080/07011784.2014.942572

Oertel, C. Matschullat, J., Zurba, K., Zimmermann, F., & Erasmi, S. (2016). Greenhouse gas emissions from soils—A review. Chemie Der Erde, 76(3), 327–352. https://doi.org/10.1016/j.chemer.2016.04.002

Panikov, N. S., Flanagan, P., Oechel, W., Mastepanov, M., & Christensen, T. (2006). Microbial activity in soils frozen to below −39 °C. Soil Biology & Biochemistry, 38(4), 785–794. https://doi.org/10.1016/j.soilbio.2005.07.004

Parkin, T. B. (1987). Soil microsites as a source of denitrification variability. Soil Science Society of America Journal, 51(5), 1194-1199.

Parkin, T.B. & Kaspar, T. C. (2003). Temperature Controls on Diurnal Carbon Dioxide Flux. Soil Science Society of America Journal, 67(6), 1763–1772. https://doi.org/10.2136/sssaj2003.1763

Paustian, K., Lehmann, J., Ogle, S., Reay, D., Robertson, G. P., & Smith, P. (2016). Climate-smart soils. Nature, 532(7597), 49–57. https://doi.org/10.1038/nature17174

Pearce, N. J. T., & Yates, A. G. (2017). Intra-annual variation of the association between agricultural best management practices and stream nutrient concentrations. The Science of the Total Environment, 586, 1124–1134. https://doi.org/10.1016/j.scitotenv.2017.02.102

Peng, Q., Dong, Y., Qi, Y., Xiao, S., He, Y., & Ma, T. (2010). Effects of nitrogen fertilization on soil respiration in temperate grassland in Inner Mongolia, China. Environmental Earth Sciences, 62(6), 1163–1171. https://doi.org/10.1007/s12665-010-0605-4

Pilegaard, K., Skiba, U., Ambus, P., Beier, C., Brüggemann, N., Butterbach-Bahl, K., Dick, J., Dorsey, J., Duyzer, J., Gallagher, M., Gasche, R., Horvath, L., Kitzler, B., Leip, A., Pihlatie, M. K., Rosenkranz, P., Seufert, G., Vesala, T., Westrate, H., & Zechmeister-Boltenstern, S. (2006). Factors controlling regional differences in forest soil emission of nitrogen oxides (NO and N 2 O). Biogeosciences, 3(4), 651–661. https://doi.org/10.5194/bg-3-651-2006

Pregitzer, K. S., Zak, D. R., Loya, W. M., Karberg, N. J., King, J. S., & Burton, A. J. (2007). Chapter 7 - The Contribution of Root - Rhizosphere interactions to Biogeochemical Cycles in a Changing World. In The Rhizosphere (pp. 155–178). Elsevier Inc. https://doi.org/10.1016/B978-012088775-0/50009-4

Raich, J. W., Tufekcioglu, A., Rustad, L. E., Huntington, T. G., & Boone, R. D. (2000). Vegetation and soil respiration; correlations and controls. Biogeochemistry, 48(1), 71–90. https://doi.org/10.1023/A:1006112000616

Reichstein, M., Rey, A., Freibauer, A., Tenhunen, J., Valentini, R., Banza, J., Casals, P., Cheng, Y., Grünzweig, J. M., Irvine, J., Joffre, R., Law, B. E., Loustau, D., Miglietta, F., Oechel, W., Ourcival, J.-M., Pereira, J. S., Peressotti, A., Ponti, F., … Yakir, D. (2003). Modeling temporal and large-scale spatial variability of soil respiration from soil water availability, temperature and vegetation productivity indices. Global Biogeochemical Cycles, 17(4), 1104–n/a. https://doi.org/10.1029/2003GB002035

Riveros-Iregui, D. A., Emanuel, R. E., Muth, D. J., McGlynn, B. L., Epstein, H. E., Welsch, D. L., Pacific, V. J., & Wraith, J. M. (2007). Diurnal hysteresis between soil CO2 and soil temperature is controlled by soil water content. Geophysical Research Letters, 34(17), L17404–n/a. https://doi.org/10.1029/2007GL030938

Rochette, P., Ellert, B., Gregorich, E. G., Desjardins, R. L., Pattey, E., Lessard, R., & Johnson, B. G. (1997). Description of a dynamic closed chamber for measuring soil respiration and its comparison with other techniques. Canadian Journal of Soil Science, 77(2), 195–203. https://doi.org/10.4141/S96-110

Rochette, P. & Hutchinson, G.L. (2005). Measuring soil respiration in situ: Chamber techniques. In J.L. Hatfield and J.M. Baker, Eds., Micrometeorology in Agricultural Systems. ASA Monograph. No. 47, American Society of Agronomy, Madison, WI, pp. 247–286.

Rosch, A., Schmidbauer, H. (2018). WaveletComp 1.1: A guided tour through the R package.

Rumble, J. R. (2018). CRC Handbook of Chemistry and Physics. (F. CRC Press/Taylor & Francis, Boca Raton, Ed.) (99th ed.). Boca Raton. Retrieved from http://hbcponline.com/faces/documents/06_40/06_40_0001.xhtml?search=true

Schaufler, G., Kitzler, B., Schindlbacher, A., Skiba, U., Sutton, M. A., & Zechmeister-Boltenstern, S. (2010). Greenhouse gas emissions from European soils under different land use: effects of soil moisture and temperature. European Journal of Soil Science, 61(5), 683–696. https://doi.org/10.1111/j.1365-2389.2010.01277.x

Scheer, C., Grace, P. R., Rowlings, D. W., & Payero, J. (2012). Nitrous oxide emissions from irrigated wheat in Australia: impact of irrigation management. Plant and Soil, 359(1/2), 351–362. https://doi.org/10.1007/s11104-012-1197-4

Scheer, C., Rowlings, D. W., Firrel, M., Deuter, P., Morris, S., & Grace, P. R. (2014). Impact of nitrification inhibitor (DMPP) on soil nitrous oxide emissions from an intensive broccoli production system in sub-tropical Australia. Soil Biology & Biochemistry, 77, 243–251. https://doi.org/10.1016/j.soilbio.2014.07.006

Schindlbacher, A., Zechmeister-Boltenstern, S., & Butterbach-Bahl, K. (2004). Effects of soil moisture and temperature on NO, NO2, and N2O emissions from European forest soils. Journal of Geophysical Research, 109(D17), D17302–n/a. https://doi.org/10.1029/2004JD004590

Serano-Silva, N., Sarria-Guzman, Y., Dendooven, L., Luna-Guido, M. (2014). Methanogenesis and Methanotrophy in Soil: A Review. Pedosphere, 24(3), 291–307. https://doi.org/10.1016/S1002-0160(14)60016-3

Shabaga, J.A., Basiliko, N., Caspersen, J. P., & Jones, T. A. (2015). Seasonal controls on patterns of soil respiration and temperature sensitivity in a northern mixed deciduous forest following partial-harvesting. Forest Ecology and Management, 348, 208–219. https://doi.org/10.1016/j.foreco.2015.03.022

Shurpali, N., Rannik, Ü., Jokinen, S., Lind, S., Biasi, C., Mammarella, I., Peltola, O., Pihlatie, M., Hyvönen, N., Räty, M., Haapanala, S., Zahniser, M., Virkajärvi, P., Vesala, T., & Martikainen, P. J. (2016). Neglecting diurnal variations leads to uncertainties in terrestrial nitrous oxide emissions. Scientific Reports, 6(1), 25739–25739. https://doi.org/10.1038/srep25739

Skaggs, R. W., Fausey, N. R., & Evans, R. O. (2012). Drainage water management. Journal of Soil and Water Conservation, 67(6), 167A. https://doi.org/10.2489/jswc.67.6.167A

Slessarev, E.W. & Schimel, J. P. (2020). Partitioning sources of CO2 emission after soil wetting using high-resolution observations and minimal models. Soil Biology & Biochemistry, 143, 107753–. https://doi.org/10.1016/j.soilbio.2020.107753

Smith, K. A., Ball, T., Conen, F., Dobbie, K. E., Massheder, J., & Rey, A. (2018). Exchange of greenhouse gases between soil and atmosphere: interactions of soil physical factors and biological processes. European Journal of Soil Science, 69(1), 10–20. https://doi.org/10.1111/ejss.12539

Statistics Canada. (2022). Table 32-10-0153-01 Land use, Census of Agriculture historical data. DOI: https://doi.org/10.25318/3210015301-eng

Stumm, W., & Morgan, J. J. (2012). Aquatic Chemistry: chemical equilibria and rates in natural waters (3rd ed.). New York: John Wiley & Sons.

Subke, J., Moody, C. S., Hill, T. C., Voke, N., Toet, S., Ineson, P., & Teh, Y. A. (2018). Rhizosphere activity and atmospheric methane concentrations drive variations of methane fluxes in a temperate forest soil. Soil Biology & Biochemistry, 116, 323–332. https://doi.org/10.1016/j.soilbio.2017.10.037

Sunohara M. D., Gottschall, N., Craiovan, E., Wilkes, G., Topp, E., Frey, S. K., & Lapen, D. R. (2016). Controlling tile drainage during the growing season in Eastern Canada to reduce nitrogen, phosphorus, and bacteria loading to surface water. Agricultural Water Management, 178, 159–170. https://doi.org/10.1016/j.agwat.2016.08.030

Sunohara, M. D., Craiovan, E., Topp, E., Gottschall, N., Drury, C. F., & Lapen, D. R. (2014). Comprehensive Nitrogen Budgets for Controlled Tile Drainage Fields in Eastern Ontario, Canada. Journal of Environmental Quality, 43(2), 617–630. https://doi.org/10.2134/jeq2013.04.0117

Tan, K.H. (2009). Environmental soil science (3rd ed.). CRC.

Thorstenson, D. C., & Pollock, D. W. (1989). Gas transport in unsaturated zones; multicomponent systems and the adequacy of Fick's laws. Water Resources Research, 25(3), 477–507. https://doi.org/10.1029/WR025i003p00477

Trumbore, S. E. (1993). Comparison of carbon dynamics in tropical and temperate soils using radiocarbon measurements. Global Biogeochemical Cycles, 7(2), 275–290. https://doi.org/10.1029/93GB00468

Unger, S., Máguas, C., Pereira, J. S., David, T. S., & Werner, C. (2010). The influence of precipitation pulses on soil respiration – Assessing the "Birch effect" by stable carbon isotopes. Soil Biology & Biochemistry, 42(10), 1800–1810. https://doi.org/10.1016/j.soilbio.2010.06.019

van der Weerden, T.J., Clough, T., & Styles, T. (2013). Using near-continuous measurements of N2O emission from urine-affected soil to guide manual gas sampling regimes. New Zealand Journal of Agricultural Research, 56(1), 60–76. https://doi.org/10.1080/00288233.2012.747548

van Hulzen, J.B., Segers, R., van Bodegom, P.M., & Leffelaar, P.A. (1999). Temperature effects on soil methane production: an explanation for observed variability. Soil Biology & Biochemistry, 31(14), 1919–1929. https://doi.org/10.1016/S0038-0717(99)00109-1

Vargas, R., & Allen, M. F. (2008). Environmental Controls and the Influence of Vegetation Type, Fine Roots and Rhizomorphs on Diel and Seasonal Variation in Soil Respiration. The New Phytologist, 179(2), 460–471. https://doi.org/10.1111/j.1469-8137.2008.02481.x

Vidon, P., Allan, C., Burns, D., Duval, T. P., Gurwick, N., Inamdar, S., Lowrance, R., Okay, J., Scott, D., & Sebestyen, S. (2010). Hot Spots and Hot Moments in Riparian Zones: Potential for Improved Water Quality Management. Journal of the American Water Resources Association, 46(2), 278–298. https://doi.org/10.1111/j.1752-1688.2010.00420.x

Vidon, P., Gomez, J., Mitchell, M., Beier, C., Gross, J., & Anonymous. (2014). Spatial and temporal patterns of CO2, CH4, and N2O fluxes at the soil-atmosphere interface in a forested watershed of the US Northeast. Abstracts with Programs - Geological Society of America, 46(6), 690.

Vidon, P., Marchese, S., Welsh, M., & McMillan, S. (2015). Short-term spatial and temporal variability in greenhouse gas fluxes in riparian zones. Environmental Monitoring and Assessment, 187(8), 503–503. https://doi.org/10.1007/s10661-015-4717-x

Wang, J. M., Murphy, J. G., Geddes, J. A., Winsborough, C. L., Basiliko, N., & Thomas, S. C. (2013). Methane fluxes measured by eddy covariance and static chamber techniques at a temperate forest in central Ontario, Canada. Biogeosciences, 10(6), 4371–4382. https://doi.org/10.5194/bg-10-4371-2013

Wang, J., Bogena, H., Süß, T., Graf, A., Weuthen, A., & Brüggemann, N. (2021). Investigating the controls on greenhouse gas emission in the riparian zone of a small headwater catchment using an automated monitoring system. Vadose Zone Journal, 20(5). https://doi.org/10.1002/vzj2.20149

Wang, S., Fu, B, Gao, G., Liu, Y., & Zhou, J. (2013). Responses of soil moisture in different land cover types to rainfall events in a re-vegetation catchment area of the Loess Plateau, China. Catena, 101, 122-128. https://doi.org/10.1016/j.catena.2012.10.006

Wang, Z., & Han, X.-G. (2005). Diurnal variation in methane emissions in relation to plants and environmental variables in the Inner Mongolia marshes. Atmospheric Environment (1994), 39(34), 6295–6305. https://doi.org/10.1016/j.atmosenv.2005.07.010

Warrick, A. W. (2002). Soil physics companion. CRC Press.

Waymouth, V., Miller, R. E., Ede, F., Bissett, A., & Aponte, C. (2020). Variation in soil microbial communities: elucidating relationships with vegetation and soil properties, and testing sampling effectiveness. Plant Ecology, 221(9), 837–851. https://doi.org/10.1007/s11258-020-01029-w

Wen, Y., Chen, Z., Dannenmann, M., Carminati, A., Willibald, G., Kiese, R., Wolf, B., Veldkamp, E., Butterbach-Bahl, K., & Corre, M. D. (2016). Disentangling gross N2O production and consumption in soil. Scientific Reports, 6(1), 36517–36517. https://doi.org/10.1038/srep36517

Whalen, S.C., & Reeburgh, W. S. (1996). Moisture and temperature sensitivity of CH (sub 4) oxidation in boreal soils. Soil Biology & Biochemistry, 28(10-11), 1271–1281.

Wicklund, R. E., & Richards, N. R. (1962). Soil Map of Russell County Ontario. Ontario Soil Survey, (33).

Wu, Y., Whitaker, J., Toet, S., Bradley, A., Davies, C. A., & McNamara, N. P. (2021). Diurnal variability in soil nitrous oxide emissions is a widespread phenomenon. Global Change Biology, 27(20), 4950–4966. https://doi.org/10.1111/gcb.15791

Wynn, T.M., & Mostaghimi, S. (2006). Effects of riparian vegetation on stream bank subaerial processes in southwestern Virginia, USA. Earth Surface Processes and Landforms, 31(4), 399–413. https://doi.org/10.1002/esp.1252

Xiaolu, T., Xiangjun, P., Ningfei, L., Xinrui, L., Liang, L., Leilei, S., Guo, C., & Liang, J. (2020). Global patterns of soil autotrophic respiration and its relation to climate, soil and vegetation characteristics. Geoderma, 369, 114339–. https://doi.org/10.1016/j.geoderma.2020.114339

Ying, W., Chuan-kuan, W., Min-jie, F., Shi, L., & Xing-chang, W. (2009). Soil nitrous oxide emission in four temperate forests in northeastern China. Yingyong Shengtai Xuebao, 20(5).

Zona, D., Janssens, I. A., Gioli, B., Jungkunst, H. F., Serrano, M. C., & Ceulemans, R. (2013). N2O fluxes of a bio-energy poplar plantation during a two years rotation period. Global Change Biology. Bioenergy, 5(5), 536–547. https://doi.org/10.1111/gcbb.12019